4-2017

Center Manifold Theory and Computation Using a Forward Backward Approach

Emily E. Schaal
College of William and Mary

Center Manifold Theory and Computation Using a Forward-Backward Approach

by

Emily Schaal

Submitted to the Department of Mathematics
in partial fulfillment of the requirements for

Honors in Mathematics

at the

College of William and Mary

May 2017

Accepted by

. . . . . .
Dr. Yu-Min Chung

. . . . . .
Dr. Sarah Day

. . . . . .
Dr. Rui Pereira

Acknowledgments

I want to give many thanks to my thesis advisor, Dr. Yu-Min Chung, without whom none of this would have been possible, and who has gone out of his way to encourage and assist me in my pursuit of mathematics.

I'd like to thank Professor Sarah Day and Professor Rui Pereira for serving on my defense committee. I also want to thank Professor Mike Jolly from Indiana University, Bloomington for coming up with the idea for this project and for coming to William and Mary to offer his advice and words of support.

Finally, I'd like to thank my friends here at the College and across the country, as well as my dear family, for their unfailing support during the time I worked on my thesis.

Abstract

The center manifold, an object from the field of differential equations, is useful in describing the long time behavior of the system. The most common way of computing the center manifold is by using a Taylor approximation. A different approach is to use iterative methods, as presented in [12], [9], and [19]. In particular, [19] presents a method based on a discretization of the Lyapunov-Perron (L-P) operator. One drawback is that this discretization can be expensive to compute and have error terms that are difficult to control. Using a similar framework to [19], we develop a forward-backward integration algorithm based on a boundary value problem derived from the operator. We include the details of the proofs that support this formulation; notably, we show that the operator is a contraction mapping with a fixed point that is a solution to the differential equation in our function space. We also show the first step in the induction to prove the existence of a $\mathcal{C}^k$ center manifold. We demonstrate the algorithm with Runge-Kutta (R-K) methods of $\mathcal{O}(k)$ and $\mathcal{O}(k^2)$. Finally, we present an application of our algorithm to studying a semilinear elliptic boundary value problem from [20].

Contents

Chapter 1

Introduction

In this work we develop a technique for studying the center manifold of a differential system. When present, knowledge of a unique center manifold can be useful when analyzing the entire invariant manifold for a particular system. Therefore, the motivation for this project is in its application to the study of differential equations. Having an understanding of these equations is integral to the rest of our work.

1.1 Background

Differential systems model flow, or rates of change, and have important applications to fields such as biology, physics, economics, and many others. Informally, an ordinary differential system a collection of equations relating important quantities and their rates of change. Usually, this derivative is taken with respect to time, represented as t. Ordinary differential equations are often used to model population dynamics, the behavior of neurons, and other biological processes. They also crop up in physics. For example, the Newtonian equations of motion are ordinary differential equations. These systems, although the "simpler" subset of differential equations, can still exhibit strange and unpredictable behavior. The Lorenz equations [26], which were developed by Edward Lorenz to model a leaky water wheel, is a system of only three dimensions and yet exhibits chaotic behavior.

Whereas ordinary differential equations are differentiated with respect to the same variable, partial differential equations are made up of derivatives of several variables. Consider the equation

$$\frac{\partial^2 u(x,y)}{\partial x^2} + \frac{\partial^2 u(x,y)}{\partial y^2} + \lambda u(x,y) - u(x,y)^2 = 0, \tag{1.1}$$

which has second derivatives with respect to x and y and is investigated in [20]. Other examples of partial differential equations are the wave equation, the heat equation, and Laplace's equations. The complexity of analyzing even apparently simple partial differential systems makes their study a mathematical field unto itself.

Any particular differential equation is either autonomous or non-autonomous. An autonomous equation, $\frac{dy}{dt} = f(y)$, is implicitly dependent on the independent variable, meaning that if an ordinary differential system was differentiated with respect to t, the variable t does

not appear in the equation. On the other hand, a non-autonomous equation, $\frac{dy}{dt} = f(y,t)$, is one that is explicitly dependent on the variable it was differentiated with respect to. For example,

$$\frac{dy}{dt} = -y^2 + t \tag{1.2}$$

is a non-autonomous equation, while

$$\frac{dy}{dt} = -y^2$$

is autonomous. We focus on autonomous equations.

The next distinction is between linear and nonlinear equations. An equation is linear if it is linear in the dependent variable and all of its derivatives. Otherwise, it is nonlinear. For example,

$$\frac{dy}{dt} = -y + t^2$$

is linear, but equation (1.2) is nonlinear. Whether or not an equation is linear makes a big difference for how well we can solve it. Closed-form solutions exist for linear ordinary differential equations unique up to a constant. Some nonlinear systems can be solved this way, but most cannot.

Although we are limited in the systems for which we can obtain full solutions, we can learn a lot by analyzing the behavior of the system without obtaining its solution. The first step in this process is identifying the steady states and the behavior of the system around each steady state, which is a point at which there is a constant solution to the ordinary differential equation; $y(t) = y_0$. Intuitively, if a trajectory starts at a steady state, it will stay at that steady state forever. For example, the steady state for the system

$$\begin{aligned} \dot{x} &= -x + 1 & x(0) &= x_0 \\ \dot{y} &= y & y(0) &= y_0 \end{aligned}$$

is $(1,0)$, which we find by setting $\dot{x} = 0$ and $\dot{y} = 0$. If, when the system is perturbed off of the steady state, it returns to the steady state, then the steady state is stable. If, on the other hand, it moves away from and never returns to its original position, the steady state is unstable. We determine stability by finding the eigenvalues and eigenvectors of the linearized Jacobian matrix for the system. In this case,

$$J(1,0) = \begin{pmatrix} \frac{\partial(-x+1)}{\partial x} & \frac{\partial(-x+1)}{\partial y} \\ \frac{\partial(y)}{\partial x} & \frac{\partial(y)}{\partial y} \end{pmatrix}_{(1,0)} = \begin{pmatrix} -1 & 0 \\ 0 & 1 \end{pmatrix},$$

which is already diagonal and will have eigenvectors $\begin{pmatrix} 0 & 1 \end{pmatrix}^t$ and $\begin{pmatrix} 1 & 0 \end{pmatrix}^t$. The negative eigenvalue implies that some trajectories will approach the steady state, while the positive eigenvalue implies that some trajectories will move away from the steady state. From this, we say that this steady state is a saddle node, where some trajectories that start in a ball of small enough radius will approach the steady state, while other trajectories will approach

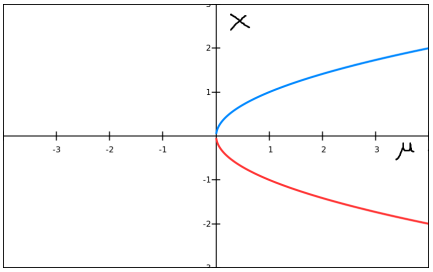

Figure 1-1: Bifurcation diagram of (1.3). Saddle Node Bifurcation at $\mu_c = 0$. The blue line represents the evolution of the stable steady state $s = \sqrt{\mu}$ and the red line represents the evolution of the unstable steady state $x = -\sqrt{\mu}$.

positive or negative infinity. Because this system is linear, the behavior of the system around this point describes the behavior of the entire system, so "near enough" could be anywhere in the phase space.

The nature of the steady states of a differential system, and the nature of the behavior of the system, can change based on the variation of a single parameter. This is a *bifurcation*, and the parameter being varied is known as the *bifurcation parameter*. Consider the system

$$\dot{x} = \mu - x^2 \qquad\qquad x(0) = x_0 \tag{1.3}$$

where x and $\mu \in \mathbb{R}$. By setting $\mu - x^2 = 0$, we can calculate the steady state as $x_0 = \pm\sqrt{\mu}$, where μ is the bifurcation parameter. When μ is negative, there are no steady states. When $\mu = 0$, the point $x_0 = 0$ is half-stable, which is a hybrid of the stable and unstable case. When μ is positive, the point $x = \sqrt{\mu}$ is stable and the point $x = -\sqrt{\mu}$ is unstable. We determine the stability by observing the change in sign of $\dot{x}$ as we vary x around the steady state. If, for a given μ, $\dot{x} < 0$ when $x < x_0$ and $\dot{x} > 0$ when $x > x_0$, then the solution $x(t)$ is increasing and the steady state x_0 is stable. If $\dot{x} > 0$ when $x < x_0$ and $\dot{x} < 0$ when $x > x_0$, then the steady state x_0 is unstable. If $\dot{x} < 0$ when $x < x_0$ and $\dot{x} < 0$ when $x > x_0$, then the steady state x_0 is half-stable. The evolution of the fixed points is described succinctly in a bifurcation diagram, which is a plot of the steady states, x, as a function of μ. The bifurcation diagram for (1.3) is in Figure 1-1. This particular bifurcation is called a saddle-node bifurcation and describes when a stable and an unstable fixed point collide and annihilate.

A Hopf bifurcation occurs when a pair of complex conjugate eigenvalues of the Jacobian matrix for a system of at least two dimensions become purely imaginary. The system evolves from one with an (un)stable spiral to one with an (un)stable limit cycle. A simple example of a system which has a subcritical pitchfork bifurcation is

$$\dot{y}_1 = \beta y_1 + y_1^3 - y_1^5 \tag{1.4}$$
$$\dot{y}_2 = \omega + b y_1^2, \tag{1.5}$$

where β is the bifurcation parameter; ω and b are other parameters that slightly modify the behavior of the system, from [33]. An example bifurcation diagram for a system like (1.4) is in Figure 1-2. We see in Figure 1-2 that the system evolves from having an unstable spiral

to an unstable limit cycle. For a rigorous and extensive discussion of Hopf bifurcations that ties in with our work, see [27].

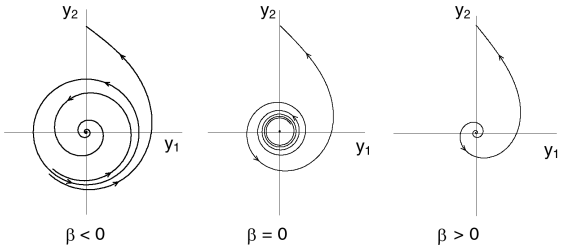

Figure 1-2: Hopf Bifurcations, from [23]

Steady states are single points on the invariant manifold associated with the differential system. Informally, the invariant manifold is a set made up of all the points such that any trajectory in the flow that starts at one of these points will only travel to other points on the same set. Intuitively, if a trajectory (a sketch of a particular solution in the phase plane) starts on the invariant manifold, it will stay on it forever. There are three distinct invariant manifolds: the stable, unstable, and center. In a linear system in $\mathbb{R}^n$ and $\mathbb{C}^n$, the manifolds are determined by the eigendecomposition of the Jacobian matrix at the steady state (for nonlinear systems, we linearize about the origin). For proofs of the existence of the invariant and center manifolds in $\mathbb{R}^n$ for a nonlinear system using the Lyapunov-Perron method, see [6].

We include a formal definition of invariant manifold from [8]:

Definition 1.1.1. (Invariant Manifold) A set $S \subseteq E$ is called an *invariant set* for the differential equation

$$\begin{aligned}\dot{x} &= Ax + F(x, y, z)\\ \dot{y} &= By + G(x, y, z)\\ \dot{z} &= Cz + H(x, y, z)\end{aligned}$$

if, for each $u = (x, y, z) \in S$, the solution $t \mapsto u(x, y, z)$, defined on $(-\infty, \infty)$ has its image in S. Alternatively, the trajectory passing through each $u \in S$ lies in S. If S is a manifold, then S is called an *invariant manifold*.

A more in-depth discussion of invariant manifolds in Banach spaces can be found in [15].

The global behavior of the system is simply the behavior of the invariant manifold for linear systems and for nonlinear systems with sufficiently controlled nonlinear terms. Otherwise, nonlinear terms can cause the system to behave "badly" - explosively or chaotically. We are interested in the invariant manifold because it often describes how the system behaves over long periods of time. Steady states appear on the manifold, and thus bifurcations show up on the manifold as well. The inertial manifold is an invariant manifold that captures all such long-term behavior. It contains the global attractor, to which all solutions will converge at an exponential rate. The attractor is what guarantees that the inertial manifold will capture the asymptotic behavior of the system [11]. A rigorous definition and discussion of the manifold can be found in [34].

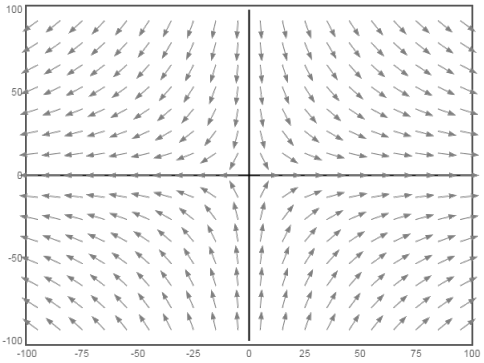

Figure 1-3: The phase portrait for (1.6), which has fixed point $(0, 0)$. The stable manifold is $x = 0$. The unstable manifold is $y = 0$.

The trajectories that start on the stable manifold will move toward the steady state at an exponential rate, while the trajectories that start on the unstable manifold will blow up to positive or negative infinity at an exponential rate. The eigenvectors associated with negative eigenvalues make up the stable subspace, and eigenvectors associated with positive eigenvalues make up the unstable subspace. As an illustration, consider the following example:

$$\begin{aligned} \dot{x} &= -x \\ \dot{y} &= y. \end{aligned} \tag{1.6}$$

The steady state for the system is $(0, 0)$, and the eigenvalue decomposition of the Jacobian gives $(-1, \begin{pmatrix} 1 & 0 \end{pmatrix}^t)$ and $(1, \begin{pmatrix} 0 & 1 \end{pmatrix}^t)$ as eigenvalue, eigenvector pairs. Thus, the invariant manifold for this system is the set of points $\{(0, y), y \in \mathbb{R}\} \cup \{(x, 0), x \in \mathbb{R}\}$, where $x = 0$ is the stable manifold and $y = 0$ is the unstable manifold. This is shown in Figure 1-3. Notice that the trajectories in Figure 1-3 move toward the origin near the $y-$axis and toward positive or negative infinity near the $x-$axis.

On the other hand, the center manifold can roughly be defined as the steady states of the system around which the trajectories neither grow nor decay exponentially over time. In other words, a steady state is in the center manifold if the behavior of the trajectories near enough to it will never be governed by either the unstable or the stable manifolds. In $\mathbb{C}^n$, the center manifold is the subspace of the eigenvector space of the Jacobian matrix of the linearized system associated with eigenvalues with zero real part. However, a system that has a zero eigenvalue is not necessarily one that has a center manifold, and the center manifold for a system is not necessarily unique. This is demonstrated in Figure 1-4, where the graph of the center manifold is shown in red but could also be described by the mirror image of the line across the x-axis.

The center manifold has a particularly nice property, which is that once we know the map whose graph is the center manifold, we can express the system only as a function of the center subspace. For example, consider this two-dimensional system:

$$\begin{aligned} \dot{x} &= -xy \\ \dot{y} &= -y + x^2 - 2y^2. \end{aligned}$$

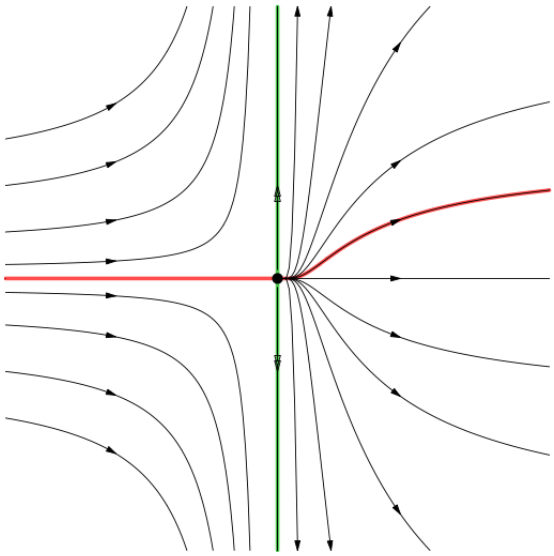

Figure 1-4: The phase portrait for the system $\dot{x} = x^2$, $\dot{y} = y$. The unstable manifold is in green and the center manifold is in red.

According to [32], it has exact center manifold $y = x^2$. We substitute in for y to get that the evolution of the system is the same as the evolution of

$$\dot{x} = -x^3.$$

This is the *center manifold reduction*, where x is the variable associated with the center subspace. The reduction results in a one-dimensional system that we can analyze for bifurcations as opposed to a two-dimensional system. In general, the reduction will always result in a lower dimensional system, and in many cases the lower dimensionality makes the system much easier to analyze.

While a number of methods for center manifold reduction already exist [35, 38, 14, 18, 25, 12, 9, 19], finding improved methods can allow us to analyze the bifurcations of (partial) differential systems with a greater degree of accuracy. One of the more common methods for computing the center manifold numerically is to do a Taylor expansion to put the system into normal form [15, 31], either manually or using software, and then implement the result as a function. This method is difficult even when using software because the risk of human error is quite high and the number of terms needed for sufficient accuracy can make the approximation slow to compute. Another method is to divide the manifold into subdivisions, as in [9]. On the other hand, [12, 19] present iterative algorithms for computing the global center manifold. The approach in [19] involves a discretization of the Lyapunov-Perron map, which they iterate on piecewise constant functions of time. An advantage of their approach is that it can compute non-smooth manifolds. However, one of the drawbacks to their algorithm is that each step in the iteration is increasingly computationally expensive. For an overview of methods for computing the invariant manifold, see [28] and [22].

The boundary value problem that we present serves as the basis for the formulation of an algorithm that uses simple numerical integration, such as the Runge-Kutta type schemes, to compute the global manifold. The limitation to using center manifold reduction in studying

partial differential equations is that the reduction itself tends to be very difficult to implement and adapt. The algorithm we present has the advantage that it is relatively simple and can be adopted using traditional numerical schemes. These schemes have the advantage that their behavior is already well understood, and the accuracy of computation can be improved with the implementation of several known updates.

In Section 2.1, we prove the existence and uniqueness of the center manifold using the Lyapunov-Perron method. First, we show that the Lyapunov-Perron map is well-defined and a contraction mapping, from [17]:

Definition 1.1.2. Let (E, d) be a metric space. A mapping $T : E \to E$ is a contraction mapping if there exists a constant c with $0 \leq c < 1$, such that $d(T(u_1), T(u_2)) \leq cd(u_1, u_2)$ for all $u_1, u_2 \in E$.

Theorem 1.1.3 (Banach Fixed Point Theorem)**.** *Let (E, d) be a Banach space with a contraction mapping $T : E \to E$. Then T admits a unique fixed-point $u^* \in E$ such that $T(u^*) = u^*$.*

Theorem 1.1.3, from [2], gives that we can iterate the operator to find a fixed point, which we show represents a unique solution in a certain function space to the ordinary differential system. These results lead us to the formulation of the boundary value problem on which we base our algorithm. In Section 2.2, we make some extensions to the framework and follow the same line of proof for the derivative of the map. We prove that the map whose graph gives the center manifold is $\mathcal{C}^1$, meaning that the derivative exists and is continuous. We also arrive at a boundary value problem for the derivative of the center manifold similar to the one we found in Section 2.1.

In Section 3.1, we present the forward/backward integration algorithm we develop based off of the boundary value problem and implement it using Runge-Kutta schemes of orders one and two. We demonstrate the accuracy of these schemes using an example from [19]. We show the results when a simple (one dimensional in each component) differential system fits the framework completely and compare them to the results we get in analyzing a simple system that does not completely fit the framework. We use this to help inform our analysis of (1.1), which does not completely satisfy the framework, in Section 3.2. We use traditional techniques to analyze the equation and compare the results to what we get using our method. We demonstrate the usefulness of our algorithm in this setting and include a discussion of some interesting behavior that arose as well as further research.

1.2 Framework

We consider nonlinear ordinary differential systems in a Banach space E where $u \in E$ takes the form $u = x + y + z$ and has an associated norm $\|u\| = \max\{\|x\|, \|y\|, \|z\|\}$:

$$\begin{aligned} \dot{x} &= Ax + F(x, y, z) \\ \dot{y} &= By + G(x, y, z) \\ \dot{z} &= Cz + H(x, y, z). \end{aligned} \tag{1.7}$$

The Banach space can be decomposed such that $E = X \times Y \times Z$. The linear terms are such that $A \in \mathcal{L}(X, X)$, $B \in \mathcal{L}(Y, Y)$, and $C \in \mathcal{L}(C, C)$, where $\mathcal{L}$ is the space of linear operators. The nonlinear terms are such that $F(x, y, z) \in \mathcal{C}(E, X)$, $G(x, y, z) \in \mathcal{C}(E, Y)$, and $H(x, y, z) \in \mathcal{C}(E, Z)$. We assume that $F(0, 0, 0) = G(0, 0, 0) = H(0, 0, 0) = 0$, which is a common assumption made for convenience. The rest of the assumptions are as follows.

A1. Exponential Trichotomy Condition: We assume that for α_x, α_y, β_y, $\beta_z \in \mathbb{R}$ such that $\alpha_x < \beta_y \leq \alpha_y < \beta_z$ and constants K_x, K_y, and $K_z \in \mathbb{R}$

$$\|e^{tA}\| \leq K_x e^{\alpha_x t},\ t \geq 0 \qquad \|e^{-tC}\| \leq K_z e^{-\beta_z t},\ t \geq 0$$
$$\|e^{-tB}\| \leq K_y e^{-\beta_y t},\ t \geq 0 \qquad \|e^{tB}\| \leq K_y e^{\alpha_y t},\ t \geq 0.$$

A2. Lipschitz Continuity of Nonlinear Terms: For all (x_1, y_1, z_1) and $(x_2, y_2, z_2) \in E$, there exist constants δ_x, δ_y, and $\delta_z \in \mathbb{R}$ such that δ_x, δ_y, and $\delta_z \geq 0$ and

$$\|F(x_1, y_1, z_1) - F(x_2, y_2, z_2)\| \leq \delta_x \|(x_1, y_1, z_1) - (x_2, y_2, z_2)\|$$
$$\|G(x_1, y_1, z_1) - G(x_2, y_2, z_2)\| \leq \delta_y \|(x_1, y_1, z_1) - (x_2, y_2, z_2)\|$$
$$\|H(x_1, y_1, z_1) - H(x_2, y_2, z_2)\| \leq \delta_z \|(x_1, y_1, z_1) - (x_2, y_2, z_2)\|.$$

A3. Gap Condition: Given the nonlinear Lipschitz constants δ_x, δ_y, and $\delta_z \geq 0$ and exponential trichotomy constants α_x, α_y, β_y, $\beta_z \in \mathbb{R}$ and K_x, K_y, and $K_z \in \mathbb{R}$, we the following inequalities hold:

$$\beta_y - \alpha_x > K_x \delta_x + K_y \delta_y$$
$$\beta_z - \alpha_y > K_y \delta_y + K_z \delta_z.$$

A1 defines bounds for the linear parts of each component. The stable component is bounded forward in time, the unstable component is bounded backward in time, and the center is bounded in both directions. This is a generalization of the exponential dichotomy condition, which pertains to the (un)stable case of the invariant manifold. A development of the exponential dichotomy condition can be found in [30]. To help understand A1, consider an ordinary differential equation in $\mathbb{C}^n$ where the real matrix A is the linear operator in the stable component. A will have eigenvalues with all negative real part, and we pick $\lambda_x \in \lambda(A)$ to be the eigenvalue such that $|\Re(\lambda_x)| \leq |\Re(\lambda)|$ for all $\lambda \in \lambda(A)$, the set of all eigenvalues of A, and $\alpha_x = \Re(\lambda_x)$, $K_x = \sup_{t \in \mathbb{R}} e^{\Im(\lambda_x)t}$. Next, A2 gives us that the behavior of the nonlinear terms will not be explosive or erratic. Then, we have A3, which allows a unique center manifold to exist. For an investigation of the gap condition that we use, see [7]. These three assumptions allow us to study the behavior of the invariant manifold as the global behavior of the system.

We define a parameter $\sigma(t)$ such that

$$\sigma(t) = \begin{cases} \sigma_p & t \geq 0 \\ \sigma_n & t \leq 0 \end{cases} \tag{1.8}$$

and define the following ordering conditions with respect to the constants in A1 and A2.

C1.

$$\alpha_x < \sigma_n < \beta_y \leq \alpha_y < \sigma_p < \beta_z,$$

C2.

$$\alpha_x + K_x\delta_x < \sigma_n < \beta_y - K_y\delta_y$$
$$\alpha_y + K_y\delta_y < \sigma_p < \beta_z - K_z\delta_z.$$

This places σ_n arbitrarily between the stable and center components and σ_p arbitrarily between the center and unstable components. We define a function space $\mathcal{F}_\sigma$ such that each global trajectory ϕ of the differential system where $\phi : Y \to E$ is found as a fixed point in

$$\mathcal{F}_\sigma = \{\phi \in \mathcal{C}(\mathbb{R} \times Y, E) : \sup_{t\in\mathbb{R}}(e^{-\sigma(t)}\|\phi(t)\|) = \|\phi\|_\sigma < \infty\}.$$

This is the space of all continuous functions from $\mathbb{R}\times Y$ to the space E that are exponentially bounded, and it is these functions that we wish to study. $\mathcal{F}_\sigma$ is also a Banach space with the $\|\cdot\|_\sigma$ norm.

Finally, let $y_0 \in Y$, $\phi(t, y_0) := \phi(t)$ and define the Lyapunov-Perron operator $\mathcal{T} : \mathcal{F}_\sigma \times Y \to \mathcal{F}_\sigma$ as

$$\mathcal{T}(\phi(t), y_0) = \underbrace{e^{tB}y_0 + \int_0^t e^{(t-s)B}G(\phi(s))ds}_{\text{I}} - \underbrace{\int_t^\infty e^{(t-s)C}H(\phi(s))ds}_{\text{II}} + \underbrace{\int_{-\infty}^t e^{(t-s)A}F(\phi(s))ds}_{\text{III}}, \tag{1.9}$$

where I is the Y component, II is the Z component, and III is the X component.

Chapter 2

Center Manifold Theory

In this chapter, we use the framework and assumptions to study the properties and regularity of the center manifold. One of the results of this study is the boundary value problem on which we base our algorithm.

2.1 Existence of the Center Manifold

We prove that the center manifold for a differential system with initial condition y_0 exists and can be defined as the graph of the X and Z components of a map $\phi \in \mathcal{F}_\sigma$. We begin by showing that the $\mathcal{T}$ map is well defined. Note that while we show a complete proof for finding continuity in each case, we omit some of the details of simplification in showing that $\mathcal{T} \in \mathcal{F}_\sigma$. These details are shown in Proposition 2.1.2.

Proposition 2.1.1. *Assume A1, A2, and C1. Let $y_0 \in Y$ and $\phi \in \mathcal{F}_\sigma$, then*

$$\mathcal{T}(\phi(t), y_0) \in \mathcal{C}(\mathbb{R} \times Y, E) \text{ and } \|\mathcal{T}(\phi, y_0)\|_\sigma < \infty.$$

Proof. First, we show that $\|\mathcal{T}(\phi, y_0)\|_\sigma < \infty$. Consider the case that $t \geq 0$. If we take the norm of (1.9) and apply assumptions A1 and A2, we obtain

$$\|\mathcal{T}(\phi(t), y_0)\| \leq \max\Bigg\{K_y e^{\alpha_y t} y_0 + K_y \delta_y e^{\alpha_y t} \int_0^t e^{-\alpha_y s} \|\phi(s)\| ds, K_z \delta_z e^{\beta_z t} \int_t^\infty e^{-\beta_z s} \|\phi(s)\| ds, \\ K_x \delta_x e^{\alpha_x t} \Big[\int_0^t e^{-\alpha_x s} \|\phi(s)\| ds + \int_{-\infty}^0 e^{-\alpha_x s} \|\phi(s)\| ds \Big] \Bigg\}.$$

Next, we multiply by one in the form of $e^{\sigma(s)s} e^{-\sigma(s)s}$ according to the sign of s in each integral:

$$\|\mathcal{T}(\phi(t), y_0)\| \leq \max\Bigg\{K_y e^{\alpha_y t} y_0 + K_y \delta_y e^{\alpha_y t} \int_0^t e^{(\sigma_p - \alpha_y)s} e^{-\sigma_p s} \|\phi(s)\| ds, \\ K_z \delta_z e^{\beta_z t} \int_t^\infty e^{(\sigma_p - \beta_z)s} e^{-\sigma_p s} \|\phi(s)\| ds, K_x \delta_x e^{\alpha_x t} \\ \Big[\int_0^t e^{(\sigma_p - \alpha_x)s} e^{-\sigma_p s} \|\phi(s)\| ds + \int_{-\infty}^0 e^{(\sigma_n - \alpha_x)s} e^{-\sigma_n s} \|\phi(s)\| ds \Big] \Bigg\}.$$

We take

$$\sup_{0\le s} e^{-\sigma_p s}\|\phi(s)\| \le \sup_{s\in\mathbb{R}} e^{-\sigma(s)s}\|\phi(s)\| = \|\phi\|_\sigma < \infty,$$
$$\sup_{s\le 0} e^{-\sigma_n s}\|\phi(s)\| \le \sup_{s\in\mathbb{R}} e^{-\sigma(s)s}\|\phi(s)\| = \|\phi\|_\sigma < \infty$$

in each integral. We also multiply through by $e^{-\sigma_p t}$:

$$e^{-\sigma_p t}\|\mathcal{T}(\phi(t), y_0)\| \le \max\Bigg\{ K_y e^{(\alpha_y-\sigma_p)t}y_0 + K_y\delta_y\|\phi\|_\sigma e^{(\alpha_y-\sigma_p)t}\int_0^t e^{(\sigma_- -\alpha_y)s}ds,$$
$$K_z\delta_z\|\phi\|_\sigma e^{(\beta_z-\sigma_p)t}\int_t^\infty e^{(\sigma_p-\beta_z)s}ds,$$
$$K_x\delta_x\|\phi\|_\sigma e^{(\alpha_x-\sigma_p)t}\Big[\int_0^t e^{(\sigma_p-\alpha_x)s}ds + \int_{-\infty}^0 e^{(\sigma_n-\alpha_x)s}ds\Big]\Bigg\}.$$

Briefly, simplifying from here gives

$$e^{-\sigma_p t}\|\mathcal{T}(\phi(t), y_0)\| \le \max\left\{ K_y e^{(\alpha_y-\sigma_p)t}y_0 + \frac{K_y\delta_y}{\sigma_p-\alpha_y}\|\phi\|_\sigma, \frac{K_z\delta_z}{\beta_z-\sigma_p}\|\phi\|_\sigma, \frac{K_x\delta_x}{\sigma_n-\alpha_x}\|\phi\|_\sigma\right\}.$$

We have by C1 that $\alpha_y < \sigma_p$ and thus $0 \le e^{(\alpha_y-\sigma_p)t} \le 1$ when $t \in [0,\infty)$, giving that each term is finite. Then,

$$\sup_{0\le t}\{e^{-\sigma_p t}\|\mathcal{T}(\phi(t), y_0)\|\} < \infty.$$

The proof for $t \le 0$ proceeds in the same fashion, giving us that

$$e^{-\sigma_n t}\|\mathcal{T}(\phi(t), y_0)\| \le \max\left\{ K_y e^{(\beta_y-\sigma_n)t}y_0 + \frac{K_y\delta_y}{\beta_y-\sigma_n}\|\phi\|_\sigma, \frac{K_z\delta_z}{\beta_z-\sigma_p}\|\phi\|_\sigma, \frac{K_x\delta_x}{\sigma_n-\alpha_x}\|\phi\|_\sigma\right\}.$$

Because $0 \le e^{(\beta_z-\sigma_n)t} \le 1$ when $t \in (-\infty, 0]$, each term is finite and we get that

$$\sup_{t\le 0}\{e^{-\sigma_n t}\|\mathcal{T}(\phi(t), y_0)\|\} < \infty.$$

Both cases together give us that that

$$\sup_{t\in\mathbb{R}} e^{-\sigma(t)t}\|\mathcal{T}(\phi(t), y_0)\| < \infty$$

and $\|\mathcal{T}(\phi, y_0)\|_\sigma < \infty$.

Next, we show that $\mathcal{T}(\phi(t), y_0)$ is continuous in t, or $\lim_{d\to t}(\mathcal{T}(\phi(t), y_0) - \mathcal{T}(\phi(d), y_0)) = 0$.

First, we calculate $\mathcal{T}(\phi(t), y_0) - \mathcal{T}(\phi(d), y_0)$:

$$\begin{aligned}\mathcal{T}(\phi(t), y_0) - \mathcal{T}(\phi(d), y_0) = (e^{tB} - e^{dB})y_0 + \int_0^t e^{(t-s)B}G(\phi(s))ds - \int_0^d e^{(d-s)B}G(\phi(s))ds \\ -\Big[\int_t^\infty e^{(t-s)C}H(\phi(s))ds - \int_d^\infty e^{(d-s)C}H(\phi(s))\Big] \\ + \int_{-\infty}^t e^{(t-s)A}F(\phi(s))ds - \int_{-\infty}^d e^{(d-s)A}F(\phi(s))ds.\end{aligned}$$

We split the proof into six cases: $t < 0$, $t > 0$, and $t = 0$ as $d \to t^+$ and $d \to t^-$. In each case, we assume that d starts in a small enough ball around t that it matches the sign of t. First, we consider $t > 0$ and take $d \to t^+$: $\mathcal{T}(\phi(t), y_0) - \mathcal{T}(\phi(d), y_0) =$

$$\begin{aligned}(e^{tB} - e^{dB})y_0 + \int_0^t (e^{(t-s)B} - e^{(d-s)B})G(\phi(s))ds - \int_t^d e^{(d-s)B}G(\phi(s))ds \\ -\Big[\int_t^d e^{(t-s)C}H(\phi(s))ds + \int_d^\infty (e^{(t-s)C} - e^{(d-s)C})H(\phi(s))\Big] \\ + \int_{-\infty}^t (e^{(t-s)A} - e^{(d-s)A})F(\phi(s))ds - \int_t^d e^{(d-s)A}F(\phi(s))ds\end{aligned}$$

$$\begin{aligned}= (e^{tB} - e^{dB})y_0 + \int_0^t [I - e^{(d-t)B}]e^{(t-s)B}G(\phi(s))ds - \int_t^d e^{(d-s)B}G(\phi(s))ds \\ -\Big[\int_t^d e^{(t-s)C}H(\phi(s))ds + \int_d^\infty [I - e^{(d-t)C}]e^{(t-s)C}H(\phi(s))ds\Big] \\ + \int_{-\infty}^t [I - e^{(d-t)A}]e^{(t-s)A}F(\phi(s))ds - \int_t^d e^{(d-s)A}F(\phi(s))ds\end{aligned}$$

$$\begin{aligned}(e^{tB} - e^{dB})y_0 + [I - e^{(d-t)B}]\int_0^t e^{(t-s)B}G(\phi(s))ds - \int_t^d e^{(d-s)B}G(\phi(s))ds \\ -\Big[\int_t^d e^{(t-s)C}H(\phi(s))ds + [I - e^{(d-t)C}]\int_d^\infty e^{(t-s)C}H(\phi(s))ds\Big] \\ +[I - e^{(d-t)A}]\int_{-\infty}^t e^{(t-s)A}F(\phi(s))ds - \int_t^d e^{(d-s)A}F(\phi(s))ds\end{aligned}$$

$$= \underbrace{(e^{tB} - e^{dB})y_0}_{\text{(I)}} - \underbrace{\sum_{n=1}^{\infty} \frac{((d-t)B)^n}{n!} \int_0^t e^{(t-s)B} G(\phi(s))ds}_{\text{(II)}} - \underbrace{\int_t^d e^{(d-s)B} G(\phi(s))ds}_{\text{(III)}}$$
$$- \Big[\underbrace{\int_t^d e^{(t-s)C} H(\phi(s))ds}_{\text{(IV)}} - \underbrace{\sum_{n=1}^{\infty} \frac{((d-t)C)^n}{n!} \int_d^{\infty} e^{(t-s)C} H(\phi(s))ds}_{\text{(V)}} \Big]$$
$$- \underbrace{\sum_{n=1}^{\infty} \frac{((d-t)A)^n}{n!} \int_{-\infty}^t e^{(t-s)A} F(\phi(s))ds}_{\text{(VI)}} - \underbrace{\int_t^d e^{(d-s)A} F(\phi(s))ds}_{\text{(VII)}}.$$

As $d \to t^+$, $e^{dB} \to e^{tB}$ and (I) will approach zero. In terms (III), (IV), and (VII), as $d \to t^+$ the bounds on the integrals contract and each integral approaches zero. In (II), the bounds on the integral are finite and thus the integral will remain bounded while $\sum_{n=1}^{\infty} \frac{((d-t)B)^n}{n!}$ will approach zero as $d \to t^+$, forcing the term to zero. The summation terms in (V) and (VI) will also converge to zero. The indefinite integrals are bounded by the boundedness of the norm of the $\mathcal{T}$ map established in the first part of the proof, and thus the terms (V) and (VI) will approach zero as $d \to t^+$ and the limit as $d \to t^+$ of this expression will be zero. The same reasoning applies to the future cases.

Next, consider $d \to t^-$ for $t > 0$: $\mathcal{T}(\phi(t), y_0) - \mathcal{T}(\phi(d), y_0) =$

$$(e^{tB} - e^{dB})y_0 + \int_d^t e^{(t-s)B} G(\phi(s))ds + \int_0^d (e^{(t-s)B} - e^{(d-s)B}) G(\phi(s))ds$$
$$- \Big[\int_t^{\infty} (e^{(t-s)C} - e^{(d-s)C}) H(\phi(s))ds - \int_d^t e^{(d-s)C} H(\phi(s)) \Big]$$
$$+ \int_{-\infty}^d (e^{(t-s)A} - e^{(d-s)A}) F(\phi(s))ds + \int_d^t e^{(d-s)A} F(\phi(s))ds$$

$$= (e^{tB} - e^{dB})y_0 + \int_d^t e^{(t-s)B} G(\phi(s))ds + [I - e^{(d-t)B}] \int_0^d e^{(t-s)B} G(\phi(s))ds$$
$$- \Big[[I - e^{(d-t)C}] \int_t^{\infty} e^{(t-s)C} H(\phi(s))ds - \int_d^t e^{(d-s)C} H(\phi(s)) \Big]$$
$$+ [I - e^{(d-t)A}] \int_{-\infty}^d e^{(t-s)A} F(\phi(s))ds + \int_d^t e^{(d-s)A} F(\phi(s))ds$$

$$= (e^{tB} - e^{dB})y_0 + \int_d^t e^{(t-s)B}G(\phi(s))ds + \sum_{n=1}^{\infty} \frac{((d-t)B)^n}{n!} \int_0^d e^{(t-s)B}G(\phi(s))ds$$
$$+ \sum_{n=1}^{\infty} \frac{((d-t)C)^n}{n!} \int_t^{\infty} e^{(t-s)C}H(\phi(s))ds - \int_d^t e^{(d-s)C}H(\phi(s))\Big]$$
$$+ \sum_{n=1}^{\infty} \frac{((d-t)A)^n}{n!} \int_{-\infty}^d e^{(t-s)A}F(\phi(s))ds + \int_d^t e^{(d-s)A}F(\phi(s))ds.$$

The limit of this expression as $d \to t^-$ is zero.

Next, we consider when $t < 0$ and $d \to t^+$: $\mathcal{T}(\phi(t), y_0) - \mathcal{T}(\phi(d), y_0) =$

$$(e^{tB} - e^{dB})y_0 + \int_0^d (e^{(t-s)B} - e^{(d-s)B})G(\phi(s))ds + \int_d^t e^{(t-s)B}G(\phi(s))ds$$
$$-\Big[\int_t^d e^{(t-s)C}H(\phi(s))ds + \int_d^{\infty} (e^{(t-s)C} - e^{(d-s)C})H(\phi(s))ds\Big]$$
$$+ \int_{-\infty}^t (e^{(t-s)A} - e^{(d-s)A})F(\phi(s))ds - \int_t^d e^{(d-s)A}F(\phi(s))ds$$

$$= (e^{tB} - e^{dB})y_0 + (I - e^{(d-t)B}) \int_0^d e^{(t-s)B}G(\phi(s))ds + \int_d^t e^{(t-s)B}G(\phi(s))ds$$
$$-\Big[\int_t^d e^{(t-s)C}H(\phi(s))ds + (I - e^{(d-t)C}) \int_d^{\infty} e^{(t-s)C}H(\phi(s))ds\Big]$$
$$+(I - e^{(d-t)A}) \int_{-\infty}^t e^{(t-s)A}F(\phi(s))ds - \int_t^d e^{(d-s)A}F(\phi(s))ds$$

$$= (e^{tB} - e^{dB})y_0 - \sum_{n=1}^{\infty} \frac{((d-t)B)^n}{n!} \int_0^d e^{(t-s)B}G(\phi(s))ds + \int_d^t e^{(t-s)B}G(\phi(s))ds$$
$$-\Big[\int_t^d e^{(t-s)C}H(\phi(s))ds - \sum_{n=1}^{\infty} \frac{((d-t)C)^n}{n!} \int_d^{\infty} e^{(t-s)C}H(\phi(s))ds\Big]$$
$$- \sum_{n=1}^{\infty} \frac{((d-t)A)^n}{n!} \int_{-\infty}^t e^{(t-s)A}F(\phi(s))ds - \int_t^d e^{(d-s)A}F(\phi(s))ds.$$

The limit of this expression as $d \to t^+$ is zero.

We consider when $t < 0$ and $d \to t^-$: $\mathcal{T}(\phi(t), y_0) - \mathcal{T}(\phi(d), y_0) =$

$$(e^{tB} - e^{dB})y_0 + \int_0^t (e^{(t-s)B} - e^{(d-s)B})G(\phi(s))ds - \int_t^d e^{(t-s)B}G(\phi(s))ds$$
$$-\Big[\int_t^\infty (e^{(t-s)C} - e^{(d-s)C})H(\phi(s))ds - \int_d^t e^{(t-s)C}H(\phi(s))ds\Big]$$
$$+\int_{-\infty}^d (e^{(t-s)A} - e^{(d-s)A})F(\phi(s))ds - \int_d^t e^{(d-s)A}F(\phi(s))ds$$

$$= (e^{tB} - e^{dB})y_0 + (I - e^{(d-t)B})\int_0^t e^{(t-s)B}G(\phi(s))ds - \int_t^d e^{(t-s)B}G(\phi(s))ds$$
$$-\Big[(I - e^{(d-t)C})\int_t^\infty e^{(t-s)C}H(\phi(s))ds - \int_d^t e^{(t-s)C}H(\phi(s))ds\Big]$$
$$+(I - e^{(d-t)A})\int_{-\infty}^d e^{(t-s)A}F(\phi(s))ds - \int_d^t e^{(d-s)A}F(\phi(s))ds$$

$$= (e^{tB} - e^{dB})y_0 - \sum_{n=1}^\infty \frac{((d-t)B)^n}{n!}\int_0^t e^{(t-s)B}G(\phi(s))ds - \int_t^d e^{(t-s)B}G(\phi(s))ds$$
$$-\Big[\sum_{n=1}^\infty \frac{((d-t)C)^n}{n!}\int_t^\infty e^{(t-s)C}H(\phi(s))ds - \int_d^t e^{(t-s)C}H(\phi(s))ds\Big]$$
$$-\sum_{n=1}^\infty \frac{((d-t)A)^n}{n!}\int_{-\infty}^d e^{(t-s)A}F(\phi(s))ds - \int_d^t e^{(d-s)A}F(\phi(s))ds.$$

The limit of this expression as $d \to t^-$ is zero.

Let $t = 0$ and consider $d \to 0^+$: $\mathcal{T}(\phi(0), y_0) - \mathcal{T}(\phi(d), y_0) =$

$$(1 - e^{dB})y_0 + \int_0^d e^{(d-s)B}G(\phi(s))ds - \Big[\int_0^d e^{-sC}H(\phi(s))ds + \int_d^\infty (e^{-sC} - e^{(d-s)C})H(\phi(s))ds\Big]$$
$$+\int_{-\infty}^0 (e^{-sA} - e^{(d-s)A})F(\phi(s))ds - \int_0^d e^{(d-s)A}F(\phi(s))ds$$

$$= (1 - e^{dB})y_0 + \int_0^d e^{(d-s)B}G(\phi(s))ds - \Big[\int_0^d e^{-sC}H(\phi(s))ds + (I - e^{dC})\int_0^\infty e^{-sC}H(\phi(s))ds\Big]$$
$$+(I - e^{dA})\int_{-\infty}^0 e^{-sA}F(\phi(s))ds - \int_0^d e^{(d-s)A}F(\phi(s))ds$$

$$= (1-e^{dB})y_0 + \int_0^d e^{(d-s)B}G(\phi(s))ds - \Big[\int_0^d e^{-sC}H(\phi(s))ds - \sum_{n=1}^{\infty}\frac{(dC)^n}{n!}\int_d^{\infty} e^{-sC}H(\phi(s))ds\Big]$$
$$- \sum_{n=1}^{\infty}\frac{(dA)^n}{n!}\int_{-\infty}^0 e^{-sA}F(\phi(s))ds - \int_0^d e^{(d-s)A}F(\phi(s))ds.$$

The limit of this expression as $d \to t^+$ is zero.

Consider as $d \to t^-$: $\mathcal{T}(\phi(t), y_0) - \mathcal{T}(\phi(d), y_0) =$

$$(1-e^{dB})y_0 - \int_0^d e^{(d-s)B}G(\phi(s))ds - \Big[\int_0^{\infty}(e^{-sC} - e^{(d-s)C})H(\phi(s))ds - \int_d^0 e^{(d-s)C}H(\phi(s))ds\Big]$$
$$+ \int_{-\infty}^d (e^{-sA} - e^{(d-s)A})F(\phi(s))ds - \int_d^0 e^{(d-s)A}F(\phi(s))ds$$

$$= (1-e^{dB})y_0 - \int_0^d e^{(d-s)B}G(\phi(s))ds - \Big[(I-e^{dC})\int_0^{\infty} e^{-sC}H(\phi(s))ds - \int_d^0 e^{-sC}H(\phi(s))ds\Big]$$
$$+(I-e^{dA})\int_{-\infty}^d e^{-sA}F(\phi(s))ds - \int_d^0 e^{(d-s)A}F(\phi(s))ds$$

$$= (1-e^{dB})y_0 - \int_0^d e^{(d-s)B}G(\phi(s))ds - \Big[\sum_{n=1}^{\infty}\frac{(dC)^n}{n!}\int_0^{\infty} e^{-sC}H(\phi(s))ds - \int_d^0 e^{-sC}H(\phi(s))ds\Big]$$
$$- \sum_{n=1}^{\infty}\frac{(dA)^n}{n!}\int_{-\infty}^d e^{-sA}F(\phi(s))ds - \int_d^0 e^{(d-s)A}F(\phi(s))ds.$$

The limit of this expression as $d \to t^-$ is zero and $\mathcal{T}$ is continuous in t. □

Now we show that the map is a contraction, meaning that as we iterate it, the distance between each successive iteration will shrink and the iterated map will converge to a fixed point. Proposition 2.1.2 is given in [19]. However, they omit a rigorous proof, which we show here. In this proof, we show each detail of the simplification of the approximation of the norm of $\mathcal{T}$. These details are referenced in later proofs as well.

Proposition 2.1.2. *Given assumptions A1, A2, A3, C1, and C2, the equation in* (1.9) *is a contraction mapping with Lipschitz constant* $\delta_\phi = \max\left\{\frac{K_y\delta_y}{\sigma_p-\alpha_y}, \frac{K_y\delta_y}{\beta_y-\sigma_n}, \frac{K_x\delta_x}{\sigma_n-\alpha_x}, \frac{K_z\delta_z}{\beta_z-\sigma_p}\right\}$.

Proof. Let ϕ_1, $\phi_2 \in \mathcal{F}_\sigma$ and denote $\mathcal{T}(\phi_1(t), y_0) := \mathcal{T}(\phi_1(t))$ for a fixed $y_0 \in Y$.

$$\mathcal{T}(\phi_1(t)) - \mathcal{T}(\phi_2(t)) = \int_0^t e^{(t-s)B}[G(\phi_1(s)) - G(\phi_2(s))]ds - \int_t^{\infty} e^{(t-s)C}[H(\phi_1(s)) - H(\phi_2(s))]ds$$
$$+ \int_{-\infty}^t e^{(t-s)A}[F(\phi_1(s)) - F(\phi_2(s))]ds.$$

Taking norms over the expression gives $\|\mathcal{T}(\phi_1(t)) - \mathcal{T}(\phi_2(t))\| \leq$

$$\max\Big\{\Big\|\int_0^t e^{(t-s)B}[G(\phi_1(s)) - G(\phi_2(s))]ds\Big\|, \Big\|\int_{-\infty}^t e^{(t-s)A}[F(\phi_1(s)) - F(\phi_2(s))]ds\Big\|, \Big\|\int_t^\infty e^{(t-s)C}[H(\phi_1(s)) - H(\phi_2(s))]ds\Big\|\Big\}$$

$$\leq \Big\{\int_0^t \|e^{(t-s)B}\|\|G(\phi_1(s)) - G(\phi_2(s))\|ds, \int_{-\infty}^t \|e^{(t-s)A}\|\|F(\phi_1(s)) - F(\phi_2(s))\|ds, \int_t^\infty \|e^{(t-s)C}\|\|H(\phi_1(s)) - H(\phi_2(s))\|ds\Big\}.$$

The interval $(-\infty, \infty)$ can be separated into $(-\infty, 0]\cup[0, \infty)$, where $t \in (-\infty, 0]$ or $t \in [0, \infty)$. The proof continues in two cases.

Case 1: Consider $t \in (-\infty, 0]$. In the X component, $s \in (-\infty, t]$, and $t - s \geq 0$ for all s in the interval. For the Y component, $s \in [t, 0]$ and $t - s \leq 0$. In the Z component, $s \in [t, \infty)$, and $t - s \leq 0$. Applying A1 and A2 gives

$$\|\mathcal{T}(\phi_1(t)) - \mathcal{T}(\phi_2(t))\| \leq \max\Big\{\int_t^0 K_y e^{\beta_y(t-s)}\delta_y\|\phi_1(s) - \phi_2(s)\|ds, \int_{-\infty}^t K_x e^{\alpha_x(t-s)}\delta_x\|\phi_1(s) - \phi_2(s)\|ds, \int_t^\infty K_z e^{\beta_z(t-s)}\delta_z\|\phi_1(s) - \phi_2(s)\|ds\Big\}.$$

In this case, $t \leq 0$ and we multiply through by $e^{-\sigma_n t}$. In the X and Y components, $s \leq 0$ because $t \leq 0$ and we multiply by one in the form $e^{\sigma_n s}e^{-\sigma_n s}$. The interval considered in the Z component is $[t, \infty)$, where $s \leq 0$ when $s \in [t, 0]$ and $s \geq 0$ when $s \in [0, \infty)$. Splitting the integral up according to these intervals gives

$$\int_t^\infty K_z e^{\beta_z(t-s)}\delta_z\|\phi_1(s) - \phi_2(s)\|ds = \int_t^0 K_z e^{\beta_z(t-s)}\delta_z\|\phi_1(s) - \phi_2(s)\|ds + \int_0^\infty K_z e^{\beta_z(t-s)}\delta_z\|\phi_1(s) - \phi_2(s)\|ds.$$

In the integral from t to zero, multiply by one in the form $e^{\sigma_n s}e^{-\sigma_n s}$. In the integral from zero to ∞, $s \geq 0$, multiply by one in the form $e^{\sigma_p s}e^{-\sigma_p s}$. Then,

$$e^{-\sigma_n t}\|\mathcal{T}(\phi_1(t)) - \mathcal{T}(\phi_2(t))\| \leq \max\Big\{K_y\delta_y e^{-\sigma_n t}\int_t^0 e^{\beta_y(t-s)}e^{\sigma_n s}e^{-\sigma_n s}\|\phi_1(s) - \phi_2(s)\|ds, K_x\delta_x e^{-\sigma_n t}\int_{-\infty}^t e^{\alpha_x(t-s)}e^{\sigma_n s}e^{-\sigma_n s}\|\phi_1(s) - \phi_2(s)\|ds, K_z\delta_z e^{-\sigma_n t}\Big(\int_t^0 e^{\beta_z(t-s)}e^{\sigma_n s}e^{-\sigma_n s}\|\phi_1(s) - \phi_2(s)\|ds + \int_0^\infty e^{\beta_z(t-s)}e^{\sigma_p s}e^{-\sigma_p s}\|\phi_1(s) - \phi_2(s)\|ds\Big)\Big\}.$$

Next, we take the supremum of the $e^{-\sigma_n s}\|\phi_1(s)-\phi_2(s)\|$ terms over the proper domain.

$$e^{-\sigma_n t}\|\mathcal{T}(\phi_1(t))-\mathcal{T}(\phi_2(t))\| \leq \max\Bigg\{K_y\delta_y e^{(\beta_y-\sigma_n)t}\int_t^0 e^{(\sigma_n-\beta_y)s}\sup_{s\in[t,0]} e^{-\sigma_n s}\|\phi_1(s)-\phi_2(s)\|ds,$$
$$K_x\delta_x e^{(\alpha_x-\sigma_n)t}\int_{-\infty}^t e^{(\sigma_n-\alpha_x)s}\sup_{s\in(-\infty,t]} e^{-\sigma_n s}\|\phi_1(s)-\phi_2(s)\|ds,$$
$$K_z\delta_z e^{(\beta_z-\sigma_n)t}\Big(\int_t^0 e^{(\sigma_n-\beta_z)s}\sup_{s\in[t,0]} e^{-\sigma_n s}\|\phi_1(s)-\phi_2(s)\|ds,$$
$$\int_0^\infty e^{(\sigma_p-\beta_z)s}\sup_{s\in[0,\infty)} e^{-\sigma_p s}\|\phi_1(s)-\phi_2(s)\|ds\Big)\Bigg\},$$

$$\leq \|\phi_1-\phi_2\|_\sigma \max\Bigg\{K_y\delta_y e^{(\beta_y-\sigma_n)t}\int_t^0 e^{(\sigma_n-\beta_y)s}e^{\sigma_n s}ds, K_x\delta_x e^{(\alpha_x-\sigma_n)t}\int_{-\infty}^t e^{(\sigma_n-\alpha_x)s}ds,$$
$$K_z\delta_z e^{(\beta_z-\sigma_n)t}\Big(\int_t^0 e^{(\sigma_n-\beta_z)s}ds+\int_0^\infty e^{(\sigma_p-\beta_z)s}ds\Big)\Bigg\}.$$

From here, we evaluate the integral expressions using classical methods.

$$e^{-\sigma_n t}\|\mathcal{T}(\phi_1(t))-\mathcal{T}(\phi_2(t))\| \leq \|\phi_1-\phi_2\|_\sigma \max\Bigg\{K_y\delta_y e^{(\beta_y-\sigma_n)t}\frac{1}{\sigma_n-\beta_y}(1-e^{(\sigma_n-\beta_y)t}),$$
$$K_x\delta_x e^{(\alpha_x-\sigma_n)t}\Big(\frac{1}{\sigma_n-\alpha_x}e^{(\sigma_n-\alpha_x)t}-\lim_{T\to-\infty}e^{(\sigma_n-\alpha_x)T}\Big),$$
$$K_z\delta_z e^{(\beta_z-\sigma_n)t}\Big[\frac{1}{\sigma_n-\beta_z}(1-e^{(\sigma_n-\beta_z)t})+\frac{1}{\sigma_p-\beta_z}\Big(\lim_{T\to\infty}e^{(\sigma_p-\beta_z)T}-1\Big)\Big]\Bigg\}.$$

Now, we know that $\sigma_n-\alpha_x>0$ and $\sigma_p-\beta_z<0$ by C1, and thus each limit evaluates to zero and we simplify the expressions further.

$$e^{-\sigma_n t}\|\mathcal{T}(\phi_1(t))-\mathcal{T}(\phi_2(t))\| \leq \max\Bigg\{\frac{K_y\delta_y}{\beta_y-\sigma_n}(1-e^{(\beta_y-\sigma_n)t}),\frac{K_x\delta_x}{\sigma_n-\alpha_x},$$
$$\frac{K_z\delta_z}{\beta_z-\sigma_p}e^{(\beta_z-\sigma_n)t}e^{(\sigma_n-\beta_z)t}\Bigg\}\|\phi_1-\phi_2\|_\sigma.$$

We want to make sure that the supremum of the left hand side stays bounded. We take the supremum over the given domain in each component as well.

$$\sup_{t\in(-\infty,0]} e^{-\sigma_n t}\|\mathcal{T}(\phi_1(t))-\mathcal{T}(\phi_2(t))\| \leq \max\Bigg\{\sup_{t\in(-\infty,0]}\frac{K_y\delta_y}{\beta_y-\sigma_n}(1-e^{(\beta_y-\sigma_n)t}),$$
$$\frac{K_x\delta_x}{\sigma_n-\alpha_x},\frac{K_z\delta_z}{\beta_z-\sigma_p}\Bigg\}\|\phi_1-\phi_2\|_\sigma.$$

Because $\beta_y-\sigma_n>0$ by C1, $e^{(\beta_y-\sigma_n)t}\leq 1$ for $t\in(-\infty,0]$, giving that $0\leq 1-e^{(\beta_y-\sigma_n)t}\leq 1$.

From this, we obtain three constants over the three components that bound the norm when $t \leq 0$.

$$\|\mathcal{T}(\phi_1) - \mathcal{T}(\phi_2)\|_\sigma \leq \max\left\{\frac{K_y\delta_y}{\beta_y - \sigma_n}, \frac{K_x\delta_x}{\sigma_n - \alpha_x}\frac{K_z\delta_z}{\beta_z - \sigma_p}\right\}\|\phi_1 - \phi_2\|_\sigma.$$

Case 2: Consider $t \in [0, \infty)$. In the X component, $s \in (-\infty, t]$ and $t - s \geq 0$. In the Z component, as $s \in [t, \infty)$ and $t - s \leq 0$. The trichotomy conditions on X and Z apply the same way as in the first case. For the Y component, as $s \in [0, t]$ and $t - s \geq 0$. The appropriate trichotomy condition is $\|e^{tB}\| \leq K_y e^{\alpha_y t}$. We have

$$\|\mathcal{T}(\phi_1(t)) - \mathcal{T}(\phi_2(t))\| \leq \max\Bigg\{\int_0^t K_y e^{\alpha_y(t-s)}\delta_y\|\phi_1(s) - \phi_2(s)\|ds,$$
$$\int_{-\infty}^t K_x e^{\alpha_x(t-s)}\delta_x\|\phi_1(s) - \phi_2(s)\|ds, \int_t^\infty K_z e^{\beta_z(t-s)}\delta_z\|\phi_1(s) - \phi_2(s)\|ds\Bigg\}.$$

Because $t \geq 0$, multiply through by $e^{-\sigma_p t}$. In the Y- and Z-components, we use $e^{-\sigma_p s}$ because $s \geq 0$ in each integral. In the X-component, the integral can be split up accordingly:

$$\int_{-\infty}^t K_x e^{\alpha_x(t-s)}\delta_x\|\phi_1(s) - \phi_2(s)\|ds = \int_{-\infty}^0 K_x e^{\alpha_x(t-s)}\delta_x\|\phi_1(s) - \phi_2(s)\|ds$$
$$+ \int_0^t K_x e^{\alpha_x(t-s)}\delta_x\|\phi_1(s) - \phi_2(s)\|ds, \qquad (2.1)$$

where $s \leq 0$ in the first integral and $s \geq 0$ in the second. Applying (2.1) this gives

$$e^{-\sigma_p t}\|\mathcal{T}(\phi_1(t)) - \mathcal{T}(\phi_2(t))\| \leq \max\Bigg\{K_y\delta_y e^{(\alpha_y - \sigma_p)t}\int_0^t e^{(\sigma_p - \alpha_y)s}e^{-\sigma_p s}\|\phi_1(s) - \phi_2(s)\|ds,$$
$$K_x\delta_x e^{(\alpha_y - \sigma_p)t}\Big[\int_{-\infty}^0 e^{(\sigma_n - \alpha_x)s}e^{-\sigma_n s}\|\phi_1(s) - \phi_2(s)\|ds + \int_0^t e^{(\sigma_p - \alpha_x)s}e^{-\sigma_p s}\|\phi_1(s) - \phi_2(s)\|ds\Big],$$
$$K_z\delta_z e^{(\beta_z - \sigma_p)t}\int_t^\infty e^{(\sigma_p - \beta_z)s}e^{-\sigma_p s}\|\phi_1(s) - \phi_2(s)\|ds\Bigg\},$$

$$\leq \max\Bigg\{K_y\delta_y e^{(\alpha_y - \sigma_p)t}\int_0^t e^{(\sigma_p - \alpha_y)s}\sup_{s\in[0,t]} e^{-\sigma_p s}\|\phi_1(s) - \phi_2(s)\|ds,$$
$$K_x\delta_x e^{(\alpha_y - \sigma_p)t}\Big[\int_{-\infty}^0 e^{(\sigma_n - \alpha_x)s}\sup_{s\in(-\infty,0]} e^{-\sigma_n s}\|\phi_1(s) - \phi_2(s)\|ds$$
$$+ \int_0^t e^{(\sigma_p - \alpha_x)s}\sup_{s\in[0,t]} e^{-\sigma_p s}\|\phi_1(s) - \phi_2(s)\|ds\Big],$$
$$K_z\delta_z e^{(\beta_z - \sigma_p)t}\int_t^\infty e^{(\sigma_p - \beta_z)s}\sup_{s\in[t,\infty)} e^{-\sigma_p s}\|\phi_1(s) - \phi_2(s)\|ds\Bigg\},$$

$$\leq \max\Bigg\{K_y\delta_y e^{(\alpha_y-\sigma_p)t}\int_0^t e^{(\sigma_p-\alpha_y)s}ds, K_x\delta_x e^{(\alpha_y-\sigma_p)t}\Big[\int_{-\infty}^0 e^{(\sigma_n-\alpha_x)s}ds+\int_0^t e^{(\sigma_p-\alpha_x)s}ds\Big],$$
$$K_z\delta_z e^{(\beta_z-\sigma_p)t}\int_t^\infty e^{(\sigma_p-\beta_z)s}ds\Bigg\}\|\phi_1-\phi_2\|_\sigma,$$

$$\leq \max\Bigg\{\frac{K_y\delta_y}{\sigma_p-\alpha_y}e^{(\alpha_y-\sigma_p)t}(e^{(\sigma_p-\alpha_y)t}-1), K_x\delta_x e^{(\alpha_y-\sigma_p)t}\Big[\frac{1}{\sigma_n-\alpha_x}+\frac{1}{\sigma_p-\alpha_x}(e^{(\sigma_p-\alpha_x)t}-1)\Big],$$
$$\frac{K_z\delta_z}{\beta_z-\sigma_p}e^{(\beta_z-\sigma_p)t}e^{(\sigma_p-\beta_z)t}\Bigg\}\|\phi_1-\phi_2\|_\sigma,$$

$$\sup_{t\in[0,\infty)} e^{-\sigma_p t}\|\mathcal{T}(\phi_1(t))-\mathcal{T}(\phi_2(t))\| \leq \max\Bigg\{\frac{K_y\delta_y}{\sigma_p-\alpha_y}\sup_{t\in[0,\infty)}(1-e^{(\alpha_y-\sigma_p)t}),$$
$$K_x\delta_x\sup_{t\in[0,\infty)}\Big[\frac{e^{(\alpha_y-\sigma_p)t}}{\sigma_n-\alpha_x}+\frac{e^{(\alpha_y-\sigma_p)t}-1}{\alpha_x-\sigma_p}\Big], \frac{K_z\delta_z}{\beta_z-\sigma_p}\Bigg\}\|\phi_1-\phi_2\|_\sigma,$$

$$\|\mathcal{T}(\phi_1)-\mathcal{T}(\phi_2)\|_\sigma \leq \max\left\{\frac{K_y\delta_y}{\sigma_p-\alpha_y}, \frac{K_x\delta_x}{\sigma_n-\alpha_x}, \frac{K_z\delta_z}{\beta_z-\sigma_p}\right\}\|\phi_1-\phi_2\|_\sigma.$$

Finally, we have that for all $t\in\mathbb{R}$,

$$\|\mathcal{T}(\phi_1)-\mathcal{T}(\phi_2)\|_\sigma \leq \max\left\{\frac{K_y\delta_y}{\sigma_p-\alpha_y}, \frac{K_y\delta_y}{\beta_y-\sigma_n}, \frac{K_x\delta_x}{\sigma_n-\alpha_x}, \frac{K_z\delta_z}{\beta_z-\sigma_p}\right\}\|\phi_1-\phi_2\|_\sigma.$$

From the conditions $\alpha_x+K_x\delta_x<\sigma_n<\beta_y-K_y\delta_y$ and $\alpha_y+K_y\delta_y<\sigma_p<\beta_z-K_z\delta_z$, we have $K_x\delta_x<\sigma_n-\alpha_x$ and $K_y\delta_y<\beta_y-\sigma_n$ as well as $K_y\delta_y<\sigma_p-\alpha_y$ and $K_z\delta_z<\beta_z-\sigma_p$. Therefore, $\delta_\phi := \max\left\{\frac{K_y\delta_y}{\sigma_p-\alpha_y}, \frac{K_y\delta_y}{\beta_y-\sigma_n}, \frac{K_x\delta_x}{\sigma_n-\alpha_x}, \frac{K_z\delta_z}{\beta_z-\sigma_p}\right\}<1$ and $\mathcal{T}(\cdot,y_0)$ is a contraction mapping in $\mathcal{F}_\sigma$. □

By the contraction mapping principle [2], there exists a unique $\phi^*\in\mathcal{F}_\sigma$ such that $\phi^*(t,y_0)=\mathcal{T}(\phi^*(t),y_0)$. Now we show that the ϕ^* is a unique solution in $\mathcal{F}_\sigma$ to the original system.

Proposition 2.1.3. *The fixed point of $\mathcal{T}(\cdot,y_0)$, denoted by $\phi^*(t,y_0)$, is characterized as the unique element in the function space that is the solution to* (1.7) *with initial condition $\phi(0,y_0)$, and satisfies the boundary value problem*

$$\begin{aligned}\dot{x}&=Ax+F(x,y,z) \quad x(-\infty)=0\\ \dot{y}&=By+G(x,y,z) \quad y(0)=y_0\\ \dot{z}&=Cz+H(x,y,z) \quad z(\infty)=0.\end{aligned} \tag{2.2}$$

Proof. We show that $\phi^*(t,y_0)$ is a solution to the system, which we do by taking derivatives

with respect to t:

$$\dot{x} = F(x,y,z) + A\int_{-\infty}^{t} e^{(t-s)A}F(\phi(s))ds$$
$$\dot{y} = G(x,y,z) + Be^{tB}y_0 + B\int_{0}^{t} e^{(t-s)B}G(\phi(s))ds$$
$$\dot{z} = H(x,y,z) - C\int_{t}^{\infty} e^{(t-s)C}H(\phi(s))ds$$

From the map, $x = \int_{-\infty}^{t} e^{(t-s)A}F(\phi(s))ds$, $y = e^{tB}y_0 + \int_0^t e^{(t-s)B}G(\phi(s))ds$, and $z = -\int_t^{\infty} e^{(t-s)C}H(\phi(s))ds$. Substituting in yields the system in (1.7) with the initial condition, which is unique given the choice of ϕ^*.

To show the second part of the proposition, simply note that for the X component of the $\mathcal{T}$ map, plugging in $t = -\infty$ yields zero, in the Y component of the $\mathcal{T}$ map, plugging in $t = 0$ yields y_0, and for the Z component, plugging in $t = \infty$ yields zero. So, we have the boundary conditions. □

Definition 2.1.4. (Center Manifold) The center manifold is

$$\mathcal{M}_c := \{u_0 \in E : u(t,u_0) \in \mathcal{F}_\sigma\}.$$

We first show the invariance of the center manifold.

Proposition 2.1.5. *$\mathcal{M}_c$ is invariant: if $u_0 \in \mathcal{M}_c$, then $u(t_0,u_0) \in \mathcal{M}_c$ for fixed t_0.*

Proof. Take $u_0 \in \mathcal{M}_c$ such that $u(t,u_0) \in \mathcal{F}_\sigma$. Fix t_0. We need that $u_1 := u(t_0,u_0) \in \mathcal{M}_c$. Since $\mathcal{M}_c = \{u_0 \in E : u(t,u_0) \in \mathcal{F}_\sigma\}$, it remains to show that $u(t,u_1) \in \mathcal{F}_\sigma$. Then, by the fact that u is autonomous, $u(t,u_1) = u(t,u(t_0,u_0)) = u(t+t_0,u_0) \in \mathcal{F}_\sigma$. □

Next, Φ is a map defined such that $\Phi : Y \to X \times Z$ by $\Phi(y_0) = \phi(0,y_0)|_{X\times Z}$. We show the following set equivalence.

Proposition 2.1.6. *Given Given A1, A2, A3, C1, and C2, we have*

$$\begin{aligned}\mathcal{M}_c &= \{u_0 : \Phi(y_0) = x_0 + z_0\}, \text{ or}\\ &= \text{graph}\Phi.\end{aligned}$$

Proof. This is a direct result of Proposition 2.1.3. □

We study the center manifold in terms of the fixed point of the $\mathcal{T}$ map. In the next proof, we use the following inequality attributed to Gronwall, a proof of which is found in [13]:

Lemma 2.1.7 (Gronwall's Inequality)**.** *If $u(t) \le p(t) + \int_{t_0}^{t} q(s)u(s)ds$ for functions $u, p,$ and q such that u and q are continuous and p is non-decreasing, then*

$$u(t) \le p(t)\exp\left(\int_{t_0}^{t} q(s)ds\right). \tag{2.3}$$

Proposition 2.1.8. *Given A1, A2 and C1, fix y_1 and $y_2 \in Y$. Then, $\mathcal{M}_c$ is Lipschitz continuous with real Lipschitz constant δ_Φ:*

$$\|\Phi(y_1) - \Phi(y_1)\| \leq \delta_\Phi \|y_1 - y_2\|.$$

Proof. Let $\phi_1^*(t) = T(\phi_1^*(t), y_1)$ and $\phi_2^*(t) = T(\phi_2^*(t), y_2)$ and note that by Proposition 2.1.6

$$\begin{aligned}\|\Phi(y_1) - \Phi(y_2)\| &= \|\phi_1^*(0)|_{X\times Z} - \phi_2^*(0)|_{X\times Z}\| \\ &\leq \|\phi_1^* - \phi_2^*\|_\sigma.\end{aligned}$$

This implies that we get a bound for $\|\Phi(y_1)-\Phi(y_2)\|$ if we bound $\|\phi_1^*-\phi_2^*\|_\sigma$. We calculate the difference using the equivalence to the $\mathcal{T}$ map:

$$\begin{aligned}\phi_1^*(t) - \phi_2^*(t) = e^{tB}(y_1 - y_2) + \int_0^t e^{(t-s)B}[G(\phi_1^*(s)) - G(\phi_2^*(s))]ds \\ - \int_t^\infty e^{(t-s)C}[H(\phi_1^*(s)) - H(\phi_2^*(s))]ds + \int_{-\infty}^t e^{(t-s)A}[F(\phi_1^*(s)) - F(\phi_2^*(s))]ds.\end{aligned}$$

As a first-pass estimation, we use the calculations from Proposition 2.1.2, to show that when $t \leq 0$:

$$\|\phi_1^* - \phi_2^*\|_\sigma \leq \sup_{t\in(-\infty,0]}(e^{(\beta_y-\sigma_n)t}\|y_1 - y_2\|) + \max\left\{\frac{K_x\delta_x}{\sigma_n - \alpha_x}, \frac{K_y\delta_y}{\beta_y - \sigma_n}, \frac{K_z\delta_z}{\beta_z - \sigma_p}\right\}\|\phi_1^* - \phi_2^*\|_\sigma$$

and when $t \geq 0$:

$$\|\phi_1^* - \phi_2^*\|_\sigma \leq \sup_{t\in(-\infty,0]}(e^{(\alpha_y-\sigma_p)t}\|y_1 - y_2\|) + \max\left\{\frac{K_x\delta_x}{\sigma_n - \alpha_x}, \frac{K_y\delta_y}{\sigma_p - \alpha_y}, \frac{K_z\delta_z}{\beta_z - \sigma_p}\right\}\|\phi_1^* - \phi_2^*\|_\sigma.$$

We have that $\delta_\phi = \max\left\{\frac{K_x\delta_x}{\sigma_n-\alpha_x}, \frac{K_y\delta_y}{\beta_y-\sigma_n}, \frac{K_y\delta_y}{\sigma_p-\alpha_y}, \frac{K_z\delta_z}{\beta_z-\sigma_p}\right\} < 1$ by Proposition 2.1.2. Because $\beta_y - \sigma_n > 0$ and $\alpha_y - \sigma_p < 0$, both $\|y_1 - y_2\|$ terms reach a supremum at $t = 0$, and each expression simplifies down to $\|\phi_1^* - \phi_2^*\|_\sigma \leq \|y_1 - y_2\| + \delta_\phi\|\phi_1^* - \phi_2^*\|_\sigma$ and

$$\|\Phi(y_1) - \Phi(y_2)\| \leq \|\phi_1^* - \phi_2^*\|_\sigma \leq \frac{1}{1-\delta_\phi}\|y_1 - y_2\|.$$

where $\delta_\Phi = \frac{1}{1-\delta_\phi}$.

However, this is unsatisfactory because as $\delta_\phi \to 1$, $\delta_\Phi \to \infty$ and we obtain a better approximation using a slightly different method. The norm $\|\phi_1^*(t) - \phi_2^*(t)\|$ is taken as the

maximum over each component. First notice that

$$\|\phi_1^*(t)-\phi_2^*(t)\| = \max\Big\{\Big\|e^{tB}(y_1-y_2)+\int_0^t e^{(t-s)B}[G(\phi_1^*(s))-G(\phi_2^*(s))]ds\Big\|,$$
$$\Big\|\int_t^\infty e^{(t-s)C}[H(\phi_1^*(s))-H(\phi_2^*(s))]ds\Big\|,\Big\|\int_{-\infty}^t e^{(t-s)A}[F(\phi_1^*(s))-F(\phi_2^*(s))]ds\Big\|\Big\},$$

$$\le \max\Big\{\|e^{tB}(y_1-y_2)\|+\Big\|\int_0^t e^{(t-s)B}[G(\phi_1^*(s))-G(\phi_2^*(s))]ds\Big\|,$$
$$\|e^{tB}(y_1-y_2)\|+\Big\|\int_t^\infty e^{(t-s)C}[H(\phi_1^*(s))-H(\phi_2^*(s))]ds\Big\|,$$
$$\|e^{tB}(y_1-y_2)\|+\Big\|\int_{-\infty}^t e^{(t-s)A}[F(\phi_1^*(s))-F(\phi_2^*(s))]ds\Big\|\Big\}.$$

$$\|\phi_1^*(t)-\phi_2^*(t)\| \le \max\Big\{\|e^{tB}\|\|y_1-y_2\|+\delta_y\int_0^t\|e^{(t-s)B}\|\|\phi_1^*(s)-\phi_1^*(s)\|ds,$$
$$\|e^{tB}\|\|y_1-y_2\|+\delta_z\int_t^\infty\|e^{(t-s)C}\|\|\phi_1^*(s)-\phi_2^*(s)\|ds,$$
$$\|e^{tB}\|\|y_1-y_2\|+\delta_x\int_{-\infty}^t\|e^{(t-s)A}\|\|\phi_1^*(s)-\phi_2^*(s)\|ds\Big\},$$

$$e^{-\sigma t}\|\phi_1^*(t)-\phi_2^*(t)\| \le \max\Big\{e^{-\sigma t}\|e^{Bt}\|\|y_1-y_2\|+\delta_y e^{-\sigma t}\int_0^t\|e^{(t-s)B}\|e^{\sigma s}e^{-\sigma s}\|\phi_1^*(s)-\phi_2^*(s)\|ds,$$
$$e^{-\sigma t}\|e^{Bt}\|\|y_1-y_2\|+\delta_z e^{-\sigma t}\int_t^\infty\|e^{(t-s)C}\|e^{\sigma s}e^{-\sigma s}\|\phi_1^*(s)-\phi_2^*(s)\|ds$$
$$e^{-\sigma t}\|e^{Bt}\|\|y_1-y_2\|+\delta_x e^{-\sigma t}\int_{-\infty}^t\|e^{(t-s)A}\|e^{\sigma s}e^{-\sigma s}\|\phi_1^*(s)-\phi_2^*(s)\|ds\Big\}.$$

We use the Gronwall inequality as in Lemma 2.3 in each component to get

$$e^{-\sigma t}\|\phi_1^*(t)-\phi_2^*(t)\| \le \max\Big\{e^{-\sigma t}\|e^{Bt}\|\|y_1-y_2\|\exp(\delta_y e^{-\sigma t}\int_0^t\|e^{(t-s)B}\|e^{\sigma s}ds),$$
$$e^{-\sigma t}\|e^{Bt}\|\|y_1-y_2\|\exp(\delta_z e^{-\sigma t}\int_t^\infty\|e^{(t-s)C}\|e^{\sigma s}ds)$$
$$e^{-\sigma t}\|e^{Bt}\|\|y_1-y_2\|\exp(\delta_x e^{-\sigma t}\int_{-\infty}^t\|e^{(t-s)A}\|e^{\sigma s}ds)\Big\}.$$

Now consider the case that $t \leq 0$:

$$e^{-\sigma_n t}\|\phi_1^*(t) - \phi_2^*(t)\| \leq \max\Big\{ K_y e^{(\beta_y-\sigma_n)t}\|y_1 - y_2\| \exp(K_y\delta_y e^{(\beta_y-\sigma_n)t}\int_0^t e^{(\sigma_n-\beta_y)s}ds),$$
$$K_y e^{(\beta_y-\sigma_n)t}\|y_1 - y_2\| \exp(K_z\delta_z e^{(\beta_z-\sigma_n)t}\Big[\int_t^0 e^{(\sigma_n-\beta_z)s}ds + \int_0^\infty e^{(\sigma_p-\beta_z)s}ds\Big])$$
$$K_y e^{(\beta_y-\sigma_n)t}\|y_1 - y_2\| \exp(K_x\delta_x e^{(\alpha_x-\sigma_n)t}\int_{-\infty}^t e^{(\sigma_n-\alpha_x)s}ds)\Big\}$$

which, using the same arguments as in Proposition 2.1.2, simplifies to

$$\|\phi_1^* - \phi_2^*\|_\sigma \leq K_y \max\left\{e^{\frac{K_x\delta_x}{\sigma_n-\alpha_x}}, e^{\frac{K_y\delta_y}{\beta_y-\sigma_n}}, e^{\frac{K_z\delta_z}{\beta_z-\sigma_p}}\right\}\|y_1 - y_2\|.$$

When $t \geq 0$:

$$e^{-\sigma_p t}\|\phi_1^*(t) - \phi_2^*(t)\| \leq \max\Big\{ K_y e^{(\beta_y-\sigma_p)t}\|y_1 - y_2\| \exp(K_y\delta_y e^{(\beta_y-\sigma_p)t}\int_0^t e^{(\sigma_p-\beta_y)s}ds),$$
$$K_y e^{(\beta_y-\sigma_p)t}\|y_1 - y_2\| \exp(K_z\delta_z e^{(\beta_z-\sigma_p)t}\int_t^\infty e^{(\sigma_p-\beta_z)s}ds)$$
$$K_y e^{(\beta_y-\sigma_p)t}\|y_1 - y_2\| \exp(K_x\delta_x e^{(\alpha_x-\sigma_p)t}\Big[\int_{-\infty}^0 e^{(\sigma_n-\alpha_x)s}ds + \int_0^t e^{(\sigma_p-\alpha_x)s}ds)\Big])\Big\}$$

and this simplifies to $\|\phi_1^* - \phi_2^*\|_\sigma \leq K_y \max\left\{e^{\frac{K_z\delta_x}{\sigma_n-\alpha_x}}, e^{\frac{K_y\delta_y}{\sigma_p-\alpha_y}}, e^{\frac{K_z\delta_z}{\beta_z-\sigma_p}}\right\}\|y_1 - y_2\|$.

Finally, we have that $\|\Phi_1 - \Phi_2\| \leq \delta_\Phi\|y_1 - y_2\|$ for all $t \in \mathbb{R}$ where

$$\delta_\Phi = K_y \max\left\{e^{\frac{K_x\delta_x}{\sigma_n-\alpha_x}}, e^{\frac{K_y\delta_y}{\beta_y-\sigma_n}}, e^{\frac{K_y\delta_y}{\sigma_p-\alpha_y}}, e^{\frac{K_z\delta_z}{\beta_z-\sigma_p}}\right\} = K_y e^{\delta_\phi}.$$

Because each exponent exists in the interval $[0, 1)$, $K_y \leq \delta_\Phi < K_y e$.

□

Now that we have that the manifold is Lipschitz, we have completed the final step in proving the following theorem:

Theorem 2.1.9. *Given Given A1, A2, A3, C1, and C2 there exists a unique Lipschitz map* $\Phi : Y \to X \times Z$ *such that graph*(Φ) *is the center manifold of* (1.7).

2.2 Regularity of the Manifold

The next step is to study the differentiability of the manifold. We add an additional assumption:

A4. Nonlinear Terms are $\mathcal{C}^1$: $F(x, y, z) \in \mathcal{C}^1(E, X)$, $G(x, y, z) \in \mathcal{C}^1(E, Y)$, and $H(x, y, z) \in \mathcal{C}^1(E, Z)$.

In other words, we assume that the derivatives of the nonlinear terms exist and are continuous. With A2 and the following theorem from [10] we have that the norm of the derivative of each nonlinear term is uniformly bounded.

Theorem 2.2.1 (Rademacher's Theorem)**.** *Given A2 and A4, the nonlinear terms are bounded such that*

$$\begin{aligned} \|DF(x,y,z)\| &\leq \delta_x \\ \|DG(x,y,z)\| &\leq \delta_y \\ \|DH(x,y,z)\| &\leq \delta_z. \end{aligned} \tag{2.4}$$

We know from Section 2.1 that for a fixed initial condition y_0 we find $\phi^*(t,y_0) = \mathcal{T}(\phi^*(t),y_0)$. Define $\phi_0(t) := \phi^*(t,y_0)$. For the most part, we drop the star notation in this section because all such ϕ that we refer to will be the fixed point of iterating the $\mathcal{T}$ map given an initial condition. We are studying the derivative of the ϕ map. To this end, define the space $\mathcal{F}_{1,\sigma}$:

$$\mathcal{F}_{1,\sigma} = \left\{\Delta \in C(\mathbb{R}\times Y, \mathcal{L}(Y,E)) : \sup_{t\in\mathbb{R}} e^{-\sigma(t)}\|\Delta(t)\|_{\mathcal{L}(Y,E)} = \|\Delta\|_{1,\sigma} < \infty\right\}$$

where $\sigma(t)$ is defined as before in (1.8).

The map $\phi_0(t)$ is written in terms of the $\mathcal{T}$ map:

$$\begin{aligned} \phi_0(t) = e^{tB}y_0 + \int_0^t e^{(t-s)B}G(\phi_0(s))ds - \int_t^\infty e^{(t-s)C}H(\phi_0(s))ds \\ + \int_{-\infty}^t e^{(t-s)A}F(\phi_0(s))ds. \end{aligned}$$

We differentiate with respect to y to get $\mathcal{T}_1 : \mathcal{F}_{1,\sigma}\times Y \to \mathcal{F}_{1,\sigma}$ such that

$$\begin{aligned} \mathcal{T}_1(\Delta(t),y_0) = \underbrace{e^{tB} + \int_0^t e^{(t-s)B}DG(\phi_0(s))\Delta(s)ds}_{Y} - \underbrace{\int_{-\infty}^t e^{(t-s)C}DH(\phi_0(s))\Delta(s)ds}_{Z} \\ + \underbrace{\int_t^\infty e^{(t-s)A}DF(\phi_0(s))\Delta(s)ds}_{X}. \end{aligned} \tag{2.5}$$

We will use this to study the map $D\Phi$ whose graph is the derivative of the manifold. Note that in the X component, $\int_t^\infty e^{(t-s)A}DF(\phi_0(s))\Delta(s)ds$ where $e^{(t-s)A}_{X\times X}$, $DF(\phi_0(s))_{X\times E}$, $\Delta(s)_{E\times Y}$. So $e^{(t-s)A}DF(\phi_0(s))\Delta(s)$ is of dimension $X\times Y$. We go through similar analyses for the other two components to get that $\mathcal{T}_1(\Delta(t),y_0)$ is of dimension $E\times Y$.

In this section, we will show that the map $\Phi \in \mathcal{C}^1(Y, X\times Z)$. As in the previous section, we first need to show that the $\mathcal{T}_1$ map is well-defined. This proof is similar to the proof for $\mathcal{T}$ and thus we leave out several details.

Proposition 2.2.2. *Given A1, A2, C1, and* (2.4)*, $\mathcal{T}_1(\Delta(t),y_0)$ is well-defined.*

Proof. First, we show $\mathcal{T}_1 : \mathcal{F}_{1,\sigma}\times Y \to \mathcal{F}_{1,\sigma}$ by showing that $\|\mathcal{T}_1(\Delta,y_0)\|_{1,\sigma} < \infty$ for any

$\Delta \in \mathcal{F}_{1,\sigma}$ and $y_0 \in Y$. When $t \leq 0$,

$$e^{-\sigma_n t}\|\mathcal{T}_1(\Delta(t), y_0)\| \leq \max\Bigg\{K_y e^{(\beta_y-\sigma_n)t} + K_y\delta_y e^{(\beta_y-\sigma_n)t}\int_0^t e^{(\sigma_n-\beta_y)s}e^{\sigma_n s}\|\Delta(s)\|ds,$$
$$K_z\delta_z e^{(\beta_z-\sigma_n)t}\Big[\int_t^0 e^{(\sigma_n-\beta_z)s}e^{\sigma_n s}\|\Delta(s)\|ds + \int_0^\infty e^{(\sigma_p-\beta_z)s}e^{-\sigma_p s}\|\Delta(s)\|ds\Big], \quad (2.6)$$
$$K_x\delta_x e^{(\alpha_x-\sigma_n)t}\int_{-\infty}^t e^{(\sigma_n-\alpha_x)s}e^{-\sigma_n s}\|\Delta(s)\|ds\Bigg\}.$$

We see that, based on the steps from Proposition 2.1.2, (2.6) will simplify down to a set of constants less than infinity.

Showing that $\mathcal{T}_1(\Delta(t), y_0)$ is continuous in t follows the same steps as in Proposition 2.1.1. □

The next step is to show that $\mathcal{T}_1(\cdot, y_0)$ is a contraction mapping. This proof is also very similar to the proof for the $\mathcal{T}$ map.

Proposition 2.2.3. *Given Given A1, A2, A3, C1, C2, and* (2.4)*, $\mathcal{T}_1(\Delta(t), y_0)$ is a contraction mapping with rate δ_ϕ.*

Proof. Take the difference $\mathcal{T}_1(\Delta_1(t), y_0) - \mathcal{T}_1(\Delta_2(t), y_0)$:

$$\begin{aligned}\mathcal{T}_1(\Delta_1(t), y_0) - \mathcal{T}_1(\Delta_2(t), y_0) = &\int_0^t e^{(t-s)B}DG(\phi_0(s))(\Delta_1(s) - \Delta_2(s))ds\\ &- \int_{-\infty}^t e^{(t-s)C}DH(\phi_0(s))(\Delta_1(s) - \Delta_2(s))ds\\ &+ \int_t^\infty e^{(t-s)A}DF(\phi_0(s))(\Delta_1(s) - \Delta_2(s))ds\end{aligned}$$

where Δ_1, Δ_2 are arbitrary functions in $\mathcal{F}_{1,\sigma}$. Then, we take norms and apply A1 and A2 in the case that $t \leq 0$:

$$\begin{aligned}\|\mathcal{T}_1(\Delta_1(t), y_0) - \mathcal{T}_1(\Delta_2(t), y_0)\| \leq \max\Bigg\{ &\int_0^t K_y e^{(t-s)\beta_y}\delta_y\|\Delta_1(s) - \Delta_2(s)\|ds,\\ &\int_{-\infty}^t K_z e^{(t-s)\beta_z}\delta_z\|\Delta_1(s) - \Delta_2(s)\|ds,\\ &\int_t^\infty K_x e^{(t-s)\alpha_y}\delta_x\|\Delta_1(s) - \Delta_2(s)\|ds\Bigg\}.\end{aligned}$$

$$e^{-\sigma_n s}\|\mathcal{T}_1(\Delta_1(t),y_0)-\mathcal{T}_1(\Delta_2(t),y_0)\| \le \max\Big\{ K_y\delta_y e^{(\beta_y-\sigma_n)t}\int_0^t e^{(\sigma_n-\beta_y)s}e^{-\sigma_n s}\|\Delta_1(s)-\Delta_2(s)\|ds$$
$$-K_z\delta_z e^{(\beta_z-\sigma_n)t}\int_{-\infty}^t e^{(\sigma_n-\beta_z)s}e^{-\sigma_n s}\|\Delta_1(s)-\Delta_2(s)\|ds$$
$$+K_x\delta_x e^{(\alpha_y-\sigma_n)t}\Big[\int_t^0 e^{(\sigma_n-\alpha_y)s}e^{-\sigma_n s}\|\Delta_1(s)-\Delta_2(s)\|ds$$
$$+\int_0^\infty e^{(\sigma_p-\alpha_y)s}e^{-\sigma_p s}\|\Delta_1(s)-\Delta_2(s)\|ds\Big]\Big\}.$$

The proof proceeds in the same way as in Proposition 2.1.2.

□

Let $\Delta^*(t)=\mathcal{T}_1(\Delta^*(t),y_0)$ be the fixed point of the $\mathcal{T}_1$ map given y_0. Before we proceed we need the following lemma.

Lemma 2.2.4. *Given A1, A2, A3, C1, C2, then let $\phi_1(t):=\phi^*(t,y_1)$ and $\phi_2(t):=\phi^*(t,y_2)$. We have the following bound on $\|\phi_1(t)-\phi_2(t)\|$:*

$$\|\phi_1(t)-\phi_2(t)\| \le \begin{cases} K_y e e^{(K_y\delta_y+\alpha_y)t}\|y_1-y_2\| & \text{when } t\ge 0 \\ K_y e e^{(\beta_y-K_y\delta_y)t}\|y_1-y_2\| & \text{when } t\le 0. \end{cases}$$

Proof. From Proposition 2.1.8, we have that

$$\|\phi_1(t)-\phi_2(t)\|e^{-\sigma_n t}\le \delta_\Phi\|y_1-y_2\|$$

where

$$\delta_\Phi = K_y\max\left\{e^{\frac{K_x\delta_x}{\sigma_n-\alpha_x}}, e^{\frac{K_y\delta_y}{\beta_y-\sigma_n}}, e^{\frac{K_z\delta_z}{\beta_z-\sigma_p}}\right\} < K_y e$$

in the case that $t\le 0$. So

$$\|\phi_1(t)-\phi_2(t)\|\le K_y e e^{\sigma_n t}\|y_1-y_2\|.$$

From C2 on σ_n, we have that $\alpha_x+K_x\delta_x<\sigma_n<\beta_y-K_y\delta_y$. If we multiply through by $t\le 0$, we get that $(\beta_y-K_y\delta_y)t<\sigma_n t<(\alpha_x+K_x\delta_x)t$. We get the most precise bound on $\|\phi(t,y_1)-\phi(t,y_2)\|$ by letting $\sigma_n\to\beta_y-K_y\delta_y$. When $t\le 0$,

$$\|\phi_1(t)-\phi_2(t)\|\le K_y e e^{(\beta_y-K_y\delta_y)t}\|y_1-y_2\|.$$

When $t\ge 0$,

$$\|\phi_1(t)-\phi_2(t)\|e^{-\sigma_p t}\le \delta_\Phi\|y_1-y_2\|$$

and

$$\|\phi_1(t)-\phi_2(t)\|\le \delta_\Phi e^{\sigma_p t}\|y_1-y_2\|.$$

As before, from C2, we get that $(\alpha_y+K_y\delta_y)t<\sigma_p t<(\beta_z-K_z\delta_z)t$. Taking $\sigma_p\to(\alpha_y+K_y\delta_y)$ gives that

$$\|\phi_1(t)-\phi_2(t)\|\le K_y e e^{(K_y\delta_y+\alpha_y)t}\|y_1-y_2\|.$$

□

We show next that $\Delta^* = \partial\phi_0/\partial y$. This follows a similar idea to the proof presented in [7].

Proposition 2.2.5. *Given A1, A2, A3, C1, C2, and* (2.4)*, we have that* $\partial\phi(y_0)/\partial y = \Delta^*$*, where* $\Delta^*(t) := \mathcal{T}_1(\Delta^*(t), y_0)$ *and* $\phi^*(t, y_0) = \mathcal{T}(\phi^*(t), y_0)$ *for a given* $y_0 \in Y$*.*

Proof. For clarity of notation in this proof, we write out $\phi^*(t, y_0)$. To get that $\partial\phi_0/\partial y = \Delta^*$, we use the representation of $\phi^*(t, y_0)$ as a fixed point of the $\mathcal{T}$ map and differentiate with respect to y using Fréchet differentiation because we are in a Banach space.

$\Delta^*(t) \in \mathcal{C}(\mathbb{R} \times Y, \mathcal{L}(Y, E))$ and therefore is bounded and linear in Y. Then, if

$$\lim_{h\to 0} \frac{\|\phi^*(y_0 + h) - \phi^*(y_0) - \Delta^* h\|_\sigma}{\|h\|} = 0 \tag{2.7}$$

where $h \in Y$, we have that $\phi^*(y_0)$ is Fréchet differentiable with derivative $\partial\phi(y_0)/\partial y = \Delta^*$.

First, let

$$\rho(t, y_0, h) = \frac{\|\phi^*(t, y_0 + h) - \phi^*(t, y_0) - \Delta^*(t)h\|_E}{\|h\|}$$

where $t \in \mathbb{R}$ and y_0, $h \in Y$. Consider this as

$$\rho(t, y_0, h) = \max\{\rho_X(t, y_0, h), \rho_Y(t, y_0, h), \rho_Z(t, y_0, h)\}$$

where

$$\begin{aligned}
\rho_X(t, y_0, h) &= \frac{\|\phi^*(t, y_0 + h)|_x - \phi^*(t, y_0)|_x - \Delta^*(t)h|_x\|}{\|h\|}, \\
\rho_Y(t, y_0, h) &= \frac{\|\phi^*(t, y_0 + h)|_y - \phi^*(t, y_0)|_y - \Delta^*(t)h|_y\|}{\|h\|}, \\
\rho_Z(t, y_0, h) &= \frac{\|\phi^*(t, y_0 + h)|_z - \phi^*(t, y_0)|_z - \Delta^*(t)h|_z\|}{\|h\|}.
\end{aligned}$$

If we show that $\sup_{t\in\mathbb{R}} e^{\sigma(t)t}\rho(t, y_0, h) \to 0$ as $h \to 0$, we will have the result.

Let $\zeta(s) := \phi^*(s, y_0)$ and $w(s) := \phi^*(s, y_0 + h) - \phi^*(s, y_0)$. We split the proof into steps and proceed accordingly.

Step 1: We establish the following estimates: for $t \leq 0$

$$\rho_Y(t, y_0, h) \leq K_y^2 e e^{\beta_y t} \int_0^t e^{-K_y\delta_y s} R_Y(\zeta(s), w(s))ds + K_y\delta_y \int_0^t e^{(t-s)\beta_y}\rho(s, y_0, h)ds,$$

$$\rho_X(t,y_0,h) \leq K_xK_yee^{\alpha_x t}\int_{-\infty}^{t} e^{(\beta_y-K_y\delta_y-\alpha_x)s}R_X(\zeta(s),w(s))ds + K_x\delta_x\int_{-\infty}^{t} e^{(t-s)\alpha_x}\rho(s,y_0,h)ds$$

$$\rho_Z(t,y_0,h) \leq K_zK_yee^{\beta_z t}\Big[\int_{t}^{0} e^{(\beta_y-K_y\delta_y-\beta_z)s}R_Z(\zeta(s),w(s))ds + \int_{0}^{\infty} e^{(K_y\delta_y+\alpha_y-\beta_z)s}R_Z(\zeta(s),w(s))ds\Big] + K_z\delta_z\int_{t}^{\infty} e^{(t-s)\beta_z}\rho(s,y_0,h)ds;$$

for $t \geq 0$

$$\rho_Y(t,y_0,h) \leq K_y^2ee^{\alpha_y t}\int_{0}^{t} e^{-K_y\delta_y s}R_Y(\zeta(s),w(s))ds + K_y\delta_y\int_{0}^{t} e^{(t-s)\alpha_y}\rho(s,y_0,h)ds$$

$$\rho_X(t,y_0,h) \leq K_xK_yee^{\alpha_x t}\Big[\int_{-\infty}^{0} e^{(\beta_y-K_y\delta_y-\alpha_x)s}R_X(\zeta(s),w(s))ds + \int_{0}^{t} e^{(K_y\delta_y+\alpha_y-\alpha_x)s}R_X(\zeta(s),w(s))ds\Big] + K_x\delta_x\int_{-\infty}^{t} e^{(t-s)\alpha_x}\rho(s,y_0,h)ds,$$

$$\rho_Z(t,y_0,h) \leq K_zK_yee^{\beta_z t}\int_{t}^{\infty} e^{(K_y\delta_y+\alpha_y-\beta_z)s}R_Z(\zeta(s),w(s))ds + K_z\delta_z\int_{t}^{\infty} e^{(t-s)\beta_z}\rho(s,y_0,h)ds.$$

Step 2: From Step 1, we obtain

$$\sup_{t\in\mathbb{R}} e^{-\sigma(t)t}\rho(t,y_0,h) \leq (1-\delta_\phi)^{-1}R(\zeta(t),w(t))$$

such that $R(\zeta(t),w(t)) = \max\{R_n(\zeta(t),w(t)), R_p(\zeta(t),w(t))\}$, where

$$R_n(\zeta(t),w(t)) = \max\Bigg\{\sup_{t\leq 0} K_y^2ee^{(\beta_y-\sigma_n)t}\int_{0}^{t} e^{-K_y\delta_y s}R_Y(\zeta(s),w(s))ds,$$
$$\sup_{t\leq 0} K_xK_yee^{(\alpha_x-\sigma_n)t}\int_{-\infty}^{t} e^{(\beta_y-K_y\delta_y-\alpha_x)s}R_X(\zeta(s),w(s))ds,$$
$$\sup_{t\leq 0} K_zK_yee^{(\beta_z-\sigma_n)t}\Big[\int_{t}^{0} e^{(\beta_y-K_y\delta_y-\beta_z)s}R_Z(\zeta(s),w(s))ds + \int_{0}^{\infty} e^{(K_y\delta_y+\alpha_y-\beta_z)s}R_Z(\zeta(s),w(s))ds\Big]\Bigg\},$$

and

$$R_p(\zeta(t),w(t)) = \max\Bigg\{ \sup_{t\geq 0} K_y^2 e e^{(\alpha_y-\sigma_p)t}\int_0^t e^{K_y\delta_y s}R_Y(\zeta(s),w(s))ds,$$
$$\sup_{t\geq 0} K_x K_y e e^{(\alpha_x-\sigma_p)t}\Big[\int_{-\infty}^0 e^{(\beta_y-K_y\delta_y-\alpha_x)s}R_X(\zeta(s),w(s))ds$$
$$+\int_0^t e^{(K_y\delta_y+\alpha_y-\alpha_x)s}R_X(\zeta(s),w(s))ds\Big],$$
$$\sup_{t\geq 0} K_z K_y e e^{(\beta_z-\sigma_p)t}\int_t^\infty e^{(K_y\delta_y+\alpha_y-\beta_z)s}R_Z(\zeta(s),w(s))ds\Bigg\}.$$

Step 3: We show that $\lim_{h\to 0} R(\zeta(t),w(t)) = \max\{\lim_{h\to 0} R_n(\zeta(t),w(t)), \lim_{h\to 0} R_p(\zeta(t),w(t))\} = 0$. Once we have this, it follows that

$$\lim_{h\to 0}\sup_{t\in\mathbb{R}} e^{-\sigma(t)t}\rho(t,y_0,h) \leq \lim_{h\to 0}(1-\delta_\phi)^{-1}R(\zeta(t),w(t)) = 0,$$

and we have shown (2.7).

Proof for Step 1: Consider ρ_Y when $t \leq 0$:

$$\rho_Y(t,y_0,h) = \frac{1}{\|h\|}\Big\| e^{tB}(y_0+h) + \int_0^t e^{(t-s)B}G(\zeta(s)+w(s))ds$$
$$- [e^{tB}y_0 + \int_0^t e^{(t-s)B}G(\zeta(s))ds]$$
$$- [e^{tB}h + \int_0^t e^{(t-s)B}DG(\zeta(s))\Delta^*(s)hds]\Big\|$$

$$= \frac{\Big\| \int_0^t e^{(t-s)B}\Big[[G(\zeta(s)+w(s)) - G(\zeta(s))] - DG(\zeta(s))\Delta^*(s)h\Big]ds\Big\|}{\|h\|}.$$

We add and subtract $DG(\zeta(s))w(s)$ in the integrand:

$$= \frac{\Big\| \int_0^t e^{(t-s)B}\big[[G(\zeta(s)+w(s)) - G(\zeta(s)) - DG(\zeta(s))w(s)] + DG(\zeta(s))w(s) - DG(\zeta(s))\Delta^*(s)h\big]ds\Big\|}{\|h\|}.$$

Then, we apply A1 and multiply by $1 = \|w(s)\|_E/\|w(s)\|_E$ to get

$$\leq K_y\int_0^t e^{(t-s)\beta_y}\frac{\|G(\zeta(s)+w(s)-G(\zeta(s))-DG(\zeta(s))w(s)\|}{\|w(s)\|_E}\frac{\|w(s)\|_E}{\|h\|}ds$$
$$+ K_y\int_0^t e^{(t-s)\beta_y}\|DG(\zeta(s))\|\frac{\|w(s)-\Delta^*(s)h\|_E}{\|h\|}ds.$$

At this point, it is convenient to establish some short-hand notation:

$$\begin{aligned} R_X(\zeta(s), w(s)) &= \frac{\|F(\zeta(s)+w(s)) - F(\zeta(s)) - DF(\zeta(s))w(s)\|}{\|w(s)\|_E} \leq 2\delta_x \\ R_Y(\zeta(s), w(s)) &= \frac{\|G(\zeta(s)+w(s)) - G(\zeta(s)) - DG(\zeta(s))w(s)\|}{\|w(s)\|_E} \leq 2\delta_y \\ R_Z(\zeta(s), w(s)) &= \frac{\|H(\zeta(s)+w(s)) - H(\zeta(s)) - DH(\zeta(s))w(s)\|}{\|w(s)\|_E} \leq 2\delta_z \end{aligned} \tag{2.8}$$

where $w(z)$ and $\zeta(z)$ are defined as before and each term is the Fréchet differentiation of the respective nonlinear term with respect to $w(z)$. The bounds come from the argument that

$$\frac{\|F(\zeta(s)+w(s)) - F(\zeta(s)) - DF(\zeta(s))w(s)\|}{\|w(s)\|_E} \leq \frac{\|F(\zeta(s)+w(s)) - F(\zeta(s))\| + \|DF(\zeta(s))\|w(s)\|}{\|w(s)\|_E},$$

applying A2 and (2.4) gives

$$\frac{\|F(\zeta(s)+w(s)) - F(\zeta(s)) - DF(\zeta(s))w(s)\|}{\|w(s)\|_E} \leq \frac{\delta_x w(s) + \delta_x\|w(s)\|}{\|w(s)\|_E} = 2\delta_x.$$

Each R_X, R_Y, and R_Z is uniformly bounded.

Note that we have $\frac{\|w(s)-\Delta^*(s)h\|_E}{\|h\|} = \rho(s, y_0, h)$. Then,

$$\rho_Y(t, y_0, h) \leq K_y \int_0^t e^{(t-s)\beta_y} R_Y(\zeta(s), w(s) \frac{\|w(s)\|_E}{\|h\|} ds + K_y\delta_y \int_0^t e^{(t-s)\beta_y}\rho(s, y_0, h) ds.$$

By Lemma 2.2.4, we have $\|w(s)\|_E \leq K_y e e^{(\beta_y - K_y\delta_y)s}\|h\|$ when $s \leq 0$ and $\|w(s)\|_E \leq K_y e e^{(K_y\delta_y+\alpha_y)s}\|h\|$ when $s \geq 0$, and

$$\rho_Y(t, y_0, h) \leq K_y^2 e e^{\beta_y t} \int_0^t e^{-K_y\delta_y s} R_Y(\zeta(s), w(s)) ds + K_y\delta_y \int_0^t e^{(t-s)\beta_y}\rho(s, y_0, h) ds.$$

We use the same steps to get that ρ_X and ρ_Z are bounded such that

$$\rho_X(t, y_0, h) \leq K_x K_y e e^{\alpha_x t} \int_{-\infty}^t e^{(\beta_y - K_y\delta_y - \alpha_x)s} R_X(\zeta(s), w(s)) ds + K_x\delta_x \int_{-\infty}^t e^{(t-s)\alpha_x}\rho(s, y_0, h) ds,$$

$$\begin{aligned} \rho_Z(t, y_0, h) \leq & K_z K_y e e^{\beta_z t}\Big[\int_t^0 e^{(\beta_y - K_y\delta_y - \beta_z)s} R_Z(\zeta(s), w(s)) ds \\ & + \int_0^\infty e^{(K_y\delta_y + \alpha_y - \beta_z)s} R_Z(\zeta(s), w(s)) ds\Big] + K_z\delta_z \int_t^\infty e^{(t-s)\beta_z}\rho(s, y_0, h) ds. \end{aligned}$$

For $t \geq 0$, we use the same process to get that

$$\rho_X(t, y_0, h) \leq K_x K_y e e^{\alpha_x t} \Big[\int_{-\infty}^{0} e^{(\beta_y - K_y\delta_y - \alpha_x)s} R_X(\zeta(s), w(s)) ds + \int_0^t e^{(K_y\delta_y + \alpha_y - \alpha_x)s} R_X(\zeta(s), w(s)) ds \Big] + K_x\delta_x \int_{-\infty}^{t} e^{(t-s)\alpha_x} \rho(s, y_0, h) ds,$$

$$\rho_Y(t, y_0, h) \leq K_y^2 e e^{\alpha_y t} \int_0^t e^{K_y\delta_y s} R_Y(\zeta(s), w(s)) ds + K_y\delta_y \int_0^t e^{(t-s)\alpha_y} \rho(s, y_0, h) ds,$$

and

$$\rho_Z(t, y_0, h) \leq K_z K_y e e^{\beta_z t} \int_t^{\infty} e^{(K_y\delta_y + \alpha_y - \beta_z)s} R_Z(\zeta(s), w(s)) ds + K_z\delta_z \int_t^{\infty} e^{(t-s)\beta_z} \rho(s, y_0, h) ds.$$

Proof for Step 2: Now that we have all the components of ρ for $t \in \mathbb{R}$, we evaluate

$$\sup_{t\in\mathbb{R}} e^{-\sigma(t)t} \rho(t, y_0, h) = \max\{\sup_{t\in\mathbb{R}} e^{-\sigma(t)t} \rho_X(t, y_0, h), \sup_{t\in\mathbb{R}} e^{-\sigma(t)t} \rho_Y(t, y_0, h), \sup_{t\in\mathbb{R}} e^{-\sigma(t)t} \rho_Z(t, y_0, h)\}.$$

When we take the supremum over each of the terms, the last integral in each expression will evaluate the same way as in Proposition 2.1.2, giving that

$$\sup_{t\in\mathbb{R}} e^{-\sigma(t)t} \rho(t, y_0, h) \leq R(\zeta(t), w(t)) + \delta_\phi \sup_{t\in\mathbb{R}} e^{-\sigma(t)t} \rho(t, y_0, h).$$

For example, consider $\sup_{t\leq 0} e^{-\sigma_n t} \rho_X(t, y_0, h)$:

$$\sup_{t\leq 0} e^{-\sigma_n t} \rho_X(t, y_0, h) \leq \sup_{t\leq 0} e^{-\sigma_n t} K_x K_y e e^{\alpha_x t} \int_{-\infty}^{t} e^{(\beta_y - K_y\delta_y - \alpha_x)s} R_X(\zeta(s), w(s)) ds + \sup_{t\leq 0} e^{-\sigma_n t} K_x\delta_x \int_{-\infty}^{t} e^{(t-s)\alpha_x} \rho(s, y_0, h) ds.$$

For now, we ignore the term dependent on R_X and consider only

$$\sup_{t\leq 0} e^{-\sigma_n t} K_x\delta_x \int_{-\infty}^{t} e^{(t-s)\alpha_x} \rho(s, y_0, h) ds \leq \sup_{t\leq 0} e^{(\alpha_x - \sigma_n)t} K_x\delta_x \int_{-\infty}^{t} e^{(\sigma_n - \alpha_x)t} \sup_{-\infty\leq s\leq t} e^{-\sigma_n s} \rho(s, y_0, h) ds.$$

Because $\rho(s, y_0, h) \in \mathcal{F}_{1,\sigma}$, $\sup_{s\in\mathbb{R}} e^{-\sigma_n s} \rho(s, y_0, h) < \infty$. We move the term outside the integral to get that

$$\sup_{t\leq 0} e^{-\sigma_n t} K_x\delta_x \int_{-\infty}^{t} e^{(t-s)\alpha_x} \rho(s, y_0, h) ds \leq \sup_{t\leq 0} e^{-\sigma_n t} \rho(t, y_0, h) \sup_{t\leq 0} e^{(\alpha_x - \sigma_n)t} K_x\delta_x \int_{-\infty}^{t} e^{(\sigma_n - \alpha_x)t} ds.$$

From Proposition 2.1.2,

$$\sup_{t\leq 0} e^{(\alpha_x-\sigma_n)t}K_x\delta_x\int_{-\infty}^{t} e^{(\sigma_n-\alpha_x)t}ds = \frac{K_x\delta_x}{\sigma_n-\alpha_x}.$$

Then we have that,

$$\sup_{t\leq 0} e^{-\sigma_n t}\rho_X(t,y_0,h) \leq \sup_{t\leq 0} e^{-\sigma_n t}K_xK_yee^{\alpha_x t}\int_{-\infty}^{t} e^{(\beta_y-K_y\delta_y-\alpha_x)s}R_X(\zeta(s),w(s))ds + \frac{K_x\delta_x}{\sigma_n-\alpha_x}\sup_{t\leq 0} e^{-\sigma_n t}\rho(t,y_0,h).$$

The simplification in the rest of the terms yield similar results.

Next, we solve for $\sup_{t\in\mathbb{R}} e^{-\sigma(t)t}\rho(t,y_0,h)$:

$$(1-\delta_\phi)\sup_{t\in\mathbb{R}} e^{-\sigma(t)t}\rho(t,y_0,h) \leq R(\zeta(t),w(t)).$$

From Proposition 2.1.2, we know $\delta_\phi < 1$. We have that $1-\delta_\phi > 0$ and we divide over to get

$$\sup_{t\in\mathbb{R}} e^{-\sigma(t)t}\rho(t,y_0,h) \leq (1-\delta_\phi)^{-1}R(\zeta(t),w(t))$$

where $R(\zeta(t),w(t)) = \max\{R_n(\zeta(t),w(t)), R_p(\zeta(t),w(t))\}$ and

$$\begin{aligned} R_n(\zeta(t),w(t)) = \max\Bigg\{ &\sup_{t\leq 0} K_y^2 ee^{(\beta_y-\sigma_n)t}\int_0^t e^{-K_y\delta_y s}R_Y(\zeta(s),w(s))ds, \\ &\sup_{t\leq 0} K_xK_yee^{(\alpha_x-\sigma_n)t}\int_{-\infty}^{t} e^{(\beta_y-K_y\delta_y-\alpha_x)s}R_X(\zeta(s),w(s))ds, \\ &\sup_{t\leq 0} K_zK_yee^{(\beta_z-\sigma_n)t}\Big[\int_t^0 e^{(\beta_y-K_y\delta_y-\beta_z)s}R_Z(\zeta(s),w(s))ds \\ &\qquad + \int_0^\infty e^{(K_y\delta_y+\alpha_y-\beta_z)s}R_Z(\zeta(s),w(s))ds\Big]\Bigg\}, \end{aligned}$$

$$\begin{aligned} R_p(\zeta(t),w(t)) = \max\Bigg\{ &\sup_{t\geq 0} K_y^2 ee^{(\alpha_y-\sigma_p)t}\int_0^t e^{K_y\delta_y s}R_Y(\zeta(s),w(s))ds, \\ &\sup_{t\geq 0} K_xK_yee^{(\alpha_x-\sigma_p)t}\Big[\int_{-\infty}^0 e^{(\beta_y-K_y\delta_y-\alpha_x)s}R_X(\zeta(s),w(s))ds \\ &\qquad + \int_0^t e^{(K_y\delta_y+\alpha_y-\alpha_x)s}R_X(\zeta(s),w(s))ds\Big], \\ &\sup_{t\geq 0} K_zK_yee^{(\beta_z-\sigma_p)t}\int_t^\infty e^{(K_y\delta_y+\alpha_y-\beta_z)s}R_Z(\zeta(s),w(s))ds\Bigg\}. \end{aligned}$$

Proof for Step 3: Now that we have $(1-\delta_\phi)^{-1}R(\zeta(t),w(t))$ is a bound for $\sup_{t\in\mathbb{R}} e^{-\sigma(t)t}\rho(t,y_0,h)$,

to show $\lim_{h\to 0}\sup_{t\in\mathbb{R}} e^{-\sigma(t)t}\rho(t,y_0,h)=0$, we show that

$$\lim_{h\to 0}(1-\delta_\phi)^{-1}R(\zeta(t),w(t))=(1-\delta_\phi)^{-1}\lim_{h\to 0}R(\zeta(t),w(t))=0.$$

To get that $\lim_{h\to 0}R(\zeta(t),w(t))=0$, we need that both $\lim_{h\to 0}R_n(\zeta(t),w(t))=0$ and $\lim_{h\to 0}R_p(\zeta(t),w(t))=0$.

First, consider $R_n(\zeta(t),w(t))$. We take the supremum over s of $R_Y(\zeta(s),w(s))$, $R_X(\zeta(s),w(s))$, and $R_Z(\zeta(s),w(s))$ and move those terms outside of the integral, which we do because R_X, R_Y, and R_Z are uniformly bounded:

$$\begin{aligned}R_n(\zeta(t),w(t))\leq\max\Bigg\{&\sup_{t\leq 0}K_y^2ee^{(\beta_y-\sigma_n)t}\sup_{t\leq s\leq 0}R_Y(\zeta(s),w(s))\int_0^t e^{-K_y\delta_y s}ds,\\&\sup_{t\leq 0}K_xK_yee^{(\alpha_x-\sigma_n)t}\sup_{-\infty\leq s\leq t}R_X(\zeta(s),w(s))\int_{-\infty}^t e^{(\beta_y-K_y\delta_y-\alpha_x)s}ds,\\&\sup_{t\leq 0}K_zK_yee^{(\beta_z-\sigma_n)t}\sup_{t\leq s\leq\infty}R_Z(\zeta(s),w(s))\Big[\int_t^0 e^{(\beta_y-K_y\delta_y-\beta_z)s}ds\\&\qquad+\int_0^\infty e^{(K_y\delta_y+\alpha_y-\beta_z)s}ds\Big]\Bigg\}.\end{aligned}$$

We make each supremum over s independent of t by extending it $s\in\mathbb{R}$. Then,

$$\begin{aligned}R_n(\zeta(t),w(t))\leq\max\Bigg\{&\sup_{s\in\mathbb{R}}R_Y(\zeta(s),w(s))\sup_{t\leq 0}K_y^2ee^{(\beta_y-\sigma_n)t}\int_0^t e^{-K_y\delta_y s}ds,\\&\sup_{s\in\mathbb{R}}R_X(\zeta(s),w(s))\sup_{t\leq 0}K_xK_yee^{(\alpha_x-\sigma_n)t}\int_{-\infty}^t e^{(\beta_y-K_y\delta_y-\alpha_x)s}ds,\\&\sup_{s\in\mathbb{R}}R_Z(\zeta(s),w(s))\sup_{t\leq 0}K_zK_yee^{(\beta_z-\sigma_n)t}\Big[\int_t^0 e^{(\beta_y-K_y\delta_y-\beta_z)s}ds\\&\qquad+\int_0^\infty e^{(K_y\delta_y+\alpha_y-\beta_z)s}ds\Big]\Bigg\}\end{aligned}$$

and we evaluate each term dependent on t. First, consider

$$\begin{aligned}\sup_{t\leq 0}K_y^2ee^{(\beta_y-\sigma_n)t}\int_0^t e^{-K_y\delta_y s}ds&=\sup_{t\leq 0}\frac{1}{K_y\delta_y}K_y^2ee^{(\beta_y-\sigma_n)t}[1-e^{-K_y\delta_y t}],\\&=\sup_{t\leq 0}\frac{K_ye}{\delta_y}[e^{(\beta_y-\sigma_n)t}-e^{(\beta_y-\sigma_n-K_y\delta_y)t}].\end{aligned}$$

By C1, $\beta_y-\sigma_n>0$ and by C2, $\beta_y-\sigma_n-K_y\delta_y>0$. Thus, when we take the supremum over $t\leq 0$ we get that

$$\sup_{t\leq 0}K_y^2ee^{(\beta_y-\sigma_n)t}\int_0^t e^{-K_y\delta_y s}ds\leq\frac{K_ye}{\delta_y}.$$

Next, consider

$$\begin{aligned}&\sup_{t\le 0} K_xK_yee^{(\alpha_x-\sigma_n)t}\int_{-\infty}^{t} e^{(\beta_y-K_y\delta_y-\alpha_x)s}ds\\&\quad=\sup_{t\le 0}\frac{K_xK_ye}{\beta_y-K_y\delta_y-\alpha_x}e^{(\alpha_x-\sigma_n)t}[e^{(\beta_y-K_y\delta_y-\alpha_x)t}-\lim_{T\to-\infty}e^{(\beta_y-K_y\delta_y-\alpha_x)T}].\end{aligned}$$

By C1 and C2, $\beta_y-K_y\delta_y-\alpha_x>0$ and $\lim_{T\to-\infty}e^{(\beta_y-K_y\delta_y-\alpha_x)T}=0$. Then,

$$\sup_{t\le 0} K_xK_yee^{(\alpha_x-\sigma_n)t}\int_{-\infty}^{t} e^{(\beta_y-K_y\delta_y-\alpha_x)s}ds=\sup_{t\le 0}\frac{K_xK_ye}{\beta_y-K_y\delta_y-\alpha_x}e^{(\beta_y-K_y\delta_y-\sigma_n)t}$$

and by C2, $\beta_y-K_y\delta_y-\sigma_n>0$. Taking the supremum of the expression over t gives that

$$\sup_{t\le 0} K_xK_yee^{(\alpha_x-\sigma_n)t}\int_{-\infty}^{t} e^{(\beta_y-K_y\delta_y-\alpha_x)s}ds=\frac{K_xK_ye}{\beta_y-K_y\delta_y-\alpha_x}.$$

Finally, consider

$$\begin{aligned}&\sup_{t\le 0} K_zK_yee^{(\beta_z-\sigma_n)t}\Big[\int_t^0 e^{(\beta_y-K_y\delta_y-\beta_z)s}ds+\int_0^\infty e^{(K_y\delta_y+\alpha_y-\beta_z)s}ds\Big]\\&\quad=\sup_{t\le 0} K_zK_yee^{(\beta_z-\sigma_n)t}\Big[\frac{1}{\beta_y-K_y\delta_y-\beta_z}(1-e^{(\beta_y-K_y\delta_y-\beta_z)t})\\&\qquad+\frac{1}{K_y\delta_y+\alpha_y-\beta_z}(\lim_{T\to\infty}e^{(K_y\delta_y+\alpha_y-\beta_z)T}-1)\Big].\end{aligned}$$

By C1 and C2, $K_y\delta_y+\alpha_y-\beta_z<0$. So,

$$\begin{aligned}&\sup_{t\le 0} K_zK_yee^{(\beta_z-\sigma_n)t}\Big[\int_t^0 e^{(\beta_y-K_y\delta_y-\beta_z)s}ds+\int_0^\infty e^{(K_y\delta_y+\alpha_y-\beta_z)s}ds\Big]\\&\quad=\sup_{t\le 0} K_zK_ye\Big[\frac{1}{\beta_y-K_y\delta_y-\beta_z}(e^{(\beta_z-\sigma_n)t}-e^{(\beta_y-K_y\delta_y-\sigma_n)t})+\frac{1}{\beta_z-K_y\delta_y-\alpha_y}\Big].\end{aligned}$$

Then, C1 gives $\beta_z-\sigma_n>0$ and C2 gives $\beta_y-K_y\delta_y-\sigma_n>0$. Thus, as we take the supremum over t, we have that

$$\begin{aligned}&\sup_{t\le 0} K_zK_yee^{(\beta_z-\sigma_n)t}\Big[\int_t^0 e^{(\beta_y-K_y\delta_y-\beta_z)s}ds+\int_0^\infty e^{(K_y\delta_y+\alpha_y-\beta_z)s}ds\Big]\\&\quad\le K_zK_ye\Big[\frac{1}{\beta_z+K_y\delta_y-\beta_y}+\frac{1}{\beta_z-K_y\delta_y-\alpha_y}\Big].\end{aligned}$$

We have that

$$R_n(\zeta(t),w(t)) \leq \max\Bigg\{ \frac{K_y e}{\delta_y} \sup_{s\in\mathbb{R}} R_Y(\zeta(s),w(s)), \frac{K_x K_y e}{\beta_y - K_y\delta_y - \alpha_x} \sup_{s\in\mathbb{R}} R_X(\zeta(s),w(s)), \\ K_z K_y e\Big[\frac{1}{\beta_z + K_y\delta_y - \beta_y} + \frac{1}{\beta_z - K_y\delta_y - \alpha_y}\Big] \sup_{s\in\mathbb{R}} R_Z(\zeta(s),w(s))\Bigg\}$$

and

$$\lim_{h\to 0} R_n(\zeta(t),w(t)) \leq \max\Bigg\{ \frac{K_y e}{\delta_y} \sup_{s\in\mathbb{R}} \lim_{h\to 0} R_Y(\zeta(s),w(s)), \frac{K_x K_y e}{\beta_y - K_y\delta_y - \alpha_x} \sup_{s\in\mathbb{R}} \lim_{h\to 0} R_X(\zeta(s),w(s)), \\ K_z K_y e\Big[\frac{1}{\beta_z + K_y\delta_y - \beta_y} + \frac{1}{\beta_z - K_y\delta_y - \alpha_y}\Big] \sup_{s\in\mathbb{R}} \lim_{h\to 0} R_Z(\zeta(s),w(s))\Bigg\}.$$

By the continuity of $w = \phi^*(s,y_0+h) - \phi^*(s,y_0)$, $w \to 0$ as $h \to 0$. Then, each $R_X(\zeta(s),w(s))$, $R_Y(\zeta(s),w(s))$, and $R_Z(\zeta(s),w(s))$ is the Fréchet differentiation of the nonlinear terms, giving that each term goes to zero as $w \to 0$. We have $\lim_{h\to 0} R_n(\zeta(t),w(t)) = 0$.

Next, we look at $R_p(\zeta(t),w(t))$. Applying the same steps as we did for $R_n(\zeta(t),w(t))$, we get that

$$R_p(\zeta(t),w(t)) \leq \max\Bigg\{ \sup_{s\in\mathbb{R}} R_Y(\zeta(s),w(s)) \sup_{t\geq 0} K_y^2 e e^{(\alpha_y-\sigma_p)t} \int_0^t e^{K_y\delta_y s} ds, \\ \sup_{s\in\mathbb{R}} R_X(\zeta(s),w(s)) \sup_{t\geq 0} K_x K_y e e^{(\alpha_x-\sigma_p)t} \Big[\int_{-\infty}^0 e^{(\beta_y - K_y\delta_y - \alpha_x)s} ds \\ + \int_0^t e^{(K_y\delta_y + \alpha_y - \alpha_x)s} ds\Big], \\ \sup_{s\in\mathbb{R}} R_Z(\zeta(s),w(s)) \sup_{t\geq 0} K_z K_y e e^{(\beta_z-\sigma_p)t} \int_t^\infty e^{(K_y\delta_y + \alpha_y - \beta_z)s} ds\Bigg\}.$$

First, consider

$$\sup_{t\geq 0} K_y^2 e e^{(\alpha_y-\sigma_p)t} \int_0^t e^{K_y\delta_y s} ds = \sup_{t\geq 0} \frac{K_y^2 e}{K_y\delta_y} e^{(\alpha_y-\sigma_p)t}[e^{K_y\delta_y t} - 1] \\ = \sup_{t\geq 0} \frac{K_y e}{\delta_y}[e^{(K_y\delta_y + \alpha_y - \sigma_p)t} - e^{(\alpha_y-\sigma_p)t}],$$

where $K_y\delta_y + \alpha_y - \sigma_p < 0$ by C2 and $\alpha_y - \sigma_p < 0$ by C1. Thus, when we take the supremum of the expression over t, we get that

$$\sup_{t\geq 0} K_y^2 e e^{(\alpha_y-\sigma_p)t} \int_0^t e^{K_y\delta_y s} ds \leq \frac{K_y e}{\delta_y}.$$

Next, consider

$$\begin{aligned}&\sup_{t\geq 0} K_x K_y e e^{(\alpha_x-\sigma_p)t}\Big[\int_{-\infty}^{0} e^{(\beta_y-K_y\delta_y-\alpha_x)s}ds+\int_{0}^{t} e^{(K_y\delta_y+\alpha_y-\alpha_x)s}ds\Big]\\ &=K_x K_y e e^{(\alpha_x-\sigma_p)t}\Big[\frac{1}{\beta_y-K_y\delta_y-\alpha_x}(1-\lim_{T\to-\infty} e^{(\beta_y-K_y\delta_y-\alpha_x)T})\\ &\quad+\frac{1}{K_y\delta_y+\alpha_y-\alpha_x}(e^{(K_y\delta_y+\alpha_y-\alpha_x)t}-1)\Big].\end{aligned}$$

Then, by C1 and C2, $\beta_y - K_y\delta_y - \alpha_x > 0$. Applying this gives

$$\begin{aligned}&\sup_{t\geq 0} K_x K_y e e^{(\alpha_x-\sigma_p)t}\Big[\int_{-\infty}^{0} e^{(\beta_y-K_y\delta_y-\alpha_x)s}ds+\int_{0}^{t} e^{(K_y\delta_y+\alpha_y-\alpha_x)s}ds\Big]\\ &=K_x K_y e\Big[\frac{1}{\beta_y-K_y\delta_y-\alpha_x}e^{(\alpha_x-\sigma_p)t}+\frac{1}{K_y\delta_y+\alpha_y-\alpha_x}(e^{(K_y\delta_y+\alpha_y-\sigma_p)t}-e^{(\alpha_x-\sigma_p)t})\Big]\end{aligned}$$

where $K_y\delta_y + \alpha_y - \sigma_p < 0$ and $\alpha_x - \sigma_p < 0$. Taking the supremum over $t \geq 0$ gives that

$$\begin{aligned}&\sup_{t\geq 0} K_x K_y e e^{(\alpha_x-\sigma_p)t}\Big[\int_{-\infty}^{0} e^{(\beta_y-K_y\delta_y-\alpha_x)s}ds+\int_{0}^{t} e^{(K_y\delta_y+\alpha_y-\alpha_x)s}ds\Big]\\ &\leq K_x K_y e\Big[\frac{1}{\beta_y-K_y\delta_y-\alpha_x}+\frac{1}{K_y\delta_y+\alpha_y-\alpha_x}\Big].\end{aligned}$$

Finally, consider

$$\begin{aligned}&\sup_{t\geq 0} K_z K_y e e^{(\beta_z-\sigma_p)t}\int_{t}^{\infty} e^{(K_y\delta_y+\alpha_y-\beta_z)s}ds\\ &\quad=\sup_{t\geq 0} K_z K_y e e^{(\beta_z-\sigma_p)t}\frac{1}{K_y\delta_y+\alpha_y-\beta_z}[\lim_{T\to\infty} e^{(K_y\delta_y+\alpha_y-\beta_z)T}-e^{(K_y\delta_y+\alpha_y-\beta_z)t}].\end{aligned}$$

C1 and C2 give that $K_y\delta_y + \alpha_y - \beta_z < 0$. Applying this gives

$$\sup_{t\geq 0} K_z K_y e e^{(\beta_z-\sigma_p)t}\int_{t}^{\infty} e^{(K_y\delta_y+\alpha_y-\beta_z)s}ds=\sup_{t\geq 0}\frac{K_z K_y e}{\beta_z-K_y\delta_y-\alpha_y}[e^{(K_y\delta_y+\alpha_y-\sigma_p)t}].$$

Then, by C2, $K_y\delta_y + \alpha_y - \sigma_p < 0$. Thus, taking the supremum over $t \geq 0$ gives that

$$\sup_{t\geq 0} K_z K_y e e^{(\beta_z-\sigma_p)t}\int_{t}^{\infty} e^{(K_y\delta_y+\alpha_y-\beta_z)s}ds=\frac{K_z K_y e}{\beta_z-K_y\delta_y-\alpha_y}.$$

Then we substitute back in to get

$$R_p(\zeta(t), w(t)) \leq \max\Bigg\{ \frac{K_y e}{\delta_y} \sup_{s\in\mathbb{R}} R_Y(\zeta(s), w(s)), \\ K_x K_y e\Big[\frac{1}{\beta_y - K_y\delta_y - \alpha_x} + \frac{1}{K_y\delta_y + \alpha_y - \alpha_x}\Big] \sup_{s\in\mathbb{R}} R_X(\zeta(s), w(s)), \\ \frac{K_z K_y e}{\beta_z - K_y\delta_y - \alpha_y} \sup_{s\in\mathbb{R}} R_Z(\zeta(s), w(s))$$

and

$$\lim_{h\to 0} R_p(\zeta(t), w(t)) \leq \max\Bigg\{ \frac{K_y e}{\delta_y} \sup_{s\in\mathbb{R}} \lim_{h\to 0} R_Y(\zeta(s), w(s)), \\ K_x K_y e\Big[\frac{1}{\beta_y - K_y\delta_y - \alpha_x} + \frac{1}{K_y\delta_y + \alpha_y - \alpha_x}\Big] \sup_{s\in\mathbb{R}} \lim_{h\to 0} R_X(\zeta(s), w(s)), \\ \frac{K_z K_y e}{\beta_z - K_y\delta_y - \alpha_y} \sup_{s\in\mathbb{R}} \lim_{h\to 0} R_Z(\zeta(s), w(s)).$$

By the same reasoning as for $R_n(\zeta(t), w(t))$, $\lim_{h\to 0} R_p(\zeta(t), w(t)) = 0$. Then,

$$\lim_{h\to 0} R(\zeta(t)), w(t)) = 0$$

and Δ^* is the Fréchet derivative of ϕ^* with respect to y, and $\partial\phi^*/\partial y = \Delta^*$. □

Now we show that $\Phi \in \mathcal{C}^1(Y, X \times Z)$.

Theorem 2.2.6. *Given A1, A2, A3, C1, C2, and* (2.4)*, the map* Φ *whose graph is the center manifold for* (1.7) *is* $C^1(Y, X \times Z)$.

Proof. We know from Proposition 2.2.5 that $\partial\phi_0/\partial y = \Delta^*$, and it follows by the definition of $\Phi(y_0) = \phi_0(0)|_X + \phi_0(0)|_Z$ that $D\Phi(y_0) = \frac{\partial\phi_0}{\partial y}(0)|_X + \frac{\partial\phi_0}{\partial y}(0)|_Z = \Delta^*(0)|_X + \Delta^*(0)|_Z$.

We also need that $D\Phi(y_0)$ is continuous in y. For y_1 and $y_2 \in Y$, $\Delta_1^*(t) = \mathcal{T}_1(\Delta_1^*(t), y_1)$ and $\Delta_2^*(t) = \mathcal{T}_1(\Delta_2^*(t), y_2)$. Then $\|D\Phi(y_1) - D\Phi(y_2)\|_{1,\sigma} \leq \|\Delta_1^* - \Delta_1^*\|_{1,\sigma}$, and we just need to check that Δ^* is continuous in y. Define a function

$$c(t) = \begin{cases} \beta_y & \text{for } t \leq 0 \\ \alpha_y & \text{for } t \geq 0. \end{cases}$$

This allows us to combine the two cases while we proceed through the proof. Take the

difference:

$$\begin{aligned}\Delta_1^*(t) - \Delta_2^*(t) = &\int_0^t e^{(t-s)B}[DG(\phi_1(s))\Delta_1^*(s) - DG(\phi_2(s))\Delta_2^*(s)]ds \\ &- \int_t^\infty e^{(t-s)C}[DH(\phi_1(s))\Delta_1^*(s) - DH(\phi_2(s))\Delta_2^*(s)]ds \\ &+ \int_{-\infty}^t e^{(t-s)A}[DF(\phi_1(s))\Delta_1^*(s) - DF(\phi_2(s))\Delta_2^*(s)]ds.\end{aligned}$$

We take norms and apply A1. Also, note that $\|DG(\phi_1(s))\Delta_1^*(s) - DG(\phi_2(s))\Delta_2^*(s)\| \leq \|DG(\phi_1(s)) - DG(\phi_2(s))\|\|\Delta_1^*(s)\| + \|DG(\phi_2(s))\|\|\Delta_1^*(s) - \Delta_2^*(s)\|$ where we add and subtract $DG(\phi_2(s))\Delta_1^*(s)$. This gives that

$$\begin{aligned}\|\Delta_1^*(t) - \Delta_2^*(t)\| \leq \max\Bigg\{ &\int_0^t K_y e^{(t-s)c(t)}\|DG(\phi_1(s)) - DG(\phi_2(s))\|\|\Delta_1^*(s)\|ds \\ &+ \int_0^t K_y e^{(t-s)c(t)}\|DG(\phi_2(s))\|\|\Delta_1^*(s) - \Delta_2^*(s)\|ds, \\ &\int_t^\infty K_z e^{(t-s)\beta_z}\|DH(\phi_1(s)) - DH(\phi_2(s))\|\|\Delta_1^*(s)\|ds \\ &+ \int_t^\infty K_z e^{(t-s)\beta_z}\|DH(\phi_2(s))\|\|\Delta_1^*(s) - \Delta_2^*(s)\|ds, \\ &\int_{-\infty}^t K_x e^{(t-s)\alpha_x}\|DF(\phi_1(s)) - DF(\phi_2(s))\|\|\Delta_1^*(s)\|ds \\ &+ \int_{-\infty}^t K_x e^{(t-s)\alpha_x}\|DF(\phi_2(s))\|\Delta_1^*(s) - \Delta_2^*(s)\|ds\Bigg\}.\end{aligned}$$

Next, we multiply through by $e^{-\sigma(t)t}$ and multiply by $1 = e^{\sigma(s)s}e^{-\sigma(s)s}$ in each integral. Also, we apply the bounds on the derivatives of the nonlinear terms in (2.4) to each of $\|DG(\phi_2(s))\|$, $\|DH(\phi_2(s))\|$, and $\|DF(\phi_2(s))\|$:

$$\begin{aligned}e^{-\sigma(t)t}\|\Delta_1^*(t) - \Delta_2^*(t)\| \leq \max\Big\{&e^{-\sigma(t)t}\int_0^t K_y e^{(t-s)c(t)}\|DG(\phi_1(s)) - DG(\phi_2(s))\|e^{\sigma(s)s}e^{-\sigma(s)s}\|\Delta_1^*(s)\|ds \\ &+e^{-\sigma(t)t}\delta_y\int_0^t K_y e^{(t-s)c(t)}e^{\sigma(s)s}e^{-\sigma(s)s}\|\Delta_1^*(s) - \Delta_2^*(s)\|ds, \\ &e^{-\sigma(t)t}\int_t^\infty K_z e^{(t-s)\beta_z}\|DH(\phi_1(s)) - DH(\phi_2(s))\|e^{\sigma(s)s}e^{-\sigma(s)s}\|\Delta_1^*(s)\|ds \\ &+e^{-\sigma(t)t}\delta_z\int_t^\infty K_z e^{(t-s)\beta_z}e^{\sigma(s)s}e^{-\sigma(s)s}\|\Delta_1^*(s) - \Delta_2^*(s)\|ds, \\ &e^{-\sigma(t)t}\int_{-\infty}^t K_x e^{(t-s)\alpha_x}\|DF(\phi_1(s)) - DF(\phi_2(s))\|e^{\sigma(s)s}e^{-\sigma(s)s}\|\Delta_1^*(s)\|ds \\ &+e^{-\sigma(t)t}\delta_x\int_{-\infty}^t K_x e^{(t-s)\alpha_x}e^{\sigma(s)s}e^{-\sigma(s)s}\|\Delta_1^*(s) - \Delta_2^*(s)\|ds\Big\}.\end{aligned}$$

Taking the supremum over the expression allows us to simplify using the same process as

in Proposition 2.1.2. We also pull out all terms dependent only on t from the integrals

$$\begin{aligned}\|\Delta_1^* - \Delta_2^*\|_{1,\sigma} \leq \|\Delta_1^*\|_{1,\sigma} \max\Bigg\{ &\sup_{t\in\mathbb{R}} e^{(c(t)-\sigma(t))t} \int_0^t K_y e^{(\sigma(s)-c(t))s} \|DG(\phi_1(s)) - DG(\phi_2(s))\| ds, \\ &\sup_{t\in\mathbb{R}} e^{(\beta_z-\sigma(t))t} \int_t^\infty K_z e^{(\sigma(s)-\beta_z)s} \|DH(\phi_1(s)) - DH(\phi_2(s))\| ds, \\ &\sup_{t\in\mathbb{R}} e^{(\alpha_x-\sigma(t))t} \int_{-\infty}^t K_x e^{(\sigma(s)-\alpha_x)s} \|DF(\phi_1(s)) - DF(\phi_2(s))\| ds \Bigg\} \\ &+ \max\left\{ \frac{K_x\delta_x}{\sigma_n - \alpha_x}, \frac{K_y\delta_y}{\beta_y - \sigma_n}, \frac{K_y\delta_y}{\sigma_p - \alpha_y}, \frac{K_z\delta_z}{\beta_z - \sigma_p} \right\} \|\Delta_1^* - \Delta_2^*\|_{1,\sigma}.\end{aligned}$$

Subtract over and divide by the coefficient on $\|\Delta_1^* - \Delta_2^*\|_{1,\sigma}$. We want the right hand side to approach zero as $y_1 \to y_2$:

$$\begin{aligned}\|\Delta_1^* - \Delta_2^*\|_{1,\sigma} \leq \|\Delta_1^*\|_{1,\sigma} (1 - \max&\left\{ \frac{K_x\delta_x}{\sigma_n - \alpha_x}, \frac{K_y\delta_y}{\beta_y - \sigma_n}, \frac{K_y\delta_y}{\sigma_p - \alpha_y}, \frac{K_z\delta_z}{\beta_z - \sigma_p} \right\})^{-1} \\ \max\Bigg\{ &\sup_{t\in\mathbb{R}} e^{(c(t)-\sigma(t))t} \int_0^t K_y e^{(\sigma(s)-c(t))s} \|DG(\phi_1(s)) - DG(\phi_2(s))\| ds, \\ &\sup_{t\in\mathbb{R}} e^{(\beta_z-\sigma(t))t} \int_t^\infty K_z e^{(\sigma(s)-\beta_z)s} \|DH(\phi_1(s)) - DH(\phi_2(s))\| ds, \\ &\sup_{t\in\mathbb{R}} e^{(\alpha_x-\sigma(t))t} \int_{-\infty}^t K_x e^{(\sigma(s)-\alpha_x)s} \|DF(\phi_1(s)) - DF(\phi_2(s))\| ds \Bigg\}.\end{aligned}$$

Before we take $y_1 \to y_2$, we need to show that each integral is bounded, especially the indefinite integrals. This way, the behavior of the integral will be dominated by the behavior of the terms dependent on y_1, y_2, e.g., $\|DG(\phi_1(s)) - DG(\phi_2(s))\|$, as we take the limit. Evaluating each integral gives that

$$\sup_{t\in\mathbb{R}} e^{(c(t)-\sigma(t))t} \int_0^t K_y e^{(\sigma(s)-c(t))s} \|DG(\phi_1(s)) - DG(\phi_2(s))\| ds \leq \max\left\{ \frac{2K_y\delta_y}{\beta_y - \sigma_n}, \frac{2K_y\delta_y}{\sigma_p - \alpha_y} \right\},$$

$$\sup_{t\in\mathbb{R}} e^{(\beta_z-\sigma(t))t} \int_t^\infty K_z e^{(\sigma(s)-\beta_z)s} \|DH(\phi_1(s)) - DH(\phi_2(s))\| ds \leq \frac{2K_x\delta_x}{\sigma_n - \alpha_x},$$

and

$$\sup_{t\in\mathbb{R}} e^{(\alpha_x-\sigma(t))t} \int_{-\infty}^t K_x e^{(\sigma(s)-\alpha_x)s} \|DF(\phi_1(s)) - DF(\phi_2(s))\| ds \leq \frac{2K_z\delta_z}{\beta_z - \sigma_p}.$$

Now, by the continuity of $\phi_1(s)$ and $DF(x,y,z), DG(x,y,z)$, and $DH(x,y,z)$, $\|DG(\phi_1(s)) - DG(\phi_2(s))\|, \|DH(\phi_1(s)) - DH(\phi_2(s))\|$, and $\|DF(\phi_1(s)) - DF(\phi_2(s))\| \to 0$ as $y_1 \to y_2$, and by dominated convergence the right hand side converges to zero. Then, $\|\Delta_1^* - \Delta_2^*\|_{1,\sigma} \to 0$ as $y_1 \to y_2$. Finally, $D\Phi(\cdot)$ is continuous. □

The next step in developing the theory is to show that given certain conditions, we have

$\Phi \in C^k(Y, E)$. This proof requires the assumption that $F \in \mathcal{C}^k(E, X), G \in \mathcal{C}^k(E, Y)$, and $H \in \mathcal{C}^k(E, Z)$, and an additional condition on $\sigma(t)$. We do not present a formal proof for this result. However, it can be obtained by following the proof scheme for the (un)stable case presented in [7]. The proof is by induction, where the result in Theorem 2.2.6 amounts to the $k = 1$ case. The induction step involves defining the $\mathcal{T}_k$ map and $\mathcal{F}_{k,\sigma}$ function space, then showing each step we include in this section to show $\Phi \in \mathcal{C}^1$ for the new map, using the induction assumption to get that the fixed point of each $\mathcal{T}_i$ map is continuous, where $i = 1, \ldots, k-1$.

We extend the boundary value problem from Section 2.1 to the case of the derivative.

Proposition 2.2.7. *The fixed point of $\mathcal{T}_1(\Delta^*(t), y_0)$, denoted $\Delta^*(t, y_0)$ is characterized as the unique element in the function space with initial condition $\Delta^*(0, y_0)$ and satisfies the boundary value problem*

$$\begin{aligned} \dot{\Delta}^*(t)|_x &= A\Delta^*(t)|_x + DF(\phi_0(t))\Delta^*(t) & \dot{\Delta}^*(-\infty)|_x &= 0 \\ \dot{\Delta}^*(t)|_y &= B\Delta^*(t)|_y + DG(\phi_0(t))\Delta^*(t) & \dot{\Delta}^*(0)|_y &= I_Y \\ \dot{\Delta}^*(t)|_z &= C\Delta^*(t)|_z + DH(\phi_0(t))\Delta^*(t) & \dot{\Delta}^*(\infty)|_z &= 0. \end{aligned} \tag{2.9}$$

Proof. The first result follows directly from Proposition 2.2.5. Next, note that substituting in the boundary conditions in each component will yield back the initial condition. □

While in the next section we present the forward-backward algorithm based on Proposition 2.1.3, it is possible to develop a similar algorithm to solve for the derivative of the manifold based on Proposition 2.2.7.

Chapter 3

Center Manifold Computation

In this chapter, we develop an algorithm based on Proposition 2.1.4 to find the function $\Phi(y) = x + z$ whose graph is the center manifold. Then we include several examples to demonstrate the algorithm and discuss how well it performs. We will see also how the algorithm behaves when the equation we are studying does not satisfy our framework completely. Lastly, we apply the algorithm to a partial differential equation from fluid dynamics. We use a particular example from a class of semilinear elliptic boundary value problems studied in [20].

3.1 Algorithm

To motivate the development of our algorithm, consider an example of an ordinary differential equation:

$$\begin{aligned} \dot{x} &= -\lambda_3 x + \lambda_3 g_3(y) + g_3'(y)(f_2(y) - \lambda_2 y) \\ \dot{y} &= -\lambda_2 y + f_2(y) \\ \dot{z} &= -\lambda_1 z + \lambda_1 g_1(y) + g_1'(y)(f_2(y) - \lambda_2 y). \end{aligned} \tag{3.1}$$

The center manifold for this system is given by $x_0 = g_3(y_0)$ and $z_0 = g_1(y_0)$; see [19] for the derivation. We choose $\lambda_1 = -10$, $\lambda_2 = 0$, and $\lambda_3 = 10$, which is the classical case of the center manifold. We also choose $g_1(y) = \sin(y)$, $g_2 = \cos(y)$, and $f_2(y) = \sin(y)$ to get

$$\begin{aligned} \dot{x} &= -10x + 10\cos(y) - \sin^2(y) \\ \dot{y} &= \sin(y) \\ \dot{z} &= 10z - 10\sin(y) + \cos(y)\sin(y), \end{aligned} \tag{3.2}$$

the center manifold of which is $x_0 = \cos(y_0)$ and $z_0 = \sin(y_0)$.

The system has a steady state at $\begin{pmatrix} 1 & 0 & 0 \end{pmatrix}^t$ and satisfies our framework, with $\alpha_x = -10$, $\beta_y = 0$, $\alpha_y = 0$, and $\beta_z = 10$, $K_x = K_y = K_z = 1$. The nonlinear terms $F(x, y, z) = 10\cos(y) - \sin^2(y)$, $G(x, y, z) = \sin(y)$, $H(x, y, z) = -10\sin(y) + \cos(y)\sin(y)$ are Lipschitz continuous, with $\delta_x = \delta_z = 20/\pi \approx 6.3662$ and $\delta_y = 1$. The gap is $10 > 7.3662$ and the range

for $\sigma(t)$ given by C2 is

$$\begin{aligned} -10 + 6.3662 <&\sigma_n < 0 - 1 \\ 0 + 1 <&\sigma_p < 10 - 6.3662. \end{aligned}$$

The boundary value problem from Proposition 2.1.3 gives that we are searching for the solution to

$$\begin{aligned} \dot{x} &= f(x,y,z), \qquad x(-\infty) = 0 \\ \dot{y} &= g(x,y,z), \qquad y(0) = y_0 \\ \dot{z} &= h(x,y,z), \qquad z(\infty) = 0 \end{aligned} \tag{3.3}$$

where $f(x,y,z) = Ax + F(x,y,z)$, $g(x,y,z) = By + G(x,y,z)$, and $h(x,y,z) = Cz + H(x,y,z)$. Then, we begin to discretize the system to adapt it to a numerical algorithm by implementing an approximation to the boundary value problem. This problem is similar to the so-called asymptotic boundary value problem in [1, 36]. It would be interesting to investigate the connection between these two fields. However, it is beyond the scope of this paper. We substitute some finite T for infinity. Then, the system in (3.3) becomes

$$\begin{aligned} \dot{x} &= f(x,y,z), \qquad x(-T) = 0 \\ \dot{y} &= g(x,y,z), \qquad y(0) = y_0 \\ \dot{z} &= h(x,y,z), \qquad z(T) = 0. \end{aligned} \tag{3.4}$$

Formally speaking, (3.4) converges to (2.2) as $T \to \infty$.

The intuition behind the algorithm is that we numerically integrate the X component forward from $t = -T$ where $x(-T) = 0$, the Z component backward from $t = T$ where $z(T) = 0$, and the Y component in the negative and positive directions from $t = 0$ where $y(0) = y_0$. This is the forward-backward (FB) part of the algorithm, as in [5]. The number of steps in a given direction from zero is N, and we use k to denote step size. Then, we generate mesh points $t_i = ik$ for $i = -N, -N+1, \ldots, 0, \ldots, N-1, N$, and we index each variable by time, defining $x_i = x(t_i)$, $y_i = y(t_i)$, and $z_i = z(t_i)$ where $kN = T$.

The approximations we make will create error in our algorithm. These two approximations are our truncation of infinity at T and our discretization of time by k. Our error will therefore be composed of these two components: $e = e_1(T) + e_2(k)$, where our choice of T controls the truncation error, while our choice of k controls our step size error. In general, the larger the value of T, the smaller our truncation error; the smaller the value of k, the smaller the error due to step size.

We want to integrate each component separately and in different directions, and can do this if we adopt a waveform relaxation, which is just an update to our iterative technique and is denoted with a superscript j index. Without the waveform relaxation, each equation must be discretized identically and evaluated simultaneously. With the waveform relaxation, we fix all but the differentiated variable in each equation and evaluate the integration. The solutions obtained at each waveform are then used to evaluate the next iteration. For an overview of the waveform relaxation algorithm and its extensions, see [37]. For a discussion of the waveform relaxation in the context of the methods we use, including the Jacobi and Gauss-Seidel updates, see [5].

Now we can apply known methods of numerical integration. We first use the Euler method, which is a first-order Runge Kutta method. For a differential system of the form

$$\dot{u} = p(t, u), \text{ and } u_0 = a$$

the scheme for finding a solution via the Euler method has general form

$$u_{i+1} = u_i + kp(t_i, u_i) \tag{3.5}$$

for $i = 0, 1, \ldots, N$ with $u_0 = a$. Let the superscript j refer to the waveform relaxation index; then, denote x_i^j, y_i^j, and z_i^j. The FB-RK1-J method is

$$\begin{aligned} y_{i+1}^{j+1} &= y_i^j + kg(x_i^j, y_i^j, z_i^j) \\ y_{-i-1}^{j+1} &= y_{-i}^j - kg(x_{-i}^j, y_{-i}^j, z_{-i}^j) \end{aligned} \tag{3.6}$$

for $i = 0, 1, \ldots, N-1$ and

$$\begin{aligned} x_{i+1}^{j+1} &= x_i^j + kf(x_i^j, y_i^j, z_i^j) \\ z_{-i}^{j+1} &= z_{-i-1}^j - kh(x_{-i-1}^j, y_{-i-1}^j, z_{-i-1}^j) \end{aligned} \tag{3.7}$$

for $i = -N, -N+1, \ldots, 0, \ldots, N-1$ with initial conditions y_0, $z_N = 0$, and $x_{-N} = 0$. Here, the naming convention is as follows: FB refers to the forward-backward nature of the algorithm, RK1 refers to the method being a first-order Runge Kutta type method, and J referring to the implementation using the Jacobi update. In (3.6), notice that the scheme is simple numerical integration forward in time starting at y_0 to y_N and backward in time starting at y_0 to y_{-N}. The X component is integrated forward in time from $x_{-N} = 0$ to x_N and the Z component is integrated backward in time from $z_N = 0$ to z_{-N}, in (3.7).

Algorithm 1 FB-RK1-J Method

Input: f, g, h, y_0, k, N, and TOL.
Output: x_0, z_0.

```
Set x_{-N} = z_N = 0 and y_{i=0} = y_0.
Set error = 1.
while error > TOL do
    for i = 0 : N − 1 do
        y_{i+1}^{j+1} = y_i^j + kg(x_i^j, y_i^j, z_i^j)
        y_{-i-1}^{j+1} = y_{-i}^j − kg(x_{-i}^j, y_{-i}^j, z_{-i}^j)
    end for
    for i = −N : N − 1 do
        x_{i+1}^{j+1} = x_i^j + kf(x_i^j, y_i^j, z_i^j)
        z_{-i}^{j+1} = z_{-i-1}^j − kh(x_{-i-1}^j, y_{-i-1}^j, z_{-i-1}^j)
    end for
    Update error = ||[x^{j+1}, y^{j+1}, z^{j+1}] − [x^j, y^j, z^j]||.
end while
Return x_0, z_0.
```

Algorithm 1 is the implementation of the FB-RK1-J method. The results from testing FB-RK1-J on the example in (3.2) with different values of k and N are in Table 3.1. We observe that for each fixed value of k, the error tends to decrease as we increase N up to the value at which $kN = 1$, and when $1 \leq kN$, the smaller the k, the smaller the error. In rows 1, 5, and 9 of Table 3.1, for which $kN = 1$, we can see that the error responds linearly to the decrease in k, suggesting that this method is $\mathcal{O}(k)$, which corresponds to the classic Euler method.

k	N	x_0	$\tilde{x_0}$	$\lvert\tilde{x_0} - x_0\rvert$	z_0	$\tilde{z_0}$	$\lvert\tilde{z_0} - z_0\rvert$	J
0.1	10	0.8775826	0.8804693	0.0028868	0.4794255	0.4764654	0.0029601	13
0.1	100	0.8775826	0.8804693	0.0028868	0.4794255	0.4764654	0.0029601	103
0.1	1000	0.8775826	0.8804693	0.0028868	0.4794255	0.4764654	0.0029601	1002
0.01	10	0.8775826	0.5643989	0.3131836	0.4794255	0.2970139	0.1824117	32
0.01	100	0.8775826	0.8776088	0.0002380	0.4794255	0.4790983	0.0003273	218
0.01	1000	0.8775826	0.8778467	0.0002641	0.4794255	0.4791232	0.0003024	1045
0.001	10	0.8775826	0.0818540	0.7957285	0.4794255	0.0420236	0.4374019	32
0.001	100	0.8775826	0.5486630	0.3289195	0.4794255	0.2880647	0.1913608	302
0.001	1000	0.8775826	0.8775663	0.0000162	0.4794255	0.4793548	0.0000707	2101

Table 3.1: By FB-RK1-J method. Tested using the example in (3.2) with $y_0 = 0.5$. The center manifold of the system is $x_0 = \cos(0.5)$ and $z_0 = \sin(0.5)$. k is the step size, N the number of steps, the actual solutions are x_0 and z_0; the algorithm output is $\tilde{x_0}$ and $\tilde{z_0}$, and the error terms are $|\tilde{x_0} - x_0|$ and $|\tilde{z_0} - z_0|$. J is the number of iterations it takes for the algorithm to converge within the tolerance 10^{-6}.

A downside to the FB-RK1-J method is how many steps it takes to converge. The number of steps seems proportionate to the size of N. So, the smaller the error we want the longer it will take to converge. We can address this problem by using the Gauss-Seidel update. The Gauss-Seidel update uses values calculated in the current iteration of the algorithm when making the next update, allowing it to compute the vector faster than the Jacobi method for most cases. The FB-RK1-GS scheme is

$$\begin{aligned} y_{i+1}^{j+1} &= y_i^{j+1} + kg(x_i^j, y_i^{j+1}, z_i^j) \\ y_{-i-1}^{j+1} &= y_{-i}^{j+1} - kg(x_{-i}^j, y_{-i}^{j+1}, z_{-i}^j) \end{aligned} \tag{3.8}$$

for $i = 0, 1, \ldots, N-1$ and

$$\begin{aligned} x_{i+1}^{j+1} &= x_i^{j+1} + kf(x_i^{j+1}, y_i^{j+1}, z_i^{j+1}) \\ z_{-i}^{j+1} &= z_{-i-1}^{j+1} - kh(x_{-i-1}^j, y_{-i-1}^{j+1}, z_{-i-1}^{j+1}) \end{aligned} \tag{3.9}$$

for $i = -N, -N+1, \ldots, 0, \ldots, N-1$ with initial conditions y_0, $z_N = 0$, and $x_{-N} = 0$. Notice that the waveform relaxation index on the right hand side of equations (3.8) and (3.9) is now $j+1$ for the values whose time grid index gives that we have already computed them in the current iteration, which is different from (3.6) and (3.7). While the Gauss-Seidel

update will not decrease the error approximation over FB-RK1-J, it will cause the system to converge faster and will allow us to choose smaller k and bigger N and maintain a reasonable computation time. Algorithm 2 shows the implementation of the FB-RK1-GS scheme, and Table 3.2 presents the results we get when we test the algorithm with our example in (3.11) at different values of k and N. The only difference between Tables 3.1 and 3.2 for the common values of k and N is the speed of convergence; $J = 2$ for all cases. The speed of convergence is extremely different from the FB-RK1-J scheme, which becomes increasingly slow and has J values in the thousands.

Algorithm 2 FB-RK1-GS Method

Input: f, g, h, y_0, k, N, and TOL.
Output: x_0, z_0.

```
Set x_{-N} = z_N = 0 and y_{i=0} = y_0.
Set error = 1.
while error > TOL do
    for i = 0 : N − 1 do
        y_{i+1}^{j+1} = y_i^{j+1} + k g(x_i^j, y_i^{j+1}, z_i^j)
        y_{−i−1}^{j+1} = y_{−i}^{j+1} − k g(x_{−i}^j, y_{−i}^{j+1}, z_{−i}^j)
    end for
    for i = −N : N − 1 do
        x_{i+1}^{j+1} = x_i^{j+1} + k f(x_i^{j+1}, y_i^{j+1}, z_i^j)
        z_{−i}^{j+1} = z_{−i−1}^{j+1} − k h(x_{−i−1}^j, y_{−i−1}^{j+1}, z_{−i−1}^{j+1})
    end for
    Update error = ‖[x^{j+1}, y^{j+1}, z^{j+1}] − [x^j, y^j, z^j]‖.
end while
Return x_0, z_0.
```

k	N	x_0	$\tilde{x_0}$	$\lvert\tilde{x_0} - x_0\rvert$	z_0	$\tilde{z_0}$	$\lvert\tilde{z_0} - z_0\rvert$	J
0.1	10	0.8775826	0.8804693	0.0028868	0.4794255	0.4764654	0.0029601	2
0.1	100	0.8775826	0.8804693	0.0028868	0.4794255	0.4764654	0.0029601	2
0.1	1000	0.8775826	0.8804693	0.0028868	0.4794255	0.4764654	0.0029601	2
0.01	10	0.8775826	0.5643989	0.3131836	0.4794255	0.2970139	0.1824117	2
0.01	100	0.8775826	0.8776088	0.0002380	0.4794255	0.4790983	0.0003273	2
0.01	1000	0.8775826	0.8778467	0.0002641	0.4794255	0.4791232	0.0003024	2
0.01	10000	0.8775826	0.8778467	0.0002641	0.4794255	0.4791232	0.0003024	2
0.001	10	0.8775826	0.0818540	0.7957285	0.4794255	0.0420236	0.4374019	2
0.001	100	0.8775826	0.5486630	0.3289195	0.4794255	0.2880647	0.1913608	2
0.001	1000	0.8775826	0.8775663	0.0000162	0.4794255	0.4793548	0.0000707	2
0.001	10000	0.8775826	0.8776087	0.0000262	0.4794255	0.4793953	0.0000303	2
0.001	100000	0.8775826	0.8776087	0.0000262	0.4794255	0.4793953	0.0000303	2

Table 3.2: By FB-RK1-GS method. Tested using the example in (3.2) with $y_0 = 0.5$. The center manifold of the system is $x_0 = \cos(0.5)$ and $z_0 = \sin(0.5)$. k is the step size, N the number of steps, the actual solutions are x_0 and z_0; the algorithm output is $\tilde{x_0}$ and $\tilde{z_0}$, and the error terms are $|\tilde{x_0} - x_0|$ and $|\tilde{z_0} - z_0|$. J is the number of iterations it takes for the algorithm to converge within the tolerance 10^{-6}.

We also include the solutions for larger values of N at each value of k in Table 3.2 in order to demonstrate that the error seems minimized when $kN = 1$ and remains constant for all values of N at fixed k when $kN > 1$. This implies that after a certain value of T the error due to truncation, $e_1(T)$, is too small to contribute a significant amount to the total error, and the remaining error is governed by $e_2(k)$. At this point, the only way to decrease the error further is to make k smaller.

Finally, we maintain the Gauss-Seidel update and demonstrate the algorithm using a second-order Runge-Kutta method referred to in [4] as the Modified Euler Method. They present the method as:

$$u_{i+1} = u_i + \frac{k}{2}[p(t_i, u_i) + p(t_{i+1}, u_i + hp(t_i, u_i))] \tag{3.10}$$

for $i = 0, 1, \ldots, N-1$. Here, we adapt (3.10) to our framework to get the FB-RK2-GS scheme:

$$y_{i+1}^{j+1} = y_i^{j+1} + \frac{k}{2}[g(x_i^j, y_i^{j+1}, z_i^j) + g(x_{i+1}^j, y_{i+1}^j, z_{i+1}^j)]$$
$$y_{-i-1}^{j+1} = y_{-i}^{j+1} - \frac{k}{2}[g(x_{-i}^j, y_{-i}^{j+1}, z_{-i}^j) + g(x_{-i-1}^j, y_{-i-1}^j, z_{-i-1}^j)]$$

for $i = 0, 1, \ldots, N-1$ and

$$x_{i+1}^{j+1} = x_i^{j+1} + \frac{k}{2}[f(x_i^{j+1}, y_i^{j+1}, z_i^j) + f(x_{i+1}^j, y_{i+1}^j, z_{i+1}^j)]$$
$$z_{-i}^{j+1} = z_{-i-1}^{j+1} - \frac{k}{2}h(x_{-i-1}^j, y_{-i-1}^j, z_{-i-1}^{j+1}) + h(x_{-i}^j, y_{-i}^j, z_{-i}^j)]$$

for $i = -N, -N+1, \ldots, 0, \ldots, N-1$ with initial conditions y_0, $z_N = 0$, and $x_{-N} = 0$ and refer to this as the Trapezoidal Update to the Euler method. This method has local truncation error roughly $\mathcal{O}(k^2)$.

Algorithm 3 FB-RK2-GS Method

Input: f, g, h, y_0, k, N, and TOL.
Output: x_0, z_0.
  Set $x_{-N} = z_N = 0$ and $y_{i=0} = y_0$.
  Set $error = 1$.
  while $error > TOL$ **do**
    for $i = 0 : N-1$ **do**
      $y_{i+1}^{j+1} = y_i^{j+1} + k/2[g(x_i^j, y_i^{j+1}, z_{i+1}^j) + g(x_{i+1}^j, y_{i+1}^j, z_{i+1}^j)]$
      $y_{-i-1}^{j+1} = y_{-i}^{j+1} - k/2[g(x_{-i}^j, y_{-i}^{j+1}, z_{-i}^j) + g(x_{-i-1}^j, y_{-i-1}^j, z_{-i-1}^j)]$
    end for
    for $i = -N : N-1$ **do**
      $x_{i+1}^{j+1} = x_i^{j+1} + k/2[f(x_i^{j+1}, y_i^{j+1}, z_i^j) + f(x_{i+1}^j, y_{i+1}^j, z_{i+1}^j)]$
      $z_{-i}^{j+1} = z_{-i-1}^{j+1} - k/2[h(x_{-i-1}^j, y_{-i-1}^{j+1}, z_{-i-1}^{j+1}) + h(x_{-i}^j, y_{-i}^j, z_{-i}^j)]$
    end for
    Update $error = \|[x^{j+1}, y^{j+1}, z^{j+1}] - [x^j, y^j, z^j]\|$.
  end while
  Return x_0, z_0.

k	N	x_0	$\tilde{x_0}$	$\lvert\tilde{x_0} - x_0\rvert$	z_0	$\tilde{z_0}$	$\lvert\tilde{z_0} - z_0\rvert$	J
0.1	10	0.8775826	0.8775301	0.0000524	0.4794255	0.4794508	0.0000253	64
0.1	100	0.8775826	0.8775468	0.0000358	0.4794255	0.4794667	0.0000411	322
0.1	1000	0.8775826	0.8775468	0.0000358	0.4794255	0.4794667	0.0000411	2401
0.01	10	0.8775826	0.5472638	0.3303188	0.4794255	0.2872724	0.1921531	11
0.01	100	0.8775826	0.8775380	0.0000446	0.4794255	0.4793838	0.0000418	32
0.01	1000	0.8775826	0.8775822	0.0000004	0.4794255	0.4794260	0.0000004	172
0.01	10000	0.8775826	0.8775822	0.0000004	0.4794260	0.4794260	0.0000004	1293
0.001	10	0.8775826	0.0814521	0.7961305	0.4794255	0.0418051	0.4376205	5
0.001	100	0.8775826	0.5469910	0.3305916	0.4794255	0.2871135	0.1923121	10
0.001	1000	0.8775826	0.8775380	0.0000446	0.4794255	0.4793830	0.0000425	31
0.001	10000	0.8775826	0.8775826	0.0000000	0.4794255	0.4794255	0.0000000	167
0.001	100000	0.8775826	0.8775826	0.0000000	0.4794255	0.4794255	0.0000000	1244

Table 3.3: By FB-RK2-GS method. Tested using the example in (3.2) with $y_0 = 0.5$. The center manifold of the system is $x_0 = \cos(0.5)$ and $z_0 = \sin(0.5)$. k is the step size, N the number of steps, the actual solutions are x_0 and z_0; the algorithm output is $\tilde{x_0}$ and $\tilde{z_0}$, and the error terms are $|\tilde{x_0} - x_0|$ and $|\tilde{z_0} - z_0|$. J is the number of iterations it takes for the algorithm to converge within the tolerance 10^{-6}.

Algorithm 3 is the implementation of the FB-RK2-GS method, and the results of testing

the method on (3.2) are in Table 3.3. Using this algorithm, we observe behavior in the system due to k and N that is different to what we saw before. Here, when $k < 0.1$, the error drops significantly from when $kN < 1$ to $kN = 1$, then significantly again from when $kN = 1$ to $kN > 1$. Although the table only includes seven decimal places, the values for the computations in rows 6 and 7 and rows 11 and 12 are exactly the same, indicating again that $e_1(T)$ is too small to make a significant difference to the error term when $T > 1$. However, this difference from the FB-RK1-J and FB-RK1-GS methods implies that this higher order update is differently sensitive to the value of T. The number of steps it takes the FB-RK2-GS method to converge, J, is proportional to T and not N in this case, meaning that shrinking k and growing N does not necessarily increase the number of steps to convergence. We see this in the differences in number of steps when $kN = 10$, which are rows 2, 6, and 11 in the table.

We do not include any updates of higher order than $\mathcal{O}(k^2)$ in this work. However, an easy update based on what we have developed in this section is the most commonly used RK method, which has local truncation error of $\mathcal{O}(k^4)$:

$$\begin{aligned} w_1 &= kp(t_i, u_i), \\ w_2 &= kp(t_i + \frac{k}{2}, u_i + \frac{1}{2}w_1), \\ w_3 &= kp(t_i + \frac{k}{2}, u_i + \frac{1}{2}w_2), \\ w_4 &= kp(t_{i+1}, u_i + w_3), \\ u_{i+1} &= u_i + \frac{1}{6}(w_1 + w_2 + w_3 + w_4) \end{aligned}$$

for $i = 0, 1, \ldots, N-1$, from [4]. Other updates are possible as well.

Next, we demonstrate the usefulness of the algorithm in computing the manifold of systems that do not completely fit our framework. Consider (3.1), but choose $g_1(y) = \sin(y)$, $g_2 = \cos(y)$, and $f_2(y) = y^2$. The system becomes

$$\begin{aligned} \dot{x} &= -10x + 10\cos(y) - \sin(y)y^2 \\ \dot{y} &= y^2 \\ \dot{z} &= 10z - 10\sin(y) + \cos(y)y^2. \end{aligned} \tag{3.11}$$

The center manifold is still given by $x_0 = \cos(y_0)$ and $z_0 = \sin(y_0)$, but the nonlinear terms of this system are not globally Lipschitz because of the choice of $f_2(y)$.

k	N	x_0	$\tilde{x_0}$	$\lvert\tilde{x_0} - x_0\rvert$	z_0	$\tilde{z_0}$	$\lvert\tilde{z_0} - z_0\rvert$	J
0.1	10	0.8775826	0.8789740	0.0013915	0.4794255	0.4773625	0.0020630	13
0.01	10	0.8775826	0.5677667	0.3098159	0.4794255	0.3041693	0.1752563	32
0.01	100	0.8775826	0.8776829	0.0001004	0.4794255	0.4791711	0.0002545	217
0.001	10	0.8775826	0.0828374	0.7947452	0.4794255	0.0438479	0.4355776	32
0.001	100	0.8775826	0.5522790	0.3253036	0.4794255	0.2955396	0.1838860	302
0.001	1000	0.8775826	0.8775542	0.0000284	0.4794255	0.4793657	0.0000598	2087

Table 3.4: By FB-RK1-J method. Tested using the example in (3.11) with $y_0 = 0.5$. The center manifold of the system is $x_0 = \cos(0.5)$ and $z_0 = \sin(0.5)$. k is the step size, N the number of steps, the actual solutions are x_0 and z_0; the algorithm output is $\tilde{x_0}$ and $\tilde{z_0}$, and the error terms are $|\tilde{x_0} - x_0|$ and $|\tilde{z_0} - z_0|$. J is the number of iterations it takes for the algorithm to converge within the tolerance 10^{-6}.

k	N	x_0	$\tilde{x_0}$	$\lvert\tilde{x_0} - x_0\rvert$	z_0	$\tilde{z_0}$	$\lvert\tilde{z_0} - z_0\rvert$	J
0.1	10	0.8775826	0.8789740	0.0013915	0.4794255	0.4773625	0.0020630	2
0.01	10	0.8775826	0.5677667	0.3098159	0.4794255	0.3041693	0.1752563	2
0.01	100	0.8775826	0.8776829	0.0001004	0.4794255	0.4791711	0.0002545	2
0.001	10	0.8775826	0.0828374	0.7947452	0.4794255	0.0438479	0.4355776	2
0.001	100	0.8775826	0.5522790	0.3253036	0.4794255	0.2955396	0.1838860	2
0.001	1000	0.8775826	0.8775542	0.0000284	0.4794255	0.4793657	0.0000598	2

Table 3.5: By FB-RK1-GS method. Tested using the example in (3.11) with $y_0 = 0.5$. The center manifold of the system is $x_0 = \cos(0.5)$ and $z_0 = \sin(0.5)$. k is the step size, N the number of steps, the actual solutions are x_0 and z_0; the algorithm output is $\tilde{x_0}$ and $\tilde{z_0}$, and the error terms are $|\tilde{x_0} - x_0|$ and $|\tilde{z_0} - z_0|$. J is the number of iterations it takes for the algorithm to converge within the tolerance 10^{-6}.

k	N	x_0	$\tilde{x_0}$	$\lvert\tilde{x_0} - x_0\rvert$	z_0	$\tilde{z_0}$	$\lvert\tilde{z_0} - z_0\rvert$	J
0.1	10	0.8775826	0.8775559	0.0000267	0.4794255	0.4794237	0.0000018	64
0.01	10	0.8775826	0.5509032	0.3266794	0.4794255	0.2947749	0.1846505	11
0.01	100	0.8775826	0.8775399	0.0000427	0.4794255	0.4793878	0.0000378	32
0.001	10	0.8775826	0.0824370	0.7951455	0.4794255	0.0436300	0.4357956	5
0.001	100	0.8775826	0.5506333	0.3269493	0.4794255	0.2946224	0.1848031	10
0.001	1000	0.8775826	0.8775397	0.0000429	0.4794255	0.4793873	0.0000382	31

Table 3.6: By FB-RK2-GS method. Tested using the example in (3.11) with $y_0 = 0.5$. The center manifold of the system is $x_0 = \cos(0.5)$ and $z_0 = \sin(0.5)$. k is the step size, N the number of steps, the actual solutions are x_0 and z_0; the algorithm output is $\tilde{x_0}$ and $\tilde{z_0}$, and the error terms are $|\tilde{x_0} - x_0|$ and $|\tilde{z_0} - z_0|$. J is the number of iterations it takes for the algorithm to converge within the tolerance 10^{-6}.

The results of solving (3.11) are in Tables 3.4, 3.5, and 3.6. We can only choose values of k and N such that $kN \leq 1$. Otherwise, the iterations fail to converge. The sensitivity to T might be due to the fact that the test example not being globally Lipschitz.

Tables 3.4 and 3.5 are the same except $J = 2$ for all k and N in Table 3.5. The error is minimized when $kN = 1$, which is the largest value we can choose for T. Also in Tables 3.4 and 3.5 we can see the linear decrease in error as k decreases while $T = 1$. The results in Table 3.6 are unexpected; the smallest errors are obtained with $k = 0.1$ and $N = 10$. Also, for any $kN = 1$ where $k < 0.1$, the error terms fluctuate around 0.000038, failing to decrease for smaller values of k and larger values of N.

The nonlinear terms not being globally Lipschitz does not prevent the algorithm from computing to within a certain degree of precision. However, we can expect that once this assumption has been violated, some of the nice properties of the numerical schemes no longer hold, such as being able to control the error term through the choice of k and N. If we know that the system we are working with does not satisfy the Lipschitz condition, we can now expect that the algorithms compute the manifold but exhibit strange behavior. This is valuable knowledge as we turn to studying our partial differential equation.

3.2 Application

We begin our study of the bifurcations of the semilinear elliptic boundary value problem from [20]. This equation contains Long-Yih's equation, which describes permanent waves in density-stratified channels, and some terms which model viscous fluid flow between concentric cylinders [21]. An overview of Long-Yih's equation can be found in [16]. The equation is

$$u_{xx} + u_{yy} + \lambda u - u^2 = 0 \text{ where } u(x, 0) = u(x, \pi) = 0, \ -\infty < x < \infty \tag{3.12}$$

where $\lambda \in \mathbb{R}$ is the bifurcation parameter. Consider the eigenvalue problem

$$\begin{aligned} \psi_{yy} + \lambda\psi &= \gamma(\lambda)\psi, \\ \psi(0) = \psi(u) &= 0. \end{aligned}$$

It can be shown that the sine function satisfies this problem, where the orthogonal eigenvectors are $\psi_k(y) = \sin(ky)$ and the eigenvalues are $\gamma_k(\lambda) = k^2 - \lambda$. The nonlinear term is $f(u) = u^2$. Now, because of the eigenfunctions, we approximate using the Fourier sine series:

$$u = \sum_{m=0}^{\infty} u_m(x)\psi_m(y)$$

and

$$f = \sum_{m=0}^{\infty} f_m(u)\psi_m(y),$$

where out of convenience we set $\psi_0 = 0$. For a rigorous treatment, see [20].

We write the equation in (3.12) as a system of first-order ordinary differential equations:

$$\dot{u}_{(k)} = \begin{cases} \dot{u}_k & = u_{-k} \\ \dot{u}_{-k} & = \gamma_k(\lambda)u_k + f_k(u) \end{cases} \tag{3.13}$$

for $k = 0, 1, \ldots, W-1$. Formally speaking, $W - 1 \to \infty$, (3.13) $\to$ (3.12). We can write this system as

$$\dot{u}_{(k)} = R_{(k)}u_{(k)} + f_{(k)}(u),$$

where $\gamma_k(\lambda) := \gamma_k$, $\dot{u}_{(k)} = \begin{pmatrix} \dot{u}_k \\ \dot{u}_{-k} \end{pmatrix}$, $R_{(k)} = \begin{pmatrix} 0 & 1 \\ \gamma_k & 0 \end{pmatrix}$, $u_{(k)} = \begin{pmatrix} u_k \\ u_{-k} \end{pmatrix}$, and $f_{(k)}(u) = \begin{pmatrix} 0 \\ f_k(u) \end{pmatrix}$.

Now consider the approximation for the nonlinear term $f_{(k)}(u)$ give by

$$f(u) = u^2 = (\sum_{m=0}^{N-1} u_m(x)\psi_m(y))^2.$$

From the Fourier series, we have

$$\begin{aligned} f_{(k)}(u_0, u_1, \ldots, u_{W-1}) &= \Big\langle (\sum_{m=0}^{W-1} u_m(x)\psi_m(y))^2, \sin(ky) \Big\rangle \\ &= \frac{2}{\pi}\int_0^\pi \Big(\sum_{m=1}^{W-1} u_m(x)\sin(my)\Big)^2 \sin(ky)dy \\ &= \frac{2}{\pi}\int_0^\pi \sum_{n=1}^{W-1}\sum_{m=1}^{N-1} u_m(x)u_n(x)\sin(my)\sin(ny)\sin(ky)dy \\ &= \frac{2}{\pi}\sum_{n=1}^{N-1}\sum_{m=1}^{W-1} u_m(x)u_n(x)\int_0^\pi \sin(my)\sin(ny)\sin(ky)dy \end{aligned}$$

where

$$\begin{aligned} \int_0^\pi \sin(my)\sin(ny)\sin(ky)dy =& \frac{1}{4}\Big[\int_0^\pi \sin((k+n-m)y)dy + \int_0^\pi \sin((k+n+m)y)dy \\ &+ \int_0^\pi \sin((k-n+m)y)dy + \int_0^\pi \sin((k-n-m)y)dy\Big]. \end{aligned}$$

If $k+n-m$ is odd for any choices of k, n, and m, then $k+n+m$, $k-n+m$, and $k-n-m$ will all also be odd. Likewise, if $k+n-m$ is even, each of the other terms will be even as well. The cases where $k+n-m$ is even, each integral in the expression will evaluate to zero. If the term is odd, the expression will evaluate to

$$\int_0^\pi \sin(my)\sin(ny)\sin(ky)dy = \frac{4kmn}{(k+n-m)(k+n+m)(k-n+m)(k-n-m)} = P(k.m.n).$$

Let O be the set of odd positive natural numbers numbers from 1 to $W-1$ and E be the

set of even numbers from 1 to $W-1$. Then, we break the term into two cases depending on whether $k \in O$ or $k \in E$:

$$f_{(k)}(u) = \begin{cases} -\frac{8k}{\pi}\Big[\sum\limits_{n\in O}\sum\limits_{m\in O}\frac{mn}{P(k,m,n)}u_m u_n + \sum\limits_{n\in E}\sum\limits_{m\in E}\frac{mn}{P(k,m,n)}u_m u_n\Big] & \text{when } k \in O \\ -\frac{16k}{\pi}\sum\limits_{n\in O}\sum\limits_{m\in E}\frac{mn}{P(k,m,n)}u_m u_n & \text{when } k \in E. \end{cases} \tag{3.14}$$

Now that we have an ordinary differential system, we need to be able to identify which indices make up the stable, unstable, and center subspaces. In other words, we need to divide the eigenspace into the X, Y, and Z components according to the eigenvalues. The X component is composed of the eigenvectors associated with the eigenvalues with negative real part; the Z component is composed of the eigenvectors associated with the eigenvalues with positive real part; and the Y component is composed of the eigenvalues with zero real part.

To do this, we use a change of variable from u to v to obtain a system whose linear component is in Jordan canonical form, at which point the eigenspace can be manipulated into the different components.

There are two cases: when $k = \sqrt{\lambda}$ and when $k \neq \sqrt{\lambda}$. In the first case we have

$$\begin{pmatrix} \dot{u}_k \\ \dot{u}_{-k} \end{pmatrix} = \begin{pmatrix} 0 & 1 \\ 0 & 0 \end{pmatrix}\begin{pmatrix} u_k \\ u_{-k} \end{pmatrix} + \begin{pmatrix} 0 \\ f_k(u) \end{pmatrix}. \tag{3.15}$$

The system in (3.15) has two zero eigenvalues and cannot be simplified further. So, we let $\begin{pmatrix} v_k \\ v_{-k} \end{pmatrix} = \begin{pmatrix} u_k \\ u_{-k} \end{pmatrix}$ and

$$\begin{pmatrix} \dot{v}_k \\ \dot{v}_{-k} \end{pmatrix} = \begin{pmatrix} 0 & 1 \\ 0 & 0 \end{pmatrix}\begin{pmatrix} v_k \\ v_{-k} \end{pmatrix} + \begin{pmatrix} 0 \\ f_k(v) \end{pmatrix}. \tag{3.16}$$

In the second case, diagonalize the matrix $R_{(k)} = T_{(k)}D_{(k)}T_{(k)}^{-1}$:

$$\begin{pmatrix} 0 & 1 \\ \gamma_k & 0 \end{pmatrix} = \begin{pmatrix} 1 & -1 \\ \sqrt{\gamma_k} & \sqrt{\gamma_k} \end{pmatrix}\begin{pmatrix} \sqrt{\gamma_k} & 0 \\ 0 & -\sqrt{\gamma_k} \end{pmatrix}\begin{pmatrix} \frac{1}{2} & \frac{1}{2\sqrt{\gamma_k}} \\ -\frac{1}{2} & \frac{1}{2\sqrt{\gamma_k}} \end{pmatrix}.$$

We do a change of variable by letting $v_{(k)} = T_{(k)}^{-1}u_{(k)}$. Then,

$$\begin{aligned} \dot{v}_{(k)} &= T_{(k)}^{-1}\dot{u}_{(k)} \\ \dot{v}_{(k)} &= T_{(k)}^{-1}(A_{(k)}u_{(k)} + f_{(k)}(u) \\ \dot{v}_{(k)} &= T_{(k)}^{-1}A_{(k)}T_{(k)}v_{(k)} + T_{(k)}^{-1}f_{(k)}(Tv) \\ \dot{v}_{(k)} &= D_{(k)}v_{(k)} + T_{(k)}^{-1}f_{(k)}(Tv) \\ \begin{pmatrix} \dot{v}_k \\ \dot{v}_{-k} \end{pmatrix} &= \begin{pmatrix} \sqrt{\gamma_k} & 0 \\ 0 & -\sqrt{\gamma_k} \end{pmatrix}\begin{pmatrix} v_k \\ v_{-k} \end{pmatrix} + \frac{1}{2}\begin{pmatrix} \frac{1}{\sqrt{\gamma_k}}f_k(Tv) \\ \frac{1}{\sqrt{\gamma_k}}f_k(Tv) \end{pmatrix}. \end{aligned} \tag{3.17}$$

In order to see how this now fits the form of the ordinary differential system in (1.7), consider the system in which the second case applies for all k. We can stack the submatrices block-diagonally: $D = 0 \oplus D_{(1)} \oplus D_{(2)} \oplus \cdots \oplus D_{(W-1)}$. Let j be the index such that $\sqrt{\gamma_{j+1}} > \sqrt{\lambda}$. Then we apply a transformation matrix to get the linear term of the full system to be

$$\begin{pmatrix} -\sqrt{\gamma_{W-1}} & & & & & & & & & & \\ & \ddots & & & & & & & & & \\ & & 0 & & & & & & & & \\ & & & \ddots & & & & & & & \\ & & & & -\sqrt{\gamma_1} & & & & & & \\ & & & & & \sqrt{\gamma_1} & & & & & \\ & & & & & & \ddots & & & & \\ & & & & & & & 0 & & & \\ & & & & & & & & \ddots & & \\ & & & & & & & & & \sqrt{\gamma_{W-1}} \end{pmatrix} \left(\begin{array}{c} v_{-(W-1)} \\ \vdots \\ \hline v_{-j} \\ \vdots \\ v_{-1} \\ v_0 \\ v_1 \\ \vdots \\ v_j \\ \hline \vdots \\ v_{W-1} \end{array}\right),$$

where the v vector corresponds to $\left(\begin{array}{c} X \\ \hline Y \\ \hline Z \end{array}\right)$. Otherwise, consider the system in which there is an index j such that $R_{(j)} = \begin{pmatrix} 0 & 1 \\ 0 & 0 \end{pmatrix}$. Then, we stack the matrices $D = 0 \oplus D_{(1)} \oplus D_{(2)} \oplus \cdots \oplus R_{(j)} \oplus \cdots \oplus D_{(W-1)}$. Applying the same transformation matrix as before gives

$$\begin{pmatrix} -\sqrt{\gamma_{W-1}} & & & & & & & & & & \\ & \ddots & & & & & & & & & \\ & & 0 & & & & & & & & \\ & & & \ddots & & & & & & & \\ & & & & -\sqrt{\gamma_1} & & & & & & \\ & & \vdots & & & 0 & & & & & \\ & & & & & & \sqrt{\gamma_1} & & & & \\ & & & & & & & \ddots & & & \\ & & 1 & & & \cdots & & & 0 & & \\ & & & & & & & & & \ddots & \\ & & & & & & & & & & \sqrt{\gamma_{W-1}} \end{pmatrix} \left(\begin{array}{c} v_{-(W-1)} \\ \vdots \\ \hline v_{-j} \\ \vdots \\ v_{-1} \\ v_0 \\ v_1 \\ \vdots \\ v_j \\ \hline \vdots \\ v_{W-1} \end{array}\right).$$

The stable component X for the system is the set $\{v_k : k \in \mathbb{Z} \cap [-W+1, -\sqrt{\lambda})\}$. The unstable component Z is the set $\{v_k : k \in \mathbb{Z} \cap (\sqrt{\lambda}, W-1]\}$, and the center component Y is the set $\{v_k : k \in \mathbb{Z} \cap [-\sqrt{\lambda}, \sqrt{\lambda}]\}$.

Now we need to implement the change of variables in the nonlinear term. In other words, find $f_k(Tv)$. First consider a system in which we have both types of subsystems. This means that for the the $f_k(v)$ when $k = \sqrt{\lambda}$, we have to apply two different changes of variables in

the summation terms:

$$u_k = \begin{cases} v_k & \text{when } \sqrt{\lambda} = k \\ v_k - v_{-k} & \text{when } \sqrt{\lambda} \neq k, \end{cases} \tag{3.18}$$

and thus have to separate out every time we have an index n or $m = \sqrt{\lambda}$. The resulting nonlinear term is included in Appendix 4.1.

For the rest of $f_k(Tv)$ in the case of the system with both types of subsystems and all the nonlinear terms in the case of the system with only subsystems of the form (3.17), the nonlinear term we get under the change of variable is obtained simply by substituting in $u_k = v_k - v_{-k}$:

$$f_k(v) = \begin{cases} -\frac{8k}{\pi}\Big[\sum\limits_{n\in O}\sum\limits_{m\in O}\frac{mn}{P(k,m,n)}(v_m - v_{-m})(v_n - v_{-n}) \\ +\sum\limits_{n\in E}\sum\limits_{m\in E}\frac{mn}{P(k,m,n)}(v_m - v_{-m})(v_n - v_{-n})\Big] & \text{for } k \in O \\ -\frac{16k}{\pi}\sum\limits_{n\in O}\sum\limits_{m\in E}\frac{mn}{P(k,m,n)}(v_m - v_{-m})(v_n - v_{-n}) & \text{for } k \in E. \end{cases} \tag{3.19}$$

We have that $\beta_y = -\sqrt{\gamma_{-j}}$, $\alpha_y = \sqrt{\gamma_j}$, $\alpha_x = -\sqrt{\gamma_{-j-1}}$, and $\beta_z = \sqrt{\gamma_{j+1}}$. K_x, K_y, and $K_z = 1$. We cannot estimate δ_x, δ_y, and δ_z because the nonlinear term is not globally Lipschitz continuous. One common technique for dealing with this difficulty is to apply a cutoff function as discussed in [24]. An example is in [19]. However, working with the system in the original form reveals interesting behavior in our algorithm that is worth noting for future study. Hence, we leave these constants ambiguous.

The system in v is now in the form of our framework. We implement the system in (3.13) with the nonlinear term in (3.14) in Fortran to perform bifurcation analysis using the package AUTO [29]. In Figure 3-1, notice that each bifurcation starts at an integer square. As λ grows in a positive direction, it will move pairs (u_k, u_{-k}) into the center subspace, creating Hopf bifurcations.

Recall that the center manifold is $\mathcal{M}_c = \{u_0 \in E : u(t, u_0) \in \mathcal{F}_\sigma\}$. Let u_0 be a steady state of the system in (3.13) for a given bifurcation parameter λ, and define $u(t, u_0) = u_0$. Then, $\|u(t, u_0)\|_\sigma = \sup_{t\in\mathbb{R}} e^{-\sigma(t)t}\|u_0\|$, where $\|u_0\|$ is some finite constant. By the definition of $\sigma(t)$ in (1.8), $e^{-\sigma(t)t}$ will be bounded for $t \in \mathbb{R}$, so $\|u_0\|_\sigma < \infty$ and $u_0 \in \mathcal{M}_c$. We have then that each steady state shown in Figure 3-1 will be on the manifold. We arbitrarily pick points 39, 72, and 94 to study further. Once we have our steady states in terms of u, we can use the change of variables $v_{(k)} = T^{-1}_{(k)} u_{(k)}$ to get

$$\begin{aligned} v_k &= \frac{1}{2}u_k + \frac{1}{2\sqrt{\gamma_k}}u_{-k} \\ v_{-k} &= -\frac{1}{2}u_k + \frac{1}{2\sqrt{\gamma_k}}u_{-k} \end{aligned} \tag{3.20}$$

to calculate the steady states in terms of v. These example points, as well as the results of the change of variable, are described in Table 4.1 in Appendix 4.2.

The X, Y, and Z components of points 39, 72, and 94 will be determined by their

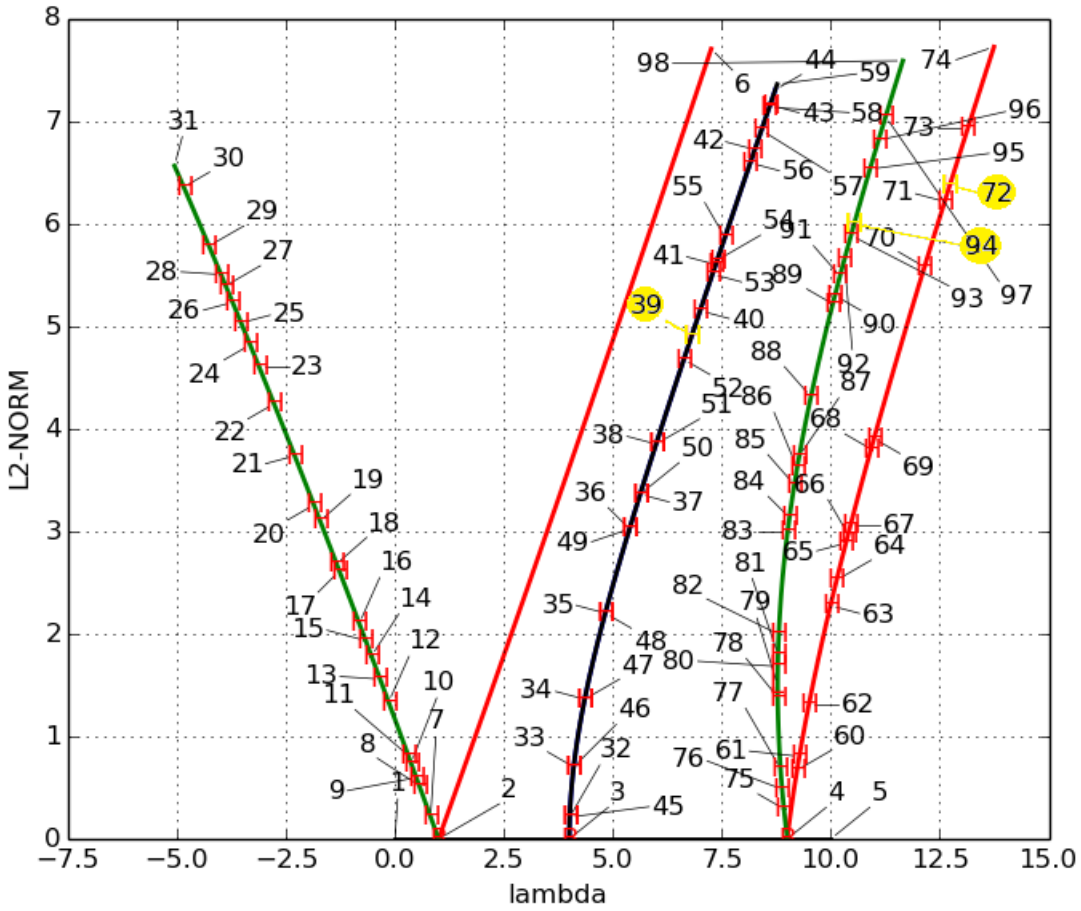

Figure 3-1: Bifurcation diagram obtained from analyzing the system in (3.15) with nonlinear term given by (3.14) choosing $W - 1 = 12$. The plot is λ versus $\|\cdot\|_2$. Each bifurcation starts at a positive integer; the ones shown here are 1, 4, and 9, which agrees with analysis of our system using the change of variables. Each label represents a point computed and output in AUTO.

respective λ values. We need to use the system as written in terms of v when using our algorithm. Because $\sqrt{\lambda} \notin O \cup E$ for any of our steady states, we implement the system in (3.17) with the nonlinear term in (3.19) in Julia [3]. We implement the entire system as a function without decomposing the vector into the different subspaces, then construct artificial functions $f(x, y, z)$, $g(x, y, z)$, and $h(x, y, z)$, corresponding to inputs in our algorithm, that assemble the different sections into the vector v, call the function with the whole system, and then disassemble the result, returning only the section of the vector corresponding to the X, Y, or Z component, respectively. This assembly and disassembly is what allows us to evaluate each component separately from the whole vector for our forward-backward algorithm. A diagram of the process can be found in Figure 3-2.

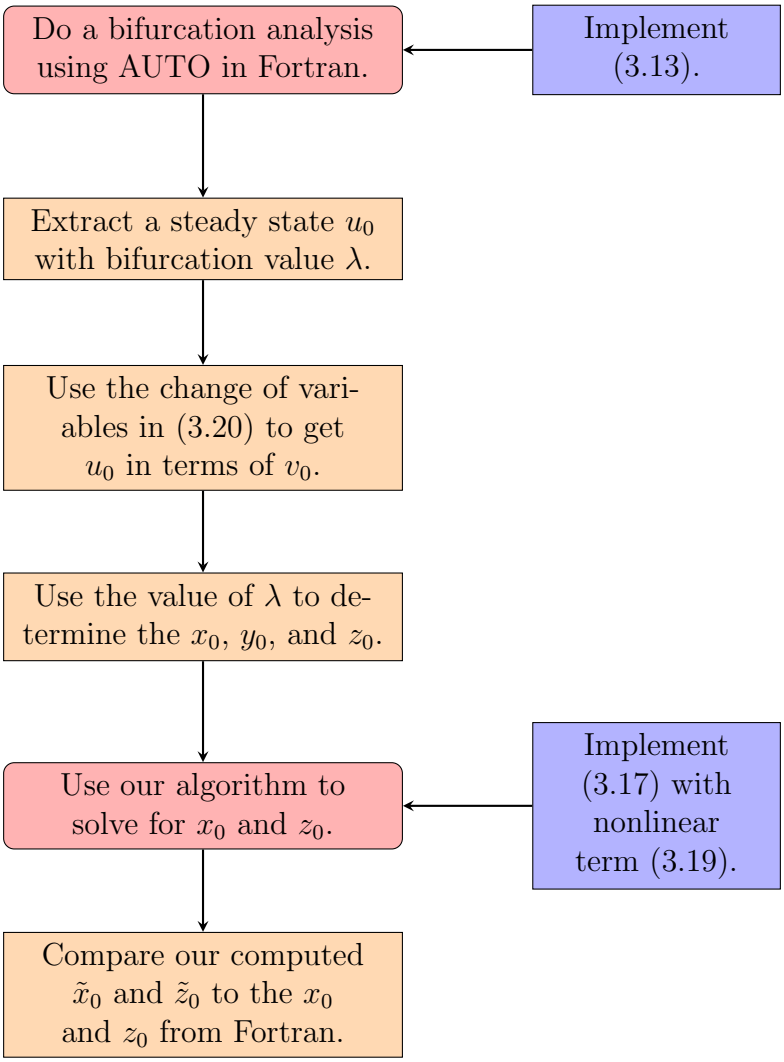

Figure 3-2: A flowchart detailing our process of analysis of the steady states of (3.13) using our algorithm.

Algorithm:	FB-RK1-J	FB-RK1-GS	FB-RK2-J	FB-RK2-GS
k, N	0.10, 20	0.02, 10	0.16, 10	0.10, 3
$\|v - \hat{v}\|_2$				
$SS - 39 - v$	0.0044979	0.5675686	0.0174135	0.4577755
$SS - 72 - v$	0.0000091	0.1903187	0.0003783	0.1254002
$SS - 94 - v$	0.0000403	0.3341094	0.0009786	0.2291970
$\|v - \hat{v}\|_2 / \|v\|_2$				
$SS - 39 - v$	0.0012961	0.1635509	0.0050179	0.1319128
$SS - 72 - v$	0.0000020	0.0422346	0.0000840	0.0278282
$SS - 94 - v$	0.0000095	0.0788823	0.0002311	0.0541127
J				
$SS - 39 - v$	252	494	1331	249
$SS - 72 - v$	78	526	407	82
$SS - 94 - v$	64	9	326	81

Table 3.7: A comparison of the effectiveness of different methods in computing the center manifold for the steady states 39, 72, and 94 in Figure 3-1, on norm, relative norm, and number of steps to convergence. The k, N were obtained experimentally; more precise values are possible. Tested with a tolerance of 10^{-6}.

We study the performance of the four different algorithms in this context. The results are in Figure 3.7 and are quite surprising. We include the relative error to help contextualize how accurate the approximations are as some of the values are quite small. First note that for each method, we select a large k and small N. These numbers are obtained with rough numerical experimentation, but can be taken as a good approximation of what the optimal values would be. The error tends to get worse when we move off of these k and N values, even if we keep T constant as we increase N and decrease k. This is very unlike the results we saw in Section 3.1, where the error tended to decrease whenever we proportionally shrank k and increased N. Also, whereas in Section 3.1 we saw that each algorithm failed to converge once we increased $T > 1$, here we have very different T sensitivities for our different algorithms. The Gauss-Seidel methods, FB-RK1-GS and FB-RK2-GS, are the most sensitive and converge only for $T < 0.2$, $T < 0.3$, respectively. This helps explain why these methods returned such high errors, as the approximations have the lowest error for $T \approx 2$. The Gauss-Seidel methods also do not show a faster rate of convergence than the Jacobi methods. On top of that, the RK2 update does not improve the error overall from the Jacobi method.

$SS-94-v$		$\tilde{SS}-94-v$		$\lvert v_k-\tilde{v}_k\rvert$	$\frac{\lvert v_k-\tilde{v}_k\rvert}{\lvert v_k\rvert}$
v_{12}	0.0000000	$\tilde{v}_{12}$	0.0000000	0.0000000	NA
v_{11}	0.0071938	$\tilde{v}_{11}$	0.0068441	0.0003497	0.0486095
v_{10}	0.0000000	$\tilde{v}_{10}$	0.0000000	0.0000000	NA
v_9	0.0232603	$\tilde{v}_9$	0.0229927	0.0002676	0.0115038
v_8	0.0000000	$\tilde{v}_8$	0.0000000	0.0000000	NA
v_7	-0.0010533	$\tilde{v}_7$	0.0034394	0.0044926	4.2654521
v_6	0.0000000	$\tilde{v}_6$	0.0000000	0.0000000	NA
v_5	-0.5343186	$\tilde{v}_5$	-0.5123375	0.0219811	0.0411391
v_4	0.0000000	$\tilde{v}_4$	0.0000000	0.0000000	NA
v_3	-2.5462873	v_3	-2.5462873	0.0000000	NA
v_2	0.0000000	v_2	0.0000000	0.0000000	NA
v_1	1.4833230	v_1	1.4833230	0.0000000	NA
v_0	0.0000000	v_0	0.0000000	0.0000000	NA
v_{-1}	-1.4833230	v_{-1}	-1.4833230	0.0000000	NA
v_{-2}	0.0000000	v_{-2}	0.0000000	0.0000000	NA
v_{-3}	2.5462873	v_{-3}	2.5462873	0.0000000	NA
v_{-4}	0.0000000	$\tilde{v}_{-4}$	0.0000000	0.0000000	NA
v_{-5}	0.5343186	$\tilde{v}_{-5}$	0.5123375	0.0219811	0.0411391
v_{-6}	0.0000000	$\tilde{v}_{-6}$	0.0000000	0.0000000	NA
v_{-7}	0.0010533	$\tilde{v}_{-7}$	-0.0034394	0.0044926	4.2654521
v_{-8}	0.0000000	$\tilde{v}_{-8}$	0.0000000	0.0000000	NA
v_{-9}	-0.0232603	$\tilde{v}_{-9}$	-0.0229927	0.0002676	0.0115038
v_{-10}	0.0000000	$\tilde{v}_{-10}$	0.0000000	0.0000000	NA
v_{-11}	-0.0071938	$\tilde{v}_{-11}$	-0.0068441	0.0003497	0.0486094
v_{-12}	0.0000000	$\tilde{v}_{-12}$	0.0000000	0.0000000	NA
$\lVert v-\tilde{v}\rVert_2 = 0.0317351$				$\frac{\lVert v-\tilde{v}\rVert_2}{\lVert v\rVert_2} = 0.0074926$	

Table 3.8: By FB-RK2-J method. $W-1=12$, $\lambda = 10.5329535$. Tolerance is 10^{-6}, $k=0.008$, and $N=100$, converges in $J=636$. Center Manifold of system: $x_0=(v_{-4},\cdots,v_{-12})$, and $z_0=(v_4,\cdots,v_{12})$. $|v_k-\tilde{v}_k|$ is the difference between each individual term and $\|v-\tilde{v}\|_2$ is the error using the ℓ_2 norm.

$SS-94-v$		$\tilde{SS}-94$		$\lvert v_k-\tilde{v}_k\rvert$	$\frac{\lvert v_k-\tilde{v}_k\rvert}{\lvert v_k\rvert}$
v_{12}	0.0000000	$\tilde{v}_{12}$	0.0000000	0.0000000	NA
v_{11}	0.0071938	$\tilde{v}_{11}$	0.0071934	0.0000004	0.0000560
v_{10}	0.0000000	$\tilde{v}_{10}$	0.0000000	0.0000000	NA
v_9	0.0232603	$\tilde{v}_9$	0.0232600	0.0000002	0.0000103
v_8	0.0000000	$\tilde{v}_8$	0.0000000	0.0000000	NA
v_7	-0.0010533	$\tilde{v}_7$	-0.0001047	0.0000061	0.0057517
v_6	0.0000000	$\tilde{v}_6$	0.0000000	0.0000000	NA
v_5	-0.5343186	$\tilde{v}_5$	-0.5342908	0.0000278	0.0000521
v_4	0.0000000	$\tilde{v}_4$	0.0000000	0.0000000	NA
v_3	-2.5462873	v_3	-2.5462873	0.0000000	NA
v_2	0.0000000	v_2	0.0000000	0.0000000	NA
v_1	1.4833230	v_1	1.4833230	0.0000000	NA
v_0	0.0000000	v_0	0.0000000	0.0000000	NA
v_{-1}	-1.4833230	v_{-1}	-1.4833230	0.0000000	NA
v_{-2}	0.0000000	v_{-2}	0.0000000	0.0000000	NA
v_{-3}	2.5462873	v_{-3}	2.5462873	0.0000000	NA
v_{-4}	0.0000000	$\tilde{v}_{-4}$	0.0000000	0.0000000	NA
v_{-5}	0.5343186	$\tilde{v}_{-5}$	0.5342908	0.0000278	0.0000521
v_{-6}	0.0000000	$\tilde{v}_{-6}$	0.0000000	0.0000000	NA
v_{-7}	0.0010533	$\tilde{v}_{-7}$	0.0001047	0.0000061	0.0057517
v_{-8}	0.0000000	$\tilde{v}_{-8}$	0.0000000	0.0000000	NA
v_{-9}	-0.0232603	$\tilde{v}_{-9}$	-0.0232600	0.0000002	0.0000103
v_{-10}	0.0000000	$\tilde{v}_{-10}$	0.0000000	0.0000000	NA
v_{-11}	-0.0071938	$\tilde{v}_{-11}$	-0.0071934	0.0000004	0.0000560
v_{-12}	0.0000000	$\tilde{v}_{-12}$	0.0000000	0.0000000	NA
$\lVert v-\tilde{v}\rVert_2 = 0.0000403$				$\frac{\lVert v-\tilde{v}\rVert_2}{\lVert v\rVert_2} = 0.000010$	

Table 3.9: By FB-RK1-J method. $W-1=12$, $\lambda = 10.5329535$. Tolerance is 10^{-6}, $k=0.1$, and $N=20$, converges in $J=112$. Center Manifold of system: $x_0=(v_{-4},\cdots,v_{-12})$, and $z_0=(v_4,\cdots,v_{12})$. $|v_k-\tilde{v}_k|$ is the difference between each individual term and $\|v-\tilde{v}\|_2$ is the error using the ℓ_2 norm. The relative error for each term is $\frac{|v_k-\tilde{v}_k|}{|v_k|}$, and the relative error using the ℓ_2 norm is $\frac{\|v-\tilde{v}\|_2}{\|v\|_2}$.

We break down the differences between the point-by-point computations for $SS-94-v$ obtained by the FB-RK2-J and the FB-RK1-J methods. These results are in Tables 3.8 and 3.9. In Table 3.8, we can see that we only get a very rough approximation, even though we use slightly more optimal values of k and N. The FB-RK2-J method is very sensitive to the values of k and N and only converges for $T<0.82$, which is much lower than the value of T we can pick when using the FB-RK1-J method. FB-RK1-J is less sensitive to k and N, and so we can choose these values for $T=2$.

The results from using the Jacobi method are in Table 3.9. The algorithm converges quickly with $J=160$ and we get relative errors of roughly 10^{-5}. This is roughly the lowest

error we get when solving for the manifold at this point.

While this is a useful example for showing the superiority of the FB-RK1-J method, it is also worthwhile to show that the algorithm can compute the manifold for a point obtained from a bifurcation analysis with higher mode. Studying the print out of point 94 in Tables 3.8 and 3.9 shows that we do not quite have the steady decrease in magnitude of points as we move farther down the vector. This indicates that we have not allowed the vector to be of large enough dimension to approximate the system in 3.12 very well. While this does not affect the demonstration of the accuracy of our algorithm, we want to make clear that our algorithm can be useful when trying to approximate the system itself.

We run the bifurcation analysis in AUTO and pick $W - 1 = 15$ based on some experimentation.

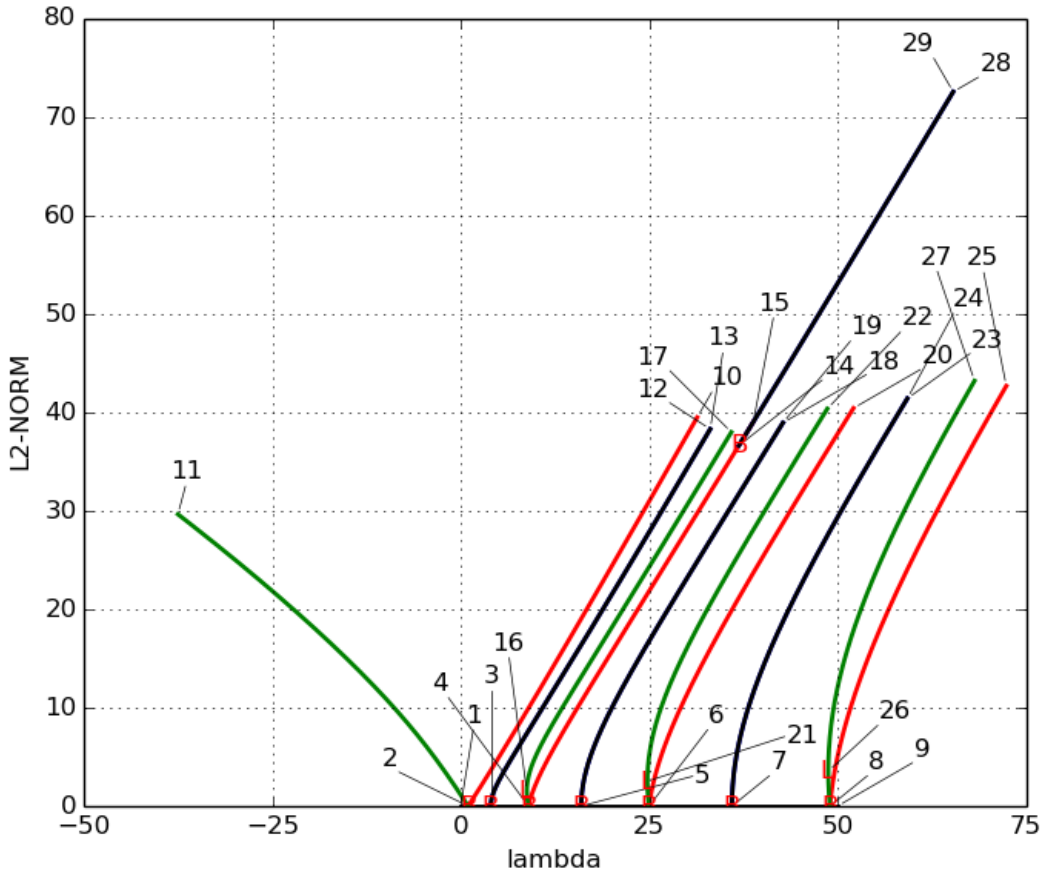

Figure 3-3: Bifurcation diagram obtained from analyzing the system in (3.15) with nonlinear term given by (3.14) choosing $W - 1 = 15$. The plot is λ versus $\|\cdot\|_2$. Each bifurcation starts at a positive integer; the ones shown here are 1, 4, 9, 16, 25, 36, and 49, which agrees with analysis of our system using the change of variables. We suppress the labeling of points for the sake of clarity.

We then pick point 428 from the output, which is not shown in Figure 3-3, to demonstrate our algorithm. The results for the X component are in Table 3.10; the Z component is just

the inverse of the X and has the same error terms. The table shows that we get error terms of roughly 10^{-5} for $W - 1 = 15$

	x_k	$\tilde{x_k}$	$\lvert\tilde{x_k} - x_k\rvert$	$\lvert\tilde{x_k} - x_k\rvert/\lvert x_k\rvert$
v_{-4}	0.0000000	0.0000000	0.0000000	NA
v_{-5}	0.4469886	0.4469659	0.0000227	0.0000508
v_{-6}	0.0000000	0.0000000	0.0000000	NA
v_{-7}	-0.0075704	-0.0075749	0.0000045	0.0005944
v_{-8}	0.0000000	0.0000000	0.0000000	NA
v_{-9}	-0.0198598	-0.0198595	0.0000003	0.0000134
v_{-10}	0.0000000	0.0000000	0.0000000	NA
v_{-11}	-0.0056845	-0.0056842	0.0000003	0.0000571
v_{-12}	0.0000000	0.0000000	0.0000000	NA
v_{-13}	-0.0014178	-0.0014177	0.0000001	0.0000689
v_{-14}	0.0000000	0.0000000	0.0000000	NA
v_{-15}	-0.0004995	-0.0004995	0.0000000	0.0000519
	$\lVert\tilde{v} - v\rVert_2$	0.0000328	$\lVert\tilde{v} - v\rVert_2/\lVert v\rVert_2$	0.0000085

Table 3.10: By FB-RK1-J method. Tested with point 428 using $W-1 = 15$, $\lambda = 10.1794919$, $k = 0.1$, and $N = 20$ with a tolerance of 10^{-6}. Converges in $J = 100$.

That the simplest algorithm converges the fastest and by far the most accurately presents some upsides as well as some problems. Using the center manifold reduction to do the bifurcation analysis presents an issue in that the computation time would include all of the time it takes to compute the manifold at each iteration. The ability of the Jacobi method to compute both the best and the fastest has a significant upside in that it reduces the amount of time we would expect it to take to compute the manifold fairly accurately and thus make the reduction more feasible.

If the Jacobi method is the absolute best for all points we wish to compute, then we have limited control over our error term; there is an upper bound on how accurately we can expect to compute the manifold. The strange behavior we see in our numerical methods is probably due to the fact that the system is not Lipschitz; we could test this by implementing the cutoff function, which we do not do here. However, as our goal is to analyze the system in (3.12), it is useful to understand why our this behavior is occurring and what we might be able to do to mitigate it without modifying the nonlinear term.

3.2.1 Discussion

We have found that our forward-backward method is useful in computing the center manifold, as well as some interesting opportunities for future work. There are two major theoretical extensions to make. One is to complete the proof for the existence of a $\mathcal{C}^k$ manifold. One of the main difficulties is to determine how to extend our assumptions. The second is to investigate the optimal truncation value T for our method based on the $\mathcal{T}$ map. This might

provide insight into why seemingly low values of $T = 1$ and $T = 2$ are enough to approximate infinity in this context.

Our computational work has several unexpected results which warrant investigation. One of the first steps in investigating these results is to perform a stability analysis for each algorithm. The stability analysis would determine the dependence of the spectral radius for each algorithm on δ_x, δ_y, and δ_z. Knowing how each algorithm is affected by the value of the Lipschitz constant might explain the behavior when we apply them to systems with nonlinear terms that are not globally Lipschitz. It also should help explain the different behavior among the four methods. Our work on the stability analysis is currently ongoing with Professor Chi-Kwong Li.

Another interesting addition is to write a forward-backward algorithm based on the boundary value problem in Proposition 2.2.7 to solve for the derivative of the manifold and compare the results to an example for which the exact derivative is known. Finally, a fairly crucial extension is to perform a bifurcation analysis using the center manifold reduction based on our algorithm and compare it to the bifurcation analysis of the full system. While at this stage we could do this experimentally, we need to develop our understanding of our methods in order to optimally implement the reduction.

The ultimate goal would be to have a systematic approach that can be applied to any differential system with a center manifold to determine the best way to implement a center manifold reduction using our algorithm and to give an estimate of how accurate the results of the algorithm will be given different methods.

Chapter 4

Appendix

4.1 Nonlinear Term

This is the nonlinear term that we get for the subsystem $v_{(k)}$ where $k = \sqrt{\lambda}$. To be able to define the term completely, we again need two different cases. First, let $\sqrt{\lambda} \in O$, and define $O_1 = O \setminus \{\sqrt{\lambda}\}$. Then, we can do the change of variables to get

$$f_k(v) = \begin{cases} -\frac{8k}{\pi}\Big[\sum\limits_{n\in O_1} \sum\limits_{m\in O_1} \frac{mn}{P(k,m,n)}(v_m - v_{-m})(v_n - v_{-n}) \\ +2 \sum\limits_{m\in O_1} \frac{m\sqrt{\lambda}}{P(k,m,\sqrt{\lambda})}(v_m - v_{-m})v_{\sqrt{\lambda}} + \frac{\lambda}{k^2(k^2-4\lambda)}v_{\sqrt{\lambda}}^2 \\ + \sum\limits_{n\in E} \sum\limits_{m\in E} \frac{mn}{P(k,m,n)}(v_m - v_{-m})(v_n - v_{-n})\Big] & \text{for } k \in O \\ -\frac{16k}{\pi}\Big[\sum\limits_{n\in O_1} \sum\limits_{m\in E} \frac{mn}{P(k,m,n)}(v_m - v_{-m})(v_n - v_{-n}) \\ + \sum\limits_{m\in E} \frac{m\sqrt{\lambda}}{P(k,m,\sqrt{\lambda})}(v_m - v_{-m})v_{\sqrt{\lambda}}\Big] & \text{for } k \in E. \end{cases}$$

Next, let $\sqrt{\lambda} \in E$, and define $E_1 = E \setminus \{\sqrt{\lambda}\}$.

$$f_k(v) = \begin{cases} -\frac{8k}{\pi}\Big[\sum\limits_{n\in E_1} \sum\limits_{m\in E_1} \frac{mn}{P(k,m,n)}(v_m - v_{-m})(v_n - v_{-n}) \\ +2 \sum\limits_{m\in E_1} \frac{m\sqrt{\lambda}}{P(k,m,\sqrt{\lambda})}(v_m - v_{-m})v_{\sqrt{\lambda}} + \frac{\lambda}{k^2(k^2-4\lambda)}v_{\sqrt{\lambda}}^2 \\ + \sum\limits_{n\in O} \sum\limits_{m\in O} \frac{mn}{P(k,m,n)}(v_m - v_{-m})(v_n - v_{-n})\Big] & \text{for } k \in O \\ -\frac{16k}{\pi}\Big[\sum\limits_{n\in O} \sum\limits_{m\in E_1} \frac{mn}{P(k,m,n)}(v_m - v_{-m})(v_n - v_{-n}) \\ + \sum\limits_{m\in O} \frac{m\sqrt{\lambda}}{P(k,m,\sqrt{\lambda})}(v_m - v_{-m})v_{\sqrt{\lambda}}\Big] & \text{for } k \in E. \end{cases}$$

In order to implement the function to be robust for any value of λ, as we would if we were doing a bifurcation analysis on the reduced system, we would need to implement all three cases of the nonlinear term. However, we only consider single points on the manifold. This allows us to be judicious in our choice of λ so that we know $\lambda \notin O \cup E$, and we do not need to provide for this case in our code.

4.2 Steady State Tables

		$SS-39-u$	$SS-72-u$	$SS-94-u$
u_1	u_{12}	-0.0000074	0.0000000	0.0000000
u_2	u_{11}	0.0021231	0.0160645	0.0143877
u_3	u_{10}	-0.0010662	0.0000000	0.0000000
u_4	u_9	0.0091051	-0.0124957	0.0465206
u_5	u_8	-0.0084588	0.0000000	0.0000000
u_6	u_7	0.0341687	0.2976874	-0.0021065
u_7	u_6	0.0079876	0.0000000	0.0000000
u_8	u_5	-0.0401509	-0.6138524	-1.0686373
u_9	u_4	0.6353136	0.0000000	0.0000000
u_{10}	u_3	-1.1058651	5.9771073	-5.0925745
u_{11}	u_2	3.5418302	0.0000000	0.0000000
u_{12}	u_1	3.1482812	2.1025194	2.9666459
u_{13}	u_0	0.0000000	0.0000000	0.0000000
u_{14}	u_{-1}	0.0000000	0.0000000	0.0000000
u_{15}	u_{-2}	0.0000000	0.0000000	0.0000000
u_{16}	u_{-3}	0.0000000	0.0000000	0.0000000
u_{17}	u_{-4}	0.0000000	0.0000000	0.0000000
u_{18}	u_{-5}	0.0000000	0.0000000	0.0000000
u_{19}	u_{-6}	0.0000000	0.0000000	0.0000000
u_{20}	u_{-7}	0.0000000	0.0000000	0.0000000
u_{21}	u_{-8}	0.0000000	0.0000000	0.0000000
u_{22}	u_{-9}	0.0000000	0.0000000	0.0000000
u_{23}	u_{-10}	0.0000000	0.0000000	0.0000000
u_{24}	u_{-11}	0.0000000	0.0000000	0.0000000
u_{25}	u_{-12}	0.0000000	0.0000000	0.0000000
	λ:	6.8099949	12.7303878	10.532953

Table 4.1: Points 39, 72, and 94 in Figure 3-1 in terms of u, attained by bifurcation analysis on (3.13) with $W-1=12$. The indices that range from 1 to 25 are imposed by Fortran; the corresponding indices from 12 to -12 are from our system.

	$SS-39-v$	$SS-72-v$	$SS-94-v$
v_{12}	-0.0000037	0.0000000	0.0000000
v_{11}	0.0010616	0.0080322	0.0071938
v_{10}	-0.0005331	0.0000000	0.0000000
v_9	0.0045526	-0.0062479	0.0232602
v_8	-0.0042294	0.0000000	0.0000000
v_7	0.0170844	0.1488437	-0.0010533
v_6	0.0039938	0.0000000	0.0000000
v_5	-0.0200754	-0.3069262	0.5343186
v_4	0.3176568	0.0000000	0.0000000
v_3	-0.5529326	2.9885537	-2.5462872
v_2	1.7709151	0.0000000	0.0000000
v_1	1.5741406	1.0512597	1.4833230
v_0	0.0000000	0.0000000	0.0000000
v_{-1}	-1.5741406	-1.0512597191	-1.4833230
v_{-2}	-1.7709151	0.0000000	0.0000000
v_{-3}	0.5529326	-2.9885537	2.5462872
v_{-4}	-0.3176568	0.0000000	0.0000000
v_{-5}	0.0200754	0.3069262	-0.5343186
v_{-6}	-0.0039938	0.0000000	0.0000000
v_{-7}	-0.0170844	-0.1488437	0.0010533
v_{-8}	0.0042294	0.0000000	0.0000000
v_{-9}	-0.0045526	0.0062479	0.0232602
v_{-10}	0.0005331	0.0000000	0.0000000
v_{-11}	-0.0010616	-0.0080322	0.0071938
v_{-12}	0.0000037	0.0000000	0.0000000
	6.8099949	12.7303878	10.532953

Table 4.2: Points 39, 72, and 94 in Figure 3-1 in terms of v, attained by bifurcation analysis on (3.13) with $W-1=12$. The values for v are computed according to the transformation in (3.20).

4.3 Julia Code

Julia is a mathematical, array-based programming language that resembles Python in syntax. To assist the reader in understanding and applying our methods, we include the explicit implementations of two of our algorithms in this language.

The first algorithm we include is the one-dimensional FB-RK2-G method. This is the code we used to achieve the most accurate approximation of the manifold for (3.2). However, we need to slightly modify our code to solve systems that have multi-dimensional components that take on complex values. We include the FB-RK1-J method implemented in this way because it is the code that we used to get the most accurate approximations for the system in (3.13).

Algorithm 4 FB-RK2-G Method, One Dimensional

```
function fb-rk2-g(f, g, h, y0, k, N, tol)
x = zeros(2N+1)
y = zeros(2N+1)
z = zeros(2N+1)
px = zeros(2N+1)
py = zeros(2N+1)
pz = zeros(2N+1)
y[N+1] = y0
error = 1
j = 0
while error > tol && error < 1000 do
    for i = 1:N do
        y[N+i+1] = y[N+i] + k[g(px[N+i], y[N+i], pz[N+i])+g(px[N+i+1], py[N+i+1], pz[N+i+1])]/2
        y[N-i+1] = y[N-i+2] - k[g(px[N-i+2], y[N-i+2], pz[N-i+2])+g(px[N-i+1], py[N-i+1], pz[N-i+1])]/2
    end for
    for i = 1:2N do
        x[i+1] = x[i] + k[f(x[i],y[i],pz[i])+f(px[i+1],py[i+1],pz[i+1])]/2
        z[2N-i+1] = z[2N-i+2] - k[h(px[2N-i+2], y[2N-i+2], z[2N-i+2])+h(px[2N-i+1], py[2N-i+1], pz[2N-i+1])]/2
    end for
    error = norm(hcat(x, y, z) - hcat(px, py, pz))
    j = j+1
    px[:] = x[:]
    py[:] = y[:]
    pz[:] = z[:]
end while
return x[N+1], z[N+1], j
```

Algorithm 5 FB-RK1-J Method, Multi-Dimensional

```
function fb-rk1-j(f, g, h, y0, k, N, tol, dimx, dimz)
n1 = length(y0)
x = complex(zeros(2N+1,dimx))
y = complex(zeros(2N+1,n1))
z = complex(zeros(2N+1,dimz))
px = complex(zeros(2N+1,dimx))
py = complex(zeros(2N+1,n1))
pz = complex(zeros(2N+1,dimz))
y[N+1,:] = y0'
error = 1
j = 0
while error > tol && error < 1000 do
    for i = 1:N do
        y[N+i+1,:] = py[N+i,:] + kg(px[N+i,:]', py[N+i,:]', pz[N+i,:]')
        y[N-i+1,:] = py[N-i+2,:] - kg(px[N-i+2,:]', py[N-i+2,:]', pz[N-i+2,:]')
    end for
    for i = 1:2N do
        x[i+1,:] = px[i,:] + kf(x[i,:]',py[i,:]',pz[i,:]')
        z[2N-i+1,:] = pz[2N-i+2,:] - kh(px[2N-i+2,:]', py[2N-i+2,:]', z[2N-i+2,:]')
    end for
    error = norm(hcat(x, y, z) - hcat(px, py, pz))
    j = j+1
    px[:] = x[:]
    py[:] = y[:]
    pz[:] = z[:]
end while
return x[N+1], z[N+1], j
```

Chapter 5

Bibliography

[1] J. Andres and R. Bader. "Asymptotic boundary value problems in Banack spaces". In: *Journal of Mathematical Analysis and Applications* 274 (1 Oct. 2002), pp. 437–457.

[2] S. Banach. "Sur les opérations dans les ensembles abstraits et leur application aux équations intégrales". In: *Fundamenta Mathematicae* 3 (1 1922), pp. 133–181.

[3] J. Bezanson et al. "Julia: A Fresh Approach to Numerical Computing". In: *SIAM Review* 59.1 (2017), pp. 65–98.

[4] R.L. Burden and D.J. Faires. *Numerical Analysis*. Ninth Edition. Brooks/Cole, Cenage Learning, 2011. Chap. Initial-Value Problems for Ordinary Differential Equations, pp. 259–374. ISBN: 0-538-73351-9.

[5] K. Burrage. *Parallel and Sequential Methods for Ordinary Differential Equations*. Clarendon Press, 1995. ISBN: 0-19-853432-9.

[6] J. Carr. *Applications of Centre Manifold Theory*. Applied Mathematical Sciences 35. New York: Springer–Verlag, 1981. ISBN: 0-387-90577-4.

[7] N. Castaneda and R. Rosa. "Optimal Estimates for the Uncoupling of Differential Equations". In: *Journal of Dynamics and Differential Equations* 8 (1 Nov. 1996), pp. 103–139.

[8] C. Chicone. *Ordinary Differential Equations with Applications*. Texts in Applied Mathematics 34. Springer, 1999. Chap. Introduction to Ordinary Differential Equations, pp. 28–52. ISBN: 0-387-98535-2.

[9] M. Dellnitz and A. Hohmann. "A subdivision algorithm for the computation of unstable manifolds and global attractors". In: *Numerical Mathematics* 75 (3 Jan. 1997), pp. 293–317.

[10] H. Federer. *Geometric measure theory*. Gundlehren der mathematischen Wissenschaften. Springer, 1969. ISBN: 978-3-540-60656-7.

[11] C. Foias. "Inertial manifolds for nonlinear evolutionary equations". In: *Journal of Differential Equations* 73 (2 June 1988), pp. 309–353.

[12] M. Fuming and T. Kupper. "A numerical method to calculate center manifolds of ode's". In: *Applicable Analysis* 54 (1-2 May 1994), pp. 1–15.

[13] T.H. Gronwall. "Note on the derivatives with respect to a parameter of the solutions of a system of differential equations". In: *Annals of Mathematics* 20 (4 July 1919), pp. 292–296.

[14] B. Hamzi, W. Kang, and A.J. Krener. "The Controlled Center Dynamics". In: *Mutliscale Modeling and Simulation* 3.4 (2005), pp. 838–852.

[15] M. Haragus and G. Iooss. *Local Bifurcations, Center Manifolds, and Normal Forms in Infinite-Dimensional Dynamical Systems*. Second Edition. Springer, 2011. Chap. Center Manifolds, pp. 29–46. ISBN: 978-0-85729-111-0.

[16] M. Humi. "Long's Equation in Terrain Following Coordinates". In: *Nonlinear Processes in Geophysics* 16 (2009), pp. 533–541.

[17] J.K. Hunter. *Applied Analysis*. Texts in Applied Mathematics. World Scientific, 2001. Chap. The Contraction Mapping Theorem, pp. 61–78. ISBN: 9810241917.

[18] K. Ito and K. Kunisch. "Reduced order control based on approximate inertial manifolds". In: *Linear Algebra and its Applications* 415 (2-3 2006), pp. 531–541.

[19] M.S. Jolly and R. Rosa. "Computation of non-smooth local centre manifolds". In: *IMA Journal of Numerical Analysis* 24 (4 Oct. 2005), pp. 698–725.

[20] K. Kirchgassner. "Wave-solutions of reversible systems and applications". In: *Journal of Differential Equations* 45 (1 July 1982), pp. 113–127.

[21] K. Kirchgassner and J. Scheurle. "On the bounded solutions of a semilinear equation in a strip". In: *Journal of Differential Equations* 32 (1 Apr. 1979), pp. 119–148.

[22] B. Krauskopf. "A survey of methods for computing (un)stable manifolds of vector fields". In: *International Journal of Bifurcation and Chaos* 15 (3 Mar. 2005), pp. 763–802.

[23] Y.A. Kuznetsov. *Andronov-Hopf bifurcation*. Ed. by Eugene M. Izhikevich. 2006. URL: `http://www.scholarpedia.org/article/Andronov-Hopf_bifurcation`.

[24] J.M. Lee. *Introduction to Smooth Manifolds*. Graduate Texts in Mathematics 218. New York: Springer–Verlag, 2012. ISBN: 978-1-4419-9981-8.

[25] T.K. Leen. "A coordinate-independent center manifold reduction". In: *Physics Letters A* 174 (1-2 1993), pp. 89–93.

[26] E.N. Lorenz. "Deterministic Nonperiodic Flow". In: *Journal of the Atmospheric Sciences* 20 (Mar. 1963), pp. 130–141.

[27] J.E. Marsde and M. McCracken. *The Hopf Bifurcation and Its Applications*. Applied Mathematical Sciences 19. Springer-Verlag, 1976. ISBN: 0-387-90200-7.

[28] G. Moore and E. Hubert. "Algorithms for constructing stable manifolds of stationary solutions". In: *IMA Journal of Numerical Analysis* 19 (3 July 1999), pp. 375–424.

[29] B.E. Oldeman and E.J. Doedel. *AUTO-07P. Continuation and Bifurcation Software for Ordinary Differential Equations*. 2012.

[30] K.J. Palmer. "Exponential separation, exponential dichotomy and spectral theory for linear systems of ordinary differential equations". In: *Journal of Differential Equations* 46 (3 Dec. 1982), pp. 324–345.

[31] C. Pötzsche and M. Rasmussen. "Taylor Approximation of Integral Manifolds". In: *Journal of Dynamics and Differential Equations* 18 (2 Apr. 2006), pp. 427–460.

[32] A.J. Roberts. "Simple examples of the derivation of amplitude equations for systems of equations possessing bifurcations". In: *The ANZIAM Journal* 27 (1 July 1985), pp. 48–65.

[33] S.H. Strogatz. *Nonlinear Dynamics and Chaos*. Westview Press, 2015. Chap. Bifurcations Revisited, pp. 244–287. ISBN: 978-0-8133-4910-7.

[34] R. Temam. "Inertial manifolds and slow manifolds". In: *The Mathematics of Models for Climatology and Environment*. NATO ASI Series 48 (1997), pp. 181–214.

[35] Y.H. Wan and B. Hassard. "Bifurcation formulae derived from center manifold theory". In: *Journal of Mathematical Analysis and Applications* 63 (1 Mar. 1978), pp. 297–312.

[36] W. Wasow. "On the Asymptotic Solution of Boundary Value Problems for Ordinary Differential Equations Containing a Parameter". In: *Studies in Applied Mathematics* 23.1 (Apr. 1944), pp. 173–183.

[37] J. White et al. *Waveform Relaxation: Theory and Practice*. Tech. rep. UCB/ERL M85/65. EECS Department, University of California, Berkeley, 1985.

[38] S. Zhao and T. Kalmár-Nagy. *Delay Differential Equations: Recent Advances and New Directions*. Springer, 2009. Chap. Center Manifold Analysis of the Delayed Liénard Equation, pp. 203–219.